NOVA SCHOOL OF SCIENCE & TECHNOLOGY

DEPARTMENT OF CHEMISTRY

Carolina Guerra Neca
BSc in Biochemistry

POLYMERIC NANOPARTICLES AS VEHICLE FOR THE DELIVERY OF ANTICANCER THERAPEUTIC DEEP EUTECTIC SYSTEMS

MASTER IN BIOTECNOLOGY

NOVA University Lisbon
September, 2024

NOVA SCHOOL OF SCIENCE & TECHNOLOGY

DEPARTMENT OF CHEMISTRY

POLYMERIC NANOPARTICLES AS VEHICLE FOR THE DELIVERY OF ANTICANCER THERAPEUTIC DEEP EUTECTIC SYSTEMS

CAROLINA GUERRA NECA
BSc in Biochemistry

Supervisor: Rita Paiva de Melo
Associate Professor in TECNICO
Co- Supervisor: Ana Rita Cruz Duarte
Associate Professor, NOVA FCT University Lisbon

Júri:
Presidente: Maria Filomena Andrade de Freitas
Associate Professor, NOVA FCT University Lisbon
Arguente: Elisabete de Jesus Oliveira Marques
Associate Investigator, NOVA FCT University Lisbon
Vogais: Rita Paiva de Melo
Associate Professor in TECNICO

MASTER´S DEGREE IN BIOTECHNOLOGY

NOVA University Lisbon
September, 2024

Polymeric Nanoparticles as Vehicle for the Delivery of Anticancer Therapeutic Deep Eutectic Systems

"A person who never made a mistake never tried anything new. The most beautiful experience we can have is the mysterious. It is the fundamental emotion which stands at the cradle of true art and true science."

Albert Einstein

ACKNOWLEDGEMENTS

I would like to express my gratitude to my supervisor, Dr. Rita Paiva, for the opportunity to work under her guidance and collaboration. I appreciate her kindness and the initial direction she provided, which helped lay a solid foundation for my research.

I also want to sincerely thank my co-supervisor, Dr. Rita Duarte, for her unwavering support, guidance, and encouragement throughout this year. Your insights and dedication have been instrumental in both my personal and academic growth, and your commitment to work has been a tremendous source of inspiration for me. Thank you for the opportunities you have provided and for always being available when needed, always offering solutions and creating an environment conducive to my development. I am just starting my journey, and seeing dedicated professionals like you is truly motivating.

My deep appreciation goes to PhD student Joana Pereira for embracing this challenge and guiding me through a journey filled with daily obstacles. Your dedication and professionalism have been truly inspiring. I cannot count all the things I have learned from you—not just about nanoparticles, but also how to work in a lab, how to collaborate as a team, how to face challenges, and how to work ethically. Thank you for your patience and the countless hours we spent together in the lab, as well as for your invaluable help in reading and correcting my thesis. Your resilience, unwavering commitment to science, and never-give-up attitude are truly admirable. You are going to be an amazing doctor, and science is lucky to have you!

I would like to thank the members of the Des.Solve Group, especially to Hugo, Ana, Filipe, and Célia—along with my colleagues Andreia, Filipe, and Diogo. I am grateful for all the help and the warm welcome you provided, for the enriching discussions, and for making this an optimal working environment. You are all great professionals.

I also acknowledge NOVA University, where I completed my master's and conducted my thesis, for its support and resources throughout this journey. My gratitude extends to the PROTEOMASS Scientific Society (Caparica, Portugal) facility for the DLS analysis performed by Dr. Elisabete Oliveira, and to the Laboratory of Membrane Processes (Caparica, Portugal) for providing the sonicator, supervised by PhD student Suchintan Mondal. Additionally, I would like to thank LAQV, which is financed by national funds from FCT/MCTES (LA/P/0008/2020, UIDP/50006/2020, and UIDB/50006/2020), for their support. I also acknowledge funding from the European Union's Horizon 2020 - European Research Council (ERC) under grant agreement

CryoDESERC-2022-POC2 101101088. This work was supported by the Associate Laboratory for Green Chemistry (LAQV), funded by national funds from FCT/MCTES (UIDB/50006/2020).

I want to extend my gratitude to my close friends from Sabugal and to the friends I made in Coimbra, especially to Maria and "*mis hermanas"* Bozzo and Inês, who supported and advised me along the way, always with words of encouragement and walking this journey by my side. Thank you for helping me see the bright side, even in the not-so-good moments, and for sharing your experiences with me. I am especially grateful to the friends that Lisbon and Biotech has brought into my life: Benedita, Bruno, Bruna, Lara, Sofia, Filipa and Beatriz, each one contributing to this journey. It is truly rewarding to be part of a group where mutual support and motivation are constant and assured, with a contagious desire to grow and pursue fulfillment.

Thank you to my close family: to my cousins Flavia and Iara, two remarkable women who lived with me this year, for providing the daily motivation to move forward and believe in myself. To *mis papas*, thank you for providing me with the tools to build my future, the courage to move away, and the financial support and motivation to continue my studies and complete this thesis. I know it is not easy, and I do not take it for granted and I understand how fortunate I am. To mi *abuelita*, gracias for boosting my confidence and helping me finish my thesis. (However, *abuelita*, just between us, I should clarify that I am not a doctor, as you often tell your friends). Additionally, thanks to my brother for keeping the sarcasm alive while always standing (In secret) by his big sis.

I want to thank myself for making it this far. It was my first time doing a thesis, and I knew from the beginning that it would be a big challenge, but I took it on anyway. It has become a truly rewarding experience and has provided me with numerous skills.

And finally, to the readers of my thesis, thank you for taking the time to go through a year's worth of my work. I promise, I gave it my all!

ABSTRACT

Therapeutic Deep Eutectic Systems (THEDES)—which combine terpenes and non-steroidal anti-inflammatory drugs (NSAIDs)—are promising approach targeting colorectal cancer (CRC). The Me:IBU (3:1) combination notably enhances antiproliferative and anti-inflammatory effects, demonstrating synergistic efficacy and selective cytotoxicity while sparing normal cells. However, the hydrophobic nature of THEDES challenges the design of an effective drug delivery. The aim of this study was to develop a poly (lactic-co-glycolic acid) (PLGA) nanoparticle (NP)-based delivery system for THEDES. Both empty and Me:IBU (3:1)-loaded PLGA NPs were prepared using single-emulsion solvent evaporation and nanoprecipitation methods. In the single-emulsion method, varying polymer (PLGA) and surfactant (PVA) concentrations were tested, with a PLGA concentration of 25 mg/mL and 5% v/v PVA yielding spherical NPs (88–185 nm). However, these NPs showed instability and aggregation, likely due to residual PVA, therefore, a surfactant-free nanoprecipitation method was also tested. Using nanoprecipitation, both empty and Me:IBU (3:1)-loaded NPs were formulated with acetone and water as co-solvents. Dynamic Light Scattering (DLS) and Scanning Electron Microscopy (SEM) confirmed the aggregation of NPs upon lyophilization, as well as their instability, which is attributed to a zeta potential of -11.6 ± 0.4 mV. Following optimization, empty NPs were successfully formulated in phosphate-buffered saline (PBS) with a size of 509.9 ± 4.4 nm and a PDI of 0.081, but not in water. Me:IBU (3:1)-loaded NPs did not form in PBS but were successfully formulated in water, as confirmed by Transmission Electron Microscopy (TEM) and DLS. These NPs had a size of 246.9 ± 2.6 nm, a PDI of 0.066, and a zeta potential of -32.6 ± 2.2 mV. Furthermore, these NPs seems remained stable for two months with a PDI of 0.095. Cytotoxicity and antiproliferative assays were performed using Caco-2 cells and HT29 cells, respectively, and showed no significant impact on cell viability. Additionally, fluorescent dyes FITC and Nile Red were successfully encapsulated, and FITC-loaded NPs were effectively internalized by HT29 cells, indicating potential for the delivery of THEDES to CRC cells.

This study highlights the challenges in formulating PLGA NPs for THEDES delivery and underscores the need for further optimization, or the use of improved methods, to enhance their effectiveness in targeted CRC therapies.

Keywords: Colorectal Cancer, Drug delivery, THEDES, PLGA, Nanoparticles, Nanoprecipitation, Single emulsion solvent evaporation

RESUMO

Os Sistemas Terapêuticos Eutécticos Profundos (STEPS)—que combinam terpenos e anti-inflamatórios não esteroides (AINEs)—são uma abordagem promissora para o tratamento do cancro colorretal (CCR). A combinação Me:IBU (3:1) melhora os efeitos antiproliferativos e anti-inflamatórios, demonstrando uma eficácia sinérgica e citotoxicidade seletiva, não afetando as células normais. No entanto, a natureza hidrofóbica dos STEPS constitui um desafio no design de um sistema eficaz de entrega de fármacos. O objetivo deste estudo foi desenvolver um sistema de entrega baseado em nanopartículas (NPs) de ácido polilático-co-glicólico (PLGA) para os STEPS. Tanto NPs vazias como NPs encapsuladas com Me:IBU (3:1) foram preparadas usando os métodos de evaporação de solvente por emulsão simples e nanoprecipitação. No método de emulsão simples, foram testadas diferentes concentrações de polímero e surfactante, com uma concentração de PLGA de 25 mg/mL a produzir NPs esféricas (88–185 nm). No entanto, estas NPs mostraram instabilidade e agregação, provavelmente devido à presença de PVA residual, pelo que foi também testado um método de nanoprecipitação sem surfactante. Utilizando o método de nanoprecipitação, foram formuladas tanto NPs vazias como NPs encapsuladas com Me:IBU (3:1), com acetona e água como co solventes. A Dispersão de Luz Dinâmica (DLS) e a Microscopia Electrónica de Varrimento (SEM) confirmaram a agregação das NPs após liofilização, bem como a sua instabilidade, atribuída a um potencial zeta de -11,6 ± 0,4 mV. Após otimização, as NPs vazias foram formuladas com sucesso em solução salina tamponada com fosfato (PBS) com um tamanho de 509,9 ± 4,4 nm e um PDI de 0,081, mas não em água. As NPs encapsuladas com Me:IBU (3:1) não se formaram em PBS, mas foram formuladas com sucesso em água, conforme confirmado pela Microscopia Electrónica de Transmissão (TEM) e DLS. Estas NPs apresentaram um tamanho de 246,9 ± 2,6 nm, um PDI de 0,066 e um potencial zeta de -32,6 ± 2,2 mV. As NPs mantiveram-se estáveis durante dois meses com um PDI de 0,095. Ensaios de citotoxicidade e antiproliferativos foram realizados em células Caco-2 e HT29, respetivamente, e nenhum impacto significativo na viabilidade celular foi observado. Adicionalmente, sondas fluorescentes FITC e Nile Red foram encapsuladas com sucesso, e as NPs encapsuladas com FITC foram internalizadas eficazmente pelas células HT29, indicando potencial para a entrega de STEPS a células do CCR.

Este estudo destaca os desafios na formulação de NPs de PLGA para a entrega de STEPS e sublinha a necessidade de otimização, ou da utilização de métodos melhorados, para aumentar a sua eficácia em terapias direcionadas ao CCR.

Palavras chave: Cancro Colorrectal, Entrega de Fármacos, STEPS, PLGA, Nanopartículas, Nanoprecipitação, Evaporação de Solvente por Emulsão Simples

TABLE OF CONTENTS

LIST OF FIGURES

LIST OF TABLES

ABBREVIATIONS

5-FU	5-fluorouracil
AC	Acetone
API	Active pharmaceutical ingredient
APC	Adenomatous polyposis coli
ATR-FTIR	Attenuated Total Reflectance-Fourier Transform Infrared Spectroscopy
Bax	Bcl-2-associated X protein
BAX	BCL2-associated X apoptosis regulator
BRAF	B-Raf proto-oncogene serine/threonine kinase
CAP	Capecitabine
CIMP	CpG island methylator phenotype
CIN	Chromosome instability
COX-2	Cyclooxygenase-2
COVID-19	Coronavirus disease 2019
CRC	Colorectal Cancer
CTLA-4	Cytotoxic T-Lymphocyte-Associated Protein 4
DDS	Drug delivery system
DCM	Dichloromethane
DES	Deep Eutectic Systems
DLS	Dynamic Light Scattering
DNA	Deoxyribonucleic acid
EGRF	Epidermal Growth Factor Receptor
EGFR	Epidermal Growth Factor Receptor
EMT	Epithelial-to-mesenchymal transition
ERK	Extracellular Signal-Regulated Kinase
FBS	Fetal bovine serum
HBA	Hydrogen Bond Acceptor
HBD	Hydrogen Bond Donor
HPLC	High-Performance Liquid Chromatography
IBD	Inflammatory bowel diseases
IGF2R	Insulin-like Growth Factor 2 Receptor
IL-4	Interleukin-4
IRI	Irinotecan
KRAS	Kirsten rat sarcoma viral oncogene homolog
MAPK	Mitogen-activated protein kinase
MMR	Mismatch repair genes

MSI	Microsatellite instability
MTS	Methyltetrazolium Sal
NADES	Natural Deep Eutectic Systems
NF-κB	Nuclear factor-kappa B
NO	Nitric oxide
NSAIDs	Non-steroidal anti-inflammatory drugs
OX	Oxaliplatin
PBS	Phosphate saline buffer
PD-1	Cell Death Protein 1
PDL-1	Programmed Death-Ligand 1
PEG	Polyethylene glycol
PGs	Prostaglandins
PDI	Polydispersity index
PGE2	Prostaglandin E2
PhMV	Physalis mottle virus
PLGA	Poly (lactic-co-glycolic acid)
POH	Perillyl alcohol
PS	Penicillin-streptomycin
PTMs	Post-translation modifications
PVA	Polyvinyl alcohol
p53	Protein 53
RES	Reticuloendothelial system
ROS	Reactive oxygen species
RPMI	Gibco Roswell Park Memorial Institute
SEM	Scanning Electron Microscopy
TEM	Transmission Electron Microscopy
TGFβR	Transforming growth factor beta
THEDES	Therapeutic Deep Eutectic Systems
TME	Tumor microenvironment
TNF-α	Tumor Necrosis Factor Alpha
TP53	Tumor Protein p53
VEGF	Vascular endothelial factor
VEGF-A	Vascular Endothelial Growth Factor A
VLPs	Virus-like particles

1. INTRODUCTION

1.1. Cancer

Cancer was one of the most lethal diseases in the 20th century and remains a major global concern in the 21st century [1]. According to World Health Organization, cancer remains the primary global health challenge, accounting for approximately 20 million new cases and almost 10 million deaths in 2022, representing nearly 1 in 6 global deaths [2]. Predictions for 2040 project a significant increase in cancer cases to 28.4 million [3]. In 2022, Portugal recorded 69.567 new cases and 33.762 deaths [4]. The most prevalent types of cancer in men include lung, prostate, colorectal, stomach, and liver cancer. In women, the most common types are breast, colorectal, lung, cervical, and thyroid cancer [5].

Cancer is a complex group of diseases characterized by the abnormal and uncontrolled growth and proliferation of cells, which can occur in any tissue or organ [6]. The initiation of cancer often arises from 4/5 mutations that create an optimal environment for further mutation [7]. Most cancers have an epithelial origin with stem cell niches having a pivotal role [8]. Understanding how normal cells progress into tumor cells is crucial to develop treatments and mitigate the abrupt statistical numbers.

Genetic susceptibility, coupled with environmental factors and lifestyle choices, emerges as a potent catalyst for these mutations and subsequently cancer development. In our modern society, individuals are exposed to a myriad of potential carcinogens and hormone-disrupting agents [8]. These range from pollutants in the air and water to detrimental habits like smoking, as well as the choice of shampoos, skincare items, and household products [9]. Additionally, previous diseases that could have led to chronic inflammation can also create an optimal environment for cancer progression [10].

1.1.1. Cancer Biology

In a normal situation, the cell division cycle is highly regulated by communication between cells. When mutations occur in genes responsible for regulating cell growth, apoptosis, and deoxyribonucleic acid (DNA) damage repairing, cells undergo regulation checkpoints to

either repair the mutation or, in extreme cases, undergo apoptosis [11]. However, in abnormal situations, mutations can persist in the regulatory genes, like a) tumor suppressor genes, responsible for inhibiting growth and promoting death, b) proto-oncogenes, involved in promoting cellular growth, and c) caretaker genes, involved in genome repair and stability (Figure 1) [12]. Growth signal pathways, that are typically downstream of growth factors, and receptors tyrosine kinase are frequently hyperactivated or constitutively activated by oncogenic mutations, which reduces the dependency of cells on these signals [13]. This in combination with the loss of function of tumor suppressors and caretaker genes, creates a landscape of genomic instability, laying the groundwork for subsequent events [14], [15].

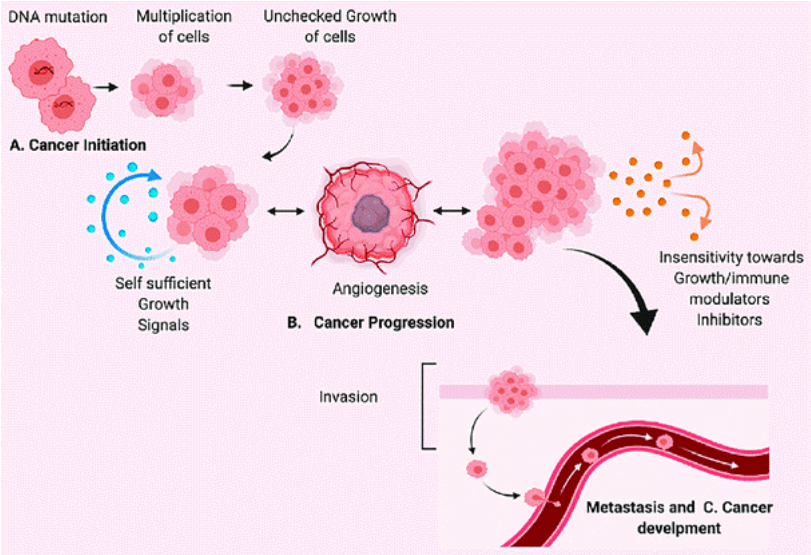

Figure 1: Carcinogenic steps: The progression of carcinogenesis is made by a multiple step process. A) Cancer initiation: involves DNA mutations, especially in proto-oncogenes and tumor suppressor genes, disrupting the delicate balance of cell growth regulation and triggering the formation of preneoplastic lesions. 2) Cancer progression: subsequent accumulation of genetic mutations leads to the proliferation of mutated cell clones that can produce self-sufficient growth signals and become insensitive to immune modulators. When the tumor rich a certain size, angiogenesis is promoted acquiring the capabilities needed to migrate to other tissues and initiate metastasis. Additionally in parallel cells communicate with a pro-inflammatory environment that also contribute to tumor progression and metastasis. Adapted from [16].

This loss of growth and survival signaling control, leads to an increase in cell division and abnormal cell shape known as dysplasia and is one of the barriers that cells need to overcome to become malignant. This stage is known as adenoma or benign tumor once it exhibits a localized growth pattern without spreading [17].

Additionally, cancer cells release signals that consistently attract mesenchymal/stromal cells such as fibroblasts and immune cells, forming a dysfunctional and pro-inflammatory tumor microenvironment (TME). In reciprocation, these stromal cells emit growth and survival signals, creating a positive feedback loop that sustains inflammation and fosters tumor growth [18]. The heightened production of reactive oxygen species (ROS) during inflammation, origi-

nally meant for pathogen elimination, can inadvertently induce DNA damage, fostering genetic mutations. This reciprocal interaction implies that cancer cells are not entirely self-sufficient in terms of growth signals, as they remain dependent on the growth factors secreted by stromal cells [19]. This clinical insight is significant, particularly when there is an increase in the expression of growth factor receptors in cancer cells, presenting potential targets for drug delivery [20]. Factors secreted by the TME, such as hormones or cytokines, promote the clonal expansion of mutated cells. In this stage, cells undergo epigenetic changes like methylation and histone modification. Epigenetic modifications, which involve alterations in gene expression without changes to the DNA sequence, contribute to tumor heterogeneity. Cancer cells with modified genetic profiles undergo continued replication, resulting in the emergence of unique mutations within different clusters of clones, explaining the tumor's diverse genetic landscape. These distinct mutations confer a selective advantage to certain cancer cells, enabling them to grow more rapidly and survive better, potentially contributing to the tumor's aggressiveness and adaptability [21], [22]. When the tumor reaches a size of 2-3 milliliters, necessitating a robust blood supply for nutrients, oxygen, and waste removal, a specialized niche of stem cells initiates the growth of tumor-related blood vessels by elevating levels of vascular endothelial growth factor (VEGF) and other pro-angiogenic factors [23].

Cancer progression towards metastasis is a nuanced process, not only involving cellular transformation but also intricate interactions within a dysfunctional TME [24], [25]. Metastasis, the intricate process of cancer cells spreading from the primary tumor to distant sites, hinges on various molecular events. In cases where cancer cells originate from epithelial tissues, they undergo a transformative process known as epithelial-to-mesenchymal transition (EMT) (Figure 2) [26]. During EMT, epithelial cells, characterized by high intercellular adhesion, low motility potential and anchored to the extracellular matrix, transit into mesenchymal cells. These mesenchymal cells exhibit heightened motility potential and low adhesion, key features that facilitate their migration and infiltration into lymphatic vessels. The EMT transition is an epigenetic alteration and evolves the downregulation of cadherins, crucial transmembrane proteins responsible for cell-to-cell adhesion. Additionally, activation of motility genes occurs, and the secretion of proteases facilitates the digestion of the extracellular membrane when epithelial cells are attached, ultimately leading to the formation of secondary tumors [27].

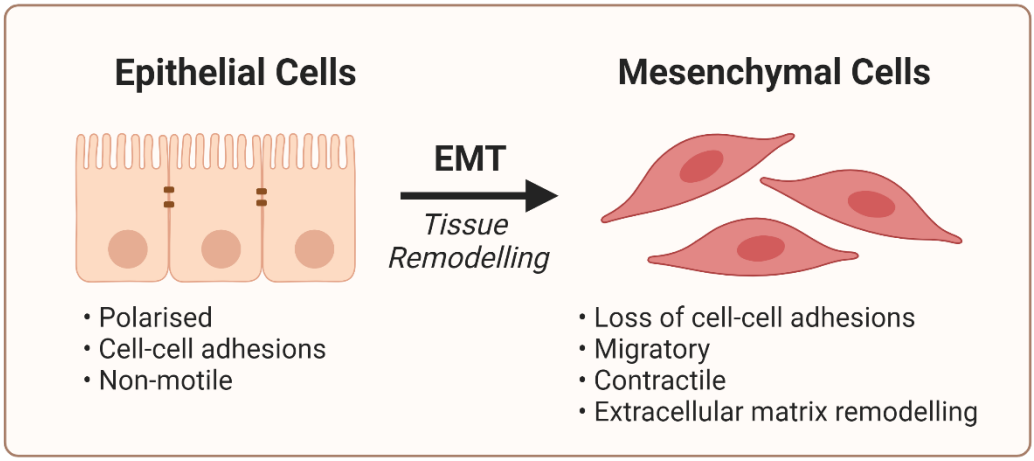

Figure 2: EMT transition of cancer cells. During EMT, cells shift from an organized and stationary epithelial state to a more migratory and invasive mesenchymal state. This involves downregulation of epithelial markers (e.g., E-cadherin), loss of apical polarity, and upregulation of mesenchymal markers (e.g., N-cadherin). Consequently, cells become more motile, lose cell-cell adhesion, and gain invasive properties, facilitating metastasis and tumor progression. Created with BioRender.com.

Moreover, inflammation holds a pivotal role in cancer progression, and its influence extends to the initiation of cancer as well. Chronic inflammation, in particular, fosters an environment conducive to both the onset and advancement of cancer. Colorectal cancer (CRC) frequently arises in the context of chronic inflammatory conditions, notably linked to disorders like inflammatory bowel diseases (IBD) [28]. This sets the stage for a microenvironment favorable to the initiation and progression of CRC. The enduring inflammatory response in the colorectal region, induced by abnormal immune reactions, results in elevated levels of pro-inflammatory cytokines, immune cell infiltration, and heightened production of ROS, that can contribute to genetic instability and tumor initiation and progression [29].

1.2. Colorectal Cancer

Currently, CRC is a significant global health challenge, ranking as the third most prevalent cancer worldwide, representing 10 % of all cancer cases. In 2020, over 1.9 million new cases of colorectal cancer and more than 930,000 related deaths was reported globally. In 2040 it is estimated an increase of 63 % in new cases and 73 % in CRC deaths [30]. In Portugal, according to Champalimaud Foundation, it is the second most frequent and the deadliest cancer with over 7.000 new cases per year [31]. The risk of developing CRC increases with age, with the majority of cases diagnosed in individuals over 50 years old [32]. Recent research indicates a decline in incidence among individuals aged 65 and older, a stabilization within the 50 to 64 age group, and a concerning upward trend observed in those aged 50 to 54 and under 50, with an annual increase of 2%, since 2011 [33]. Diet, family history, obesity, diabetes, smoking habits, history of inflammatory disease, and familial syndromes, are among the risks to the development of this malignance. Disparities in the adoption of screening practices and

access to healthcare services present significant challenges, resulting in delayed diagnoses and inferior outcomes, especially within underserved populations [32]. Furthermore, the emergence of COVID-19 (Coronavirus disease 2019), which required more resources for health services, lead to a reduction in care for other diseases as cancer [34].

1.2.1. Molecular pathways in CRC development

CRC is a complex disease affecting the large intestine and rectum [35]. Approximately 75 % of CRC cases are sporadic, meaning they do not have clear hereditary connections [36]. About 5 % are linked to hereditary syndromes like Lynch syndrome, which involves specific genetic factors [37]. There is also a unique subtype called Colitis-Associated Cancer (CAC), related to chronic inflammatory conditions in the colon [38]. The sequence of events that make normal cells start uncontrolled proliferation and growth involves three different pathways that could lead to CRC formation and progression from adenoma to carcinoma: the classical adenoma-to-carcinoma progression, CAC pathway, and Serrated pathway [39].

The classical adenoma-to-carcinoma progression representing 65-85 %, can be a consequence of two different events: chromosome instability (CIN) or microsatellite instability (MSI) [40].

CIN refers to accumulation of mutations in oncogenes and tumor suppressor genes. The loss of function of tumor suppressor gene adenomatous polyposis coli (APC) and the increase expression of Kirsten rat sarcoma viral oncogene homolog (KRAS) results in adenoma formation. Later SMAD2-4 and protein 53 (p53) mutations leads to the progression to carcinoma [41]. APC is a tumor suppressor gene and a negative regulator of the WNT pathway. APC is responsible for facilitating the degradation of β-catenin protein. β-catenin migrates to the nucleus and binds to specific genes responsible for promoting cell proliferation and survival, activating them. The APC mutations lead to the accumulation of β-catenin, which hyperactivates WNT pathway [42]. Furthermore, SMAD2 and SMAD4, key components of the TGF-β signaling pathway, act as tumor suppressor genes by modulating cell proliferation and apoptosis. Dysregulation or loss of function in SMAD2 and SMAD4 disrupts TGF-β signaling, facilitating tumorigenesis. TP53 is a tumor suppressor gene encoding the p53 protein that acts as a transcription factor, regulating the expression of genes involved in cell cycle arrest, DNA repair, and apoptosis. TP53 loss of function can result in impaired DNA damage response, allowing cells with genetic errors to evade apoptosis and continue dividing. Conversely, KRAS is a proto-oncogene and a mutation in this pathway results in uncontrolled cell growth [43].

MSI points to errors in microsatellites, short repetitive DNA sequences, causing inactivation of mismatch repair genes. In this pathway the loss of DNA mismatch repair genes (MMR), like MLH1 gene, contribute to adenoma formation. These genes are responsible for maintaining DNA integrity by identifying and correcting errors in the genetic material before they can

lead to mutations or genetic instability. Subsequently, the progression from adenoma to carcinoma occurs as a consequence of mutations in B-Raf proto-oncogene, serine/threonine kinase (BRAF), BAX gene, or transforming growth factor beta (TGFβR) signaling pathway and insulin-like growth factor 2 receptor (IGF2R) [44], [45]. Typically, 70-85 % of CRC present higher levels of CIN than MSI [41]. The BRAF mutation upregulates cell signaling proteins, disrupting pathways like mitogen-activated protein kinase/extracellular signal-regulated kinase (MAPK/ERK). This prompts uncontrolled cell growth, survival, and proliferation [46]. BCL2-associated X, apoptosis regulator (BAX) is a pro-apoptotic gene having a role in promoting apoptosis. Dysregulation of Bcl-2-associated X protein (Bax) expression or function can disrupt apoptosis, enabling cancer cells to evade programmed cell death, thereby promoting tumor survival and progression [47]. Additionally, TGFβR is part of the TGF-β signaling pathway, which typically has tumor-suppressive functions. The IGF2R acts as a tumor suppressor by binding to IGF2 and targeting it for lysosomal degradation, thereby inhibiting its mitogenic effects. A mutation in these receptors lead to the loss of the ability to control cell proliferation (Figure 3) [48], [49].

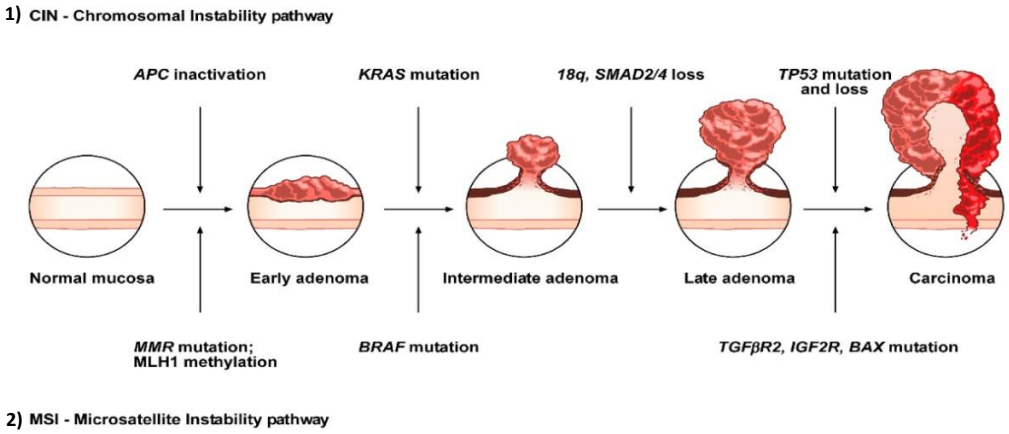

Figure 3: Classical adenoma to carcinoma progression by two different pathways: 1) CIN is consequence of an accumulation of genetic alterations: gain or loss of chromosomes or chromosomal segments and, alterations in tumor suppressor genes (APC, SMAD2/4, TP53) and proto-oncogenes (KRAS). 2) MSI involves mutations in shorts repetitive DNA segments, affecting DNA mismatch repair genes (MMR, MLH1), the genes responsible for correcting DNA errors. Additionally, BRAF and later BAX, TGFβR and IGF2R mutations also contribute to the progression from adenoma to carcinoma [50].

CAC arises in the context of chronic IBD like ulcerative colitis and Crohn's disease, with IBD patients having a 60 % higher CRC incidence. This shows the role of inflammation as one possible trigger for tumor development [51]. CAC pathway involves mutations in TP53, BRAF and KRAS genes, and MSI, leading to a low grade of dysplasia. In this pathway, the APC mutation comes further giving rise to angiogenesis via the NF-kB, IL-6/STAT3, or IL-23/Th17 pathways and cytokines secretion [52]. Inflammation is typically present from the beginning in conditions like inflammatory bowel disease. Concurrently, the IL-6/STAT3 pathway becomes activated, fostering an environment conducive to immune evasion, increased cell survival, and

uncontrolled proliferation [53]. Meanwhile, IL-23-mediated differentiation and maintenance of Th17 cells, helper cell subtype, produce primarily interleukin 17. The dysregulation of Th17 responses can lead to an excessive production of cytokines contributing to the inflammatory environment potentially fueling tumor development (Figure 4) [54]. Collectively, these pathways synergize to sustain chronic inflammation, creating a microenvironment that supports the initiation and progression of colorectal cancer in the context of colitis.

The serrated adenoma pathway is characterized by specific morphological features displaying a unique serrated appearance, setting them apart from conventional adenomas. This pathway is often associated with BRAF mutations and CpG island methylator phenotype (CIMP) in genes as TP53 resulting in uncontrolled proliferation [55]. Furthermore, p16 loss of function promotes progression to cancer [56]. This pathway presents higher expression of inflammatory mediators as interleukin-4 (IL-4), tumor necrosis factor alpha (TNF-α), interleukine-1 beta (IL-1β) and cyclooxygenase-2 (COX-2) compared with conventional adenomas [57]. The persistent activation of the nuclear factor-kappa B (NF-κB), a pivotal transcription factor in inflammatory responses, amplifies the expression of genes associated with inflammation, cell survival, and proliferation (Figure 4) [58].

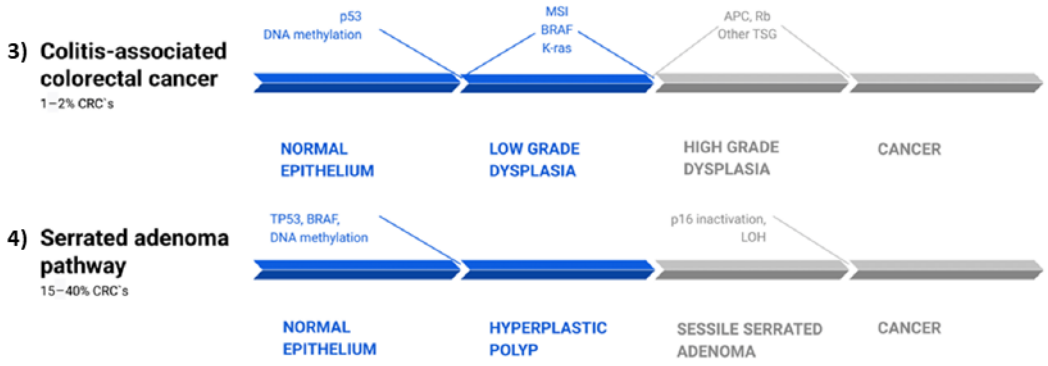

Figure 4 : Two other pathways responsible for adenoma to carcinoma progression: 3) CAC pathway: Mutations in TP53, BRAF, and KRAS, along with MSI, initiate dysplasia. Concurrently, APC mutations stimulate angiogenesis via NF-kB, IL-6/STAT3, or IL-23/Th17 pathways, contributing for tumor progression. 4) Serrated pathway: Epigenetic changes and mutations in genes like BRAF, KRAS, and CpG island methylator phenotype (CIMP) genes drive CRC development [59].

The genetic differences in pathways responsible for the progression from adenoma to carcinoma influence prognosis and treatment outcome. Consequently, identical treatments may have different responses.

1.2.2. CRC and inflammation

Inflammation plays a pivotal role, not only in establishing a conducive environment for cancer initiation in chronic inflammatory diseases but also in driving tumor progression and metastasis. Inflammation is a common factor in all types of CRC, although the degree is variable. It could be associated with the initiation, progression or both phases. CRC is not just

characterized by cells that accumulate mutations, but it also includes the communication between them and with a dysfunctional TME [48]. Key pathways have been identified as deregulated in CRC, like NF-κB, WNT/β-catenin pathway, COX-2, and MAPK pathway, resulting in an inflammatory microenvironment [60].

When NF-κB is activated, it migrates to the nucleus leading to the transcription of genes involved in cell survival, proliferation, and inflammation. Persistent activation of NF-κB in CRC can promote a pro-tumorigenic microenvironment by enhancing cell survival and the production of pro-inflammatory cytokines [61]. Additionally, inflammation can impact the WNT/β-catenin pathway, by promoting the release of WNT ligands, molecules that activate the WNT pathway, or affecting the regulation of β-catenin degradation, leading to aberrant WNT signaling and promoting tumor development [62]. COX-2 is an enzyme involved in the conversion of arachidonic acid into prostaglandins (PGs) and is typically present in pathological conditions. Inflammatory stimuli, like cytokines, induce the expression of COX-2, leading to an increased synthesis of PGs, especially prostaglandin E2 (PGE2). This, in turn, further exacerbates inflammation, creating a positive feedback loop that not only sustains the inflammatory milieu within TME but also supports the uncontrolled growth of cancer cells. COX-2 is overexpressed in 80 % of colorectal carcinomas and it is known to lead to cancer progression [63]. Multiple *in vivo* studies have shown that the inhibition of COX 2 in mice, used as a model for CRC, results in a decrease in size and number of intestinal polyps [64], [65]. The PGs produced by COX-2 lead to an increase in β-catenin that migrates to the nucleus and activates WNT signaling. Studies show that the administration of non-steroidal anti-inflammatory drugs (NSAIDs), as ibuprofen and diclofenac, that are COX-2 inhibitors, show a decrease in β-catenin content suggesting their anti-tumor effect [66]. Additionally, NSAIDs decrease the transcription of genes mediated by NF-κB that are involved in metastasis and cancer cells growth [67]. Furthermore, MAPK pathway dysregulation leads to increased cell proliferation, survival, and migration. Inflammatory mediators, such as growth factors and cytokines, contribute to the sustained activation of the MAPK/ERK pathway in CRC [68]. However, the type of mutations, the time of occurrence and the location is different between the various subtypes of CRC what makes difficult to find a treatment that is effect for all colorectal cancer subtypes [40].

1.2.3. CRC Treatments

Colorectal cancer treatments include surgery, chemotherapy and targeted therapies. However, these treatments exhibit inherent limitations. In response, scientists are exploring novel approaches, such as the application of nanoparticles, to enhance the effectiveness of drugs and improve CRC treatments [39], [40].

1.2.3.1. Conventional treatments

Conventional treatments for CRC encompass a multidisciplinary approach addressing various stages of the disease. The treatment regimen is determined based on various factors such as the location of the primary tumor, the extent of cancer spread to lymph nodes, and

the presence or absence of metastasis. These treatments can be local or systemic, depending on whether they are administered directly to the tumor site or delivered via the bloodstream, respectively (Figure 5) [69]. Surgical intervention, such as open surgery or laparoscopic, is local and remains the primary treatment, particularly for localized tumors, involving the removal of the cancerous tissue and surrounding lymph nodes [70]. Open surgery allows better view of the tumor, but laparoscopic is a less invasive approach, since it involves small incisions decreasing the risk of infection and improving recovery time. However, the choice depends mainly on cancer stage and the patient`s medical conditions [71].

Despite an improvement in screening, the majority of CRCs are detected in advanced stages often with metastasis present [72]. In such cases, adjuvant treatments applied before or after the surgery, become essential to stabilize the tumor, suppress tumor growth, and prevent invasion into other surrounding tissues. A combination treatment regimen is often applied.

Chemotherapy, a systemic treatment, is the centerpiece in colorectal cancer treatment since it can increase the survival rate. It can be implemented alone, or complementary to surgery [73]. Additionally, radiation therapy, a local treatment, can also be used to shrink tumors before surgery [72].

The selection of the right chemotherapy involves the use of either single agents or a combination of multiple agents, depending on the patient's prognosis and treatment objectives [74]. Single-agent regimens, including 5-fluorouracil (5-FU), capecitabine (CAP), irinotecan (IRI), and oxaliplatin (OX), play a key role, in effectively targeting residual cancer cells and preventing recurrence. Combined regimens, such as FOLFOX (5-FU+OX), FOXFIRI (5-FU+IRI), CAPOX (CAP+OX), and CAPIRI (CAP+IRI), involve the use of two or more agents, contributing to enhanced effectiveness, particularly in advanced stages of treatment. While the use of combined therapies may introduce additional side effects, it has shown promise in reducing resistance to drugs and proving effectiveness in advanced stages of treatment [73]. However, chemotherapy have high toxicity to normal cells, often leading to negative off-target side effects and drug resistance [73].

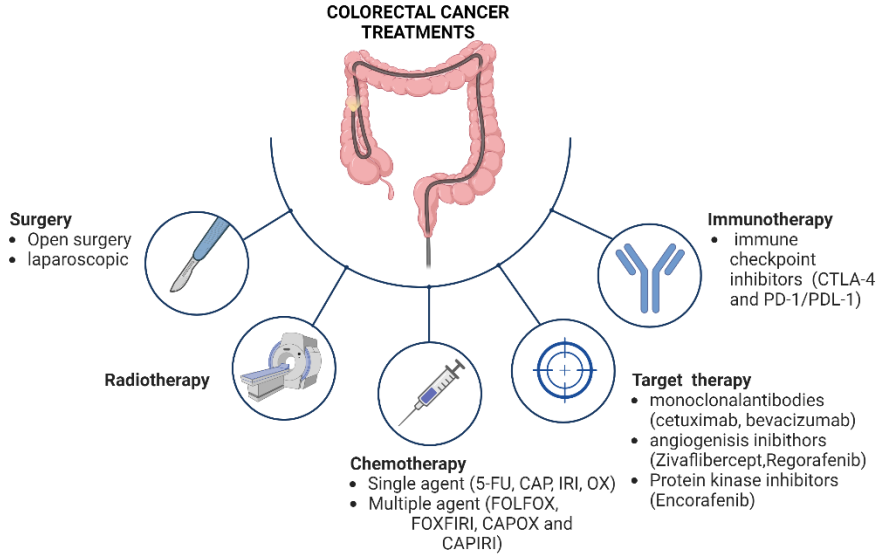

Figure 5: Conventional CRC treatments. The treatment regimen depends on cancer stage, patients age and health, and other factors. The treatment could be systemic or local and be combined in order to obtained a better outcome. Created with BioRender.com.

In response to the off-target effects, targeted therapies emerge. These targeted treatments are employed in advanced stages to target specific molecular pathways crucial for cancer progression. CRC target therapies include: 1) Monoclonal antibodies, like cetuximab that targets epidermal growth factor receptor (EGFR) (present in 80 % of CRC cases) and bevacizumab, which blocks vascular endothelial growth factor A (VEGF-A), crucial for blood vessel formation around tumors [75]; 2) Angiogenesis inhibitors, such as Zivaflibercept hinder new blood vessel growth by trapping VEGF and Regorafenib, effective in advanced stages, blocks VEGF and other proteins to slow tumor growth and angiogenesis [76]; 3) Protein kinase inhibitors, like Encorafenib, a BRAF inhibitor, targets and stop abnormal protein activity associated with mutant BRAF genes, disrupting pathways vital for CRC development and progression [77]. Moreover, in advanced stages, immunotherapy is implemented to activate the body's immune system to recognize and eliminate cancer cells. This includes immune checkpoint inhibitors like cytotoxic T-lymphocyte-associated protein 4 (CTLA-4) and programmed cell death protein 1/programmed death-ligand 1 (PD-1/PDL-1), that target receptors present in immune cells and cancer cells, respectively. This enhances the immune system's ability to fight cancer by blocking signals that typically suppress immune cells activity [78].

1.2.3.2. New treatments approaches

While these advancements hold great promise, the challenges persist, particularly in enhancing the survival rates of patients at advanced stages of CRC [69]. The complex nature of the disease, coupled with factors such as treatment resistance and metastasis, explains the ongoing efforts in research to refine existing therapies and pioneer new strategies to enhance

drug delivery, reduce cytotoxicity, and decrease the cost of the treatments [79]. Simultaneously, researchers are delving into the exploration of nanomaterials, with a focus on enhancing drug delivery mechanisms thereby optimizing the efficacy and precision of cancer treatments [80]. Furthermore, pharmaceutical industries are not only dedicated to enhance current treatments but are also actively investigating solutions in line with green chemistry principles. Hence, the quest for inherent anticancer properties in natural products and the pursuit of sustainable processes is pivotal in this endeavor [81]. This dual focus reflects a commitment to advancing therapeutic efficacy of cancer treatments.

1.3. Therapeutic Deep Eutectic Systems and their role in drug improvement

1.3.1. Deep Eutectic Systems

In the contemporary era, with a strong emphasis on global sustainability, there is a notable surge in the demand for eco-friendly alternatives in all industry fields, especially in pharmaceutical industry. Key strategies involve the substitution of hazardous solvents with environmentally friendly options, by exploring natural pharmaceuticals and enhancing existing drugs efficiency. Furthermore, optimizing drug efficiency plays a pivotal role in promoting a sustainable healthcare approach by minimizing excess production and waste [82]. The incorporation of green chemistry principles in pharmaceutic industry and health products it is imperative [83].

Deep Eutectic Systems (DES) have emerged as a revolutionary solution in this pursuit [84]. DES are formulations comprising two or more compounds selected based on their capacity to donate or accept hydrogen bonds. These hydrogen bond interactions are fundamental in determining the unique properties and behavior of DES. However, DES can also form through weaker interactions, such as Van der Waals forces. When combined in a specific ratio, a charged delocalization phenomenon occurs, leading to a depression in the melting point and a transition to a liquid state [85]. The behavior of DES can be understood by a two-phase diagram (Figure 6). Each compound has a specific temperature at which it changes from a solid to a liquid, known as its melting point. When compounds A and B are mixed in a specific ratio at a set temperature, they transit from a solid to a liquid state in what is called the eutectic point. This point reflects a unique combination of the correct ratio and temperature for this transition to occur optimally. At the eutectic point, a fraction of the mixture remains in the solid phase while the remainder shifts to a liquid state, establishing an equilibrium where both phases coexist. However, deviations from ideality can occur when compounds are combined at specific ratios and temperatures, resulting in a lower melting point than expected in an ideal scenario, a deeper eutectic point [86].

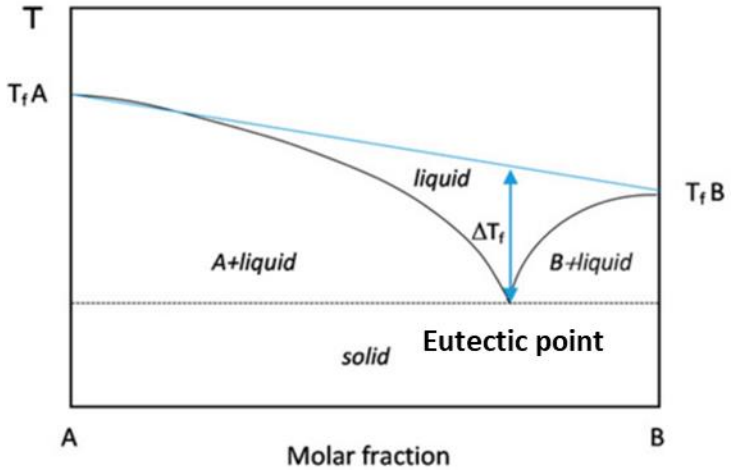

Figure 6: Phase diagram illustrating the solid-liquid behavior of a deep eutectic mixture [87].

DES have favorable physicochemical characteristics, such as low volatility and exceptional thermal stability. It stands out due to its straightforward manufacturing process, cost-effectiveness, and minimal environmental impact, making it a more practical and widely applicable option [88]. The resultant intermolecular interactions confer 100 % atom economy, with no waste and no by-product formation during preparation. Moreover, DES present highly favorable physicochemical properties: low melting points, minimal volatility, nonflammability, substantial solubilizing capacity, customizable polarity, and thermodynamic stability [89]. Furthermore, the easy preparation contributes to an exceptionally low E-factor. The E-factor measures the amount of waste produced per unit of product in a chemical process, with a lower value indicating higher efficiency and environmental friendliness. Furthermore, nearly all the DES compounds are non-toxic and biodegradable, what are align with green chemistry principles. Additionally, DES can be custom-designed, with components selected specifically to suit the intended application [90].

Their unique composition and versatility make DES essential in various domains, ranging from synthesis and processing of biopolymers [91], to solvent extraction [92], finding crucial applications in food and pharmaceutical industries [93], particularly within the realm of drug delivery science [94]. As examples, DES has been used as a green solvent in detecting and extracting neurotransmitters, that are the chemical messengers of the brain, leading to higher yields and purity compared to traditional solvents [95]. Some DES have also shown antimicrobial effects against several bacteria, fungi, and viruses [94]. For instance, a DES made of choline bicarbonate:geranic acid (1:2) has antimicrobial effects against *Mycobacterium tuberculosis*, *Staphylococcus aureus*, and *Candida albicans* [96].

The pharmaceutical industry faces challenges such as dissolving drugs with low solubility in water, creating effective drug delivery systems, and extracting natural products [97], [98], [99]. The reduction in the melting point of DES induces a state of liquidity at room temperature and, consequently, at the standard human body temperature of 37 °C. Drugs in liquid form are more efficiently absorbed, leading to heightened bioavailability, thereby enhancing the

therapeutic efficacy of pharmaceutical compounds. This characteristic, coupled with the potential versatility of DES applications, shows its significance as a promising candidate for advancing drug delivery strategies and formulations within the pharmaceutical industry. For instance, the use of graphene functionalized with the DES choline chloride:malonic acid has been explored a new approach to improve the effectiveness of the anti-cancer drug doxorubicin. The DES-functionalized graphene demonstrated high efficiency in loading the drug and showed promising results in fighting cancer cells [100].

1.3.1.1 Therapeutic Deep Eutectic System

DES could be classified based on their composition. Two of the most promising types are Natural Deep Eutectic Systems (NADES) and Therapeutic Deep Eutectic Systems (THEDES). NADES comprises at least two naturally occurring components. Alternatively, THEDES comprise two or more elements, prioritizing the integration of an active pharmaceutical ingredient (API), which may or may not be one of the compounds within the DES. In the first scenario, the API can serve as either a hydrogen bond acceptor (HBA) or an hydrogen bond donor (HBD) based on its properties. As an example, atropine acts as an HBA when intricately paired with capric acid, forming a specialized THEDES, while ibuprofen assumes the role of an HBD when combined with menthol [101]. The three-dimensional chemical and steric properties of the natural molecules, confer them distinct mechanisms of action contributing to enhance efficiency and selectivity towards specific molecular targets [102]. In the second scenario, the API is dissolved within the THEDES, without directly contributing to the formation of the eutectic system itself. Instead, the API is incorporated into the THEDES matrix, allowing it to be integrated without being a structural component of the system. In both cases the API integration in THEDES changes the API physicochemical characteristics, such as its solubility. This emphasizes the potential role of THEDES to improve the effectiveness of pharmaceutical formulations [103].

In the realm of pharmaceutical industries, a significant area of interest lies in drug repurposing. Designing new medicines from the beginning is not only costly but also takes many years to go through all the necessary stages. Drugs repurposing involves the exploration of existing drugs for alternative indications or the adaptation of their characteristics, encompassing potential modifications in formulation, delivery methods, dosage, or other attributes [104]. The utilization of THEDES may lead to improvements in the fundamental attributes of APIs. These improvements include increased permeability, better absorption, and increased solubility, all of which are important factors that improve the drug's bioavailability and, in turn, its therapeutic effectiveness and patient outcomes [105]. For instance, one of the problems is the use of poor water-soluble drugs that demonstrate poor bioavailability, which could be enhanced through their incorporation in THEDES [106].

Several APIs with anti-inflammatory activity are being integrated into THEDES formulations. An example is NSAIDs, including COX-2 inhibitors like ibuprofen, which effectively mitigate inflammation. As previously noted, inflammation plays an important role in cancer. Given

ibuprofen's limited solubility in water, its inclusion in THEDES could enhance its properties and, consequently, improve bioavailability. This ability of a eutectic to dissolve poorly water-soluble substances is knowing as hydrotropy [107]. Furthermore, the noteworthy chemical diversity and distinct mechanisms of action exhibited by natural molecules highlight their potential synergy with APIs in THEDES, promising advancements in therapeutic outcomes and the refinement of existing treatments [108].

Certain THEDES have shown significant antiproliferative effects on CRC cells. Notable examples include formulations containing limonene, menthol, and ibuprofen, which effectively inhibit cell growth, highlighting the potential of THEDES in CRC treatment [109], [110].

Pereira J *et al.*, have investigated the anti-CRC activity of several hydrophobic THEDES composed of terpenes, natural compounds, such as safranal, menthol, and linalool, combined with NSAIDs as ketoprofen, flurbiprofen, and ibuprofen. Terpenes are produced by plants and are known to have several anti-inflammatories, anti-oxidant, and anticancer effects. Combinations such as safranal:ibuprofen (3:1), safranal:ibuprofen (4:1), and menthol:ibuprofen (3:1) have exhibited selective toxicity against HT29 CRC cell line, leading to reduced cell proliferation primarily through caspase 3-mediated apoptosis in the former two combinations. Conversely, menthol:ibuprofen (3:1) induced anti-inflammatory activity by decreasing ROS levels and antiproliferative activity by activating caspase 3 [110]. Moreover, incorporating ibuprofen into different THEDES formulations has shown improved properties of the API, such as better permeability and solubility [111]. Additionally, a study reported by Pereira C *et al.*, highlighted the anti-inflammatory and antiproliferative effects of LIM:IBU (4:1) on CRC cells, while simultaneously preserving the viability of normal cells. This combination effectively combated inflammation by inhibiting ROS and NO (nitric oxide), pivotal modulators of inflammation [108]. Another study demonstrates anticancer activity of a THEDES composed of a limonene metabolite, perillyl alchool (POH) and ibuprofen. POH:IBU (3:1) was capable of inhibit cell growth by affecting cell proliferation in CRC cells [109]. Both studies further clarified the variations in proliferation activity observed between utilizing a physical mixture of the two compounds and utilizing them in THEDES form [108], [109].

However, like most anticancer drugs, these THEDES are hydrophobic, presenting poor solubility in water [112]. Furthermore, to attain optimal therapeutic effects, these THEDES must reach CRC cells at an ideal concentration and rate, minimizing potential negative side effects. Designing an efficient targeted drug delivery system (DDS) capable of delivering THEDES specifically to CRC cells could enable the effective utilization of these compounds for colorectal cancer treatment.

1.4. Drug Delivery Systems

DDS refers to the method of administering pharmaceutical substances to achieve a therapeutic effect in humans or animals [113]. As the pharmacology field progresses, it becomes

clear that the release profile of a drug has a crucial influence on the bioavailability and consequently on therapeutic efficacy.

Conventional drug administration methods, like tablets and capsules, have poor bioavailability and are rapidly absorbed and metabolized, causing fluctuations in drug concentration in the bloodstream. Bioavailability is the percentage of an API that enters the bloodstream and is accessible to act at the target site. Influenced by factors such as the route of administration, absorption, distribution, metabolism, and rate of excretion, bioavailability is an important factor in determining the effectiveness of a drug [114]. For instance, comparing oral administration with intravenous administration, the first one encounters the challenge of passing through the liver's first metabolism and facing potential degradation in the acidic stomach environment, leading to a decrease in bioavailability. Conversely, intravenous administration allows the drug to directly enter the bloodstream, bypassing the initial metabolism in the liver. Additionally, poor water-soluble drugs pose absorption difficulties, resulting in a reduced percentage reaching the bloodstream and reaching the target site [115]. In cancer, many antitumor drugs are excreted by the liver due to their small size (6 nm), which results in a lower drug circulation time. Furthermore, once these conventional DDS are non-selective, just a few percent of the administrated drug reach the target site. This compromises the effectiveness of the treatment, potentially leading to inadequate drug levels and systemic side effects. The initial approaches to address these fluctuations involve either increasing the dosage or implementing a regimen of multiple administrations. However, the single dose often gives rise to more severe side effects and the multiple doses result in drug levels that prove to be either toxic or ineffective, decreasing patient compliance [116].

To overcome these challenges and maximize bioavailability, drugs must achieve precise delivery to their target in terms of concentration, timing, and rate. This is when the emerging new era of DDS assumes a critical role [117].

1.4.1. DDS and Nanotechnology

The integration of nanotechnology into healthcare, known as nanomedicine, has propelled the creation of innovative DDSs. This encompasses intelligent systems, including NPs, that can be activated by stimuli like temperature, pH and/or radiation, facilitating the targeted release of drugs in response to specific environmental cues. Furthermore, NPs serve dual roles, functioning as both intelligent systems for drug release and as components of target delivery systems, enhancing precision in drug transportation (Figure 7) [118], [119], [120]. The primary goal of a DDS is to transport and deliver therapeutic compounds in a controlled and secure manner, ultimately enhancing drug's bioavailability. While controlled-release systems focus on regulating the gradual release of drugs over time, the integration of targeted delivery, whether through active or passive mechanisms, takes this a step further [121]. Passive DDSs, used for instance as chemotherapy agents, are systems that exploit the tumor's enhanced permeability and retention effect (EPR). This effect arises due to the abnormal structure of tumor vasculature

which exhibit both excessive growth and poorly developed structures with large spaces between the endothelial cells. These structural irregularities allow drugs to pass more easily from the bloodstream into the tumor tissue, where they accumulate due to the impaired lymphatic drainage commonly found in tumors [122]. Alternatively, active DDS involve the incorporation of specific targeting ligands, such as antibodies, peptides, or other molecules, onto the surface of the drug carriers that will interact with receptors that are overexpressed on the target cells, leading to enhanced binding and uptake of the drug delivery system (Figure 7) [123]. As Ehrlich mentioned, target delivery is a "magic bullet" hitting target cells [123], [124]. These advanced methods offer precise control over drug release kinetics, extending efficacy and minimizing adverse effects, while targeted delivery enhances therapy, selectively reaching specific sites of interest and providing control over pharmacodynamics, toxicity, immunogenicity, and overall drug efficacy [123].

NPs are characterized by their nanometer scale from 10-100 nm, once NPs smaller than 10 nm are filtered by the kidneys, and larger NPs are rationed by the liver. NPs in the range of 100 nm typically evade clearance by the liver, whereas those around 200 nm may start encountering the liver's reticuloendothelial system (RES) for potential clearance. At approximately 300 nm, NPs are significantly more likely to being cleared by the liver and spleen through the RES, resulting in reduced circulation time in the bloodstream. However, modifying the surface properties of these NPs, such as by coating them with polymers or PEGylation, provides a promising approach to evade RES recognition and uptake. This strategy could prolong their circulation in the bloodstream and enhance their effectiveness in therapy [125]. Polymer NPs, inorganic NPs, liposomes, micelles, and virus-like particles are being used in biomedical field to improve not just the monitoring and diagnosis but passive and active target delivery of drugs for the treatment of several diseases, including cancer [119], [123], [126]. Although NPs are conventionally defined as being between 1 and 100 nm, particles up to 500 nm are also used in drug delivery. Despite not fitting the strict size range, these larger NPs can still exhibit valuable nanoscale properties such as enhanced cellular uptake, targeted delivery, and controlled release.

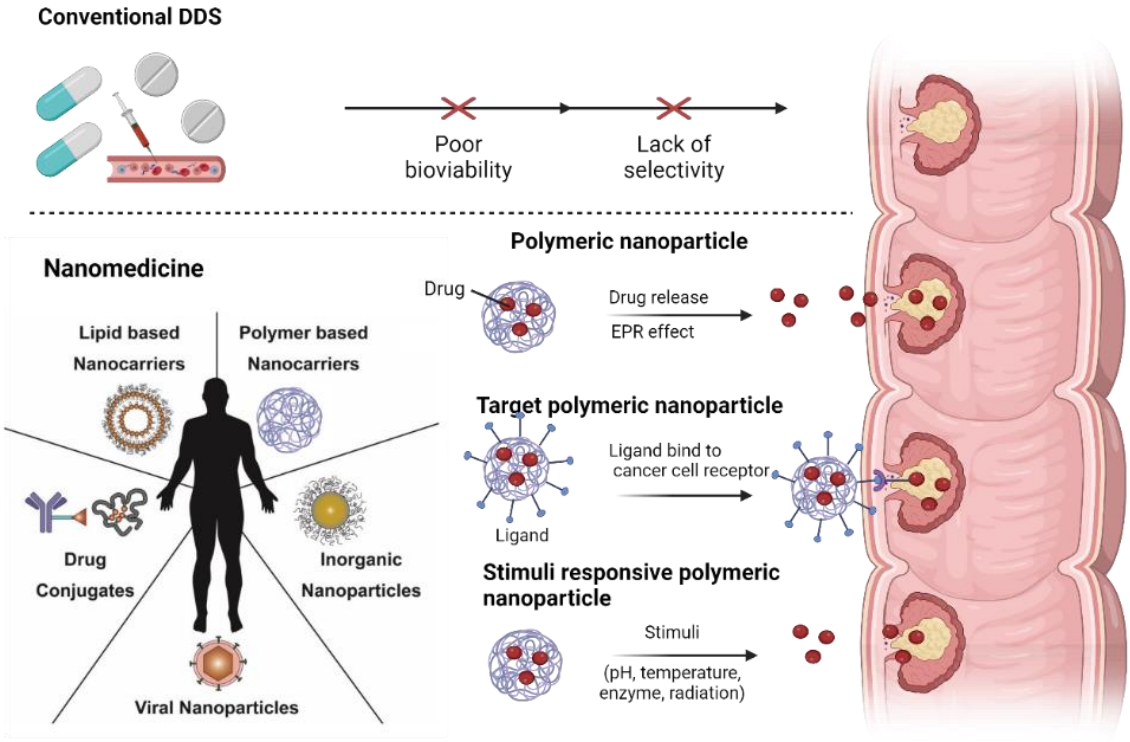

Figure 7: The different mechanism of action of conventional DDS and NPs. Created with BioRender.com.

For NP to be an ideal vehicle for drug delivery, they must possess specific characteristics. These include the ability to bypass the immune system, protect the drug from premature degradation, and release it at the intended target site at the ideal rate and concentration. Their small size, surface area, and tunable properties allow them to deliver drugs directly to the target site. The high surface area-to-volume ratio of NPs allow efficient interactions with biological entities, while their small size facilitates enhanced permeability and retention in tissues. Additionally, they could be modified at the surface, enabling the control of interactions with biological systems, including the attachment of targeting ligands for specific cell or tissue. Another factor that makes NPs so attractive for drug delivery is the ability to encapsulate or adsorb a diverse range of therapeutic agents, simultaneously providing protection from degradation. This is particularly beneficial for poorly soluble hydrophobic drugs, since NPs increase local drug concentration at the target site, enhancing intracellular penetration and improving treatment outcomes in various diseases [119], [127].

1.4.2. NPs for CRC Treatment

In biomedical applications, NPs are promising DDS that can ensure targeted and controlled release of therapeutic agents while enhancing imaging, diagnosis, and theragnostic of diverse diseases, including cancer [118]. DDS with different compositions, sizes, and properties allow the delivery of anticancer agents, decreasing drug toxicity and effectiveness [126].

A diversity of passive and target DDS based on NPs are being studied for CRC to improve the drug's bioavailability and, in consequence, treatment effectiveness [128]. The first DDSs for

CRC started to emerge in the early 1950s and have since then increased in number and diversity with the significant advancement of nanotechnology [129]. Nanocarriers based on different materials, like lipids, polymers, and inorganic substances, has been reported (Figure 8) [130], [131]. NP's versatility arises from the ability to select specific materials and formulation methods, considering the type of drug, release profile, biocompatibility, level of biodegradability, and the need for functionalization, that allow the creation of specific NPs with the desired size [121].

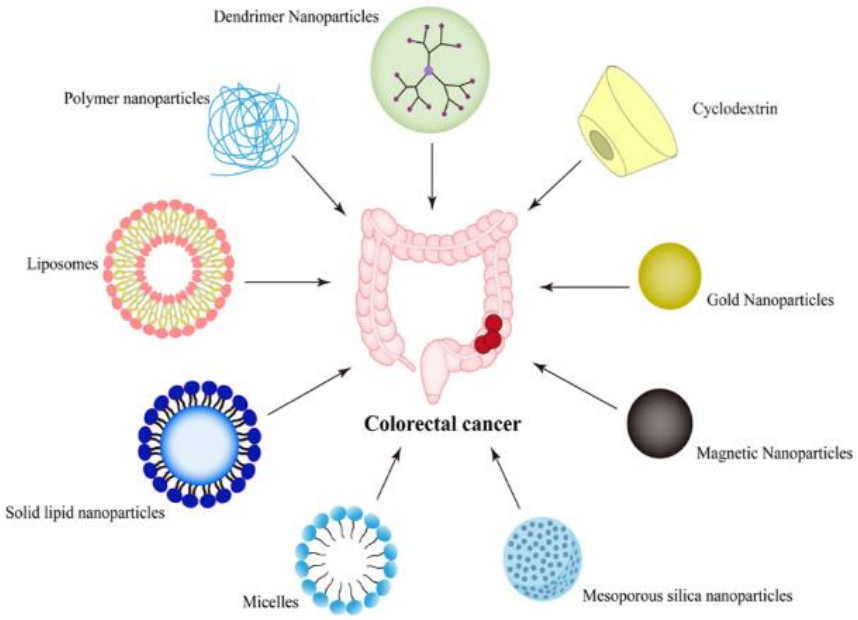

Figure 8: Different DDS for CRC treatment. Adapted from [132] and modified with BioRender.com.

Lipid-based NPs, including liposomes and micelles, are capable of encapsulating both hydrophobic and hydrophilic drugs within a lipidic environment, ensuring biocompatibility [133]. They can be tailored for targeted delivery through surface modifications, which enhances their therapeutic effectiveness and minimizes side effects. However, they can face stability issues such as leakage and fusion, and maintaining consistent release profiles can be challenging. Onivyde® a lipid formulation containing irinotecan was approved for CRC. This DDS show selective accumulation in the tumor site, an increase in drug blood circulation time, and a decrease in toxicity [134]. Additionally, inorganic NPs, like silica, gold, magnetic or quantum dots, introduce diversity and show promise for controlled drug release. Inorganic NPs, offer potential for controlled drug release via external stimuli and can serve multifunctional roles in drug delivery and diagnostics. Despite their high stability, concerns over biocompatibility and non-biodegradability pose significant limitations, as they may accumulate in tissues and cause long-term toxicity [135]. In contrast, polymeric NPs, like Poly (lactic-co-glycolic acid)

(PLGA) NPs, also provide controlled and sustained release for both hydrophobic and hydrophilic drugs, but are biocompatible and biodegradable [136]. Together, these NPs types showcase a multifaceted approach to advanced DDSs.

Examples of passive-targeting NPs designed for treating CRC consist of oxaliplatin and resveratrol enclosed within N, O-carboxymethyl chitosan NPs. These particles exhibit improved solubility, stability, and efficacy against CRC in mice with subcutaneous tumors, surpassing the performance of the free drug [137]. Lipid NPs act as efficient carriers for a variety of chemotherapeutic drugs, such as irinotecan and oxaliplatin, enhancing their stability *in vivo*, reducing systemic toxicity, and overcoming drug resistance in CRC treatment [138].

However, studies suggest that there is a low level of vascularization in CRC making passive delivery difficult [139]. To bypass this disadvantage, active delivery is being studied to target receptors overexpressed in CRC cells [140]. Receptors as CD44 receptor, folate receptor, and EGFR are usually overexpressed in CRC cells. For instance, the antibody Bortezomib encapsulated within self-assembled NPs composed of chitosan and chondroitin sulfate materials effectively targets folate receptors, resulting in notable suppression of colorectal tumor growth [141]. Additionally, polymer NPs loaded with the antibody anti-EGFR-mAb and the drug 5-Fluorouracil demonstrate enhanced drug delivery to CRC cells, showcasing the diverse strategies employed to optimize therapeutic outcomes in CRC treatment [142].

Polymeric NPs offer targeted delivery of anti-cancer drugs to CRC cells, minimizing off-target effects and enhancing therapeutic efficacy, making them a promising approach for CRC treatment. Furthermore, they stand out for their scalability, chemical and physical stability in biological environment, ease of modification, ability to be freeze-dried for storage, and their production aligns seamlessly with Good Manufacturing Practices, offering an advantage over other systems [143].

1.4.2.1. PLGA NPs

PLGA is one of the polymers often used to synthetize NPs as DDSs conferring to these systems the advantages described on Chapter 1.4.2. Ongoing research are trying to optimize polymer NPs design for clinical translation in CRC therapy [144]. PLGA is composed by lactic acid and glycolic acid units linked by ester bonds and is biodegradable, biocompatible and present lower toxicity (Figure 9). In addition, PLGA NPs are approved by FDA and EMA for use as drug delivery systems in humans, being safe and efficient. PLGA NPs can be prepared from different ratios of monomers, however, that will affect the time of degradation, changing from several months to several years [145], [146]. For instance, PLGA with a higher content of lactic acid has been reported to degrade more slowly, while the copolymer 50:50 exhibits faster degradation [147]. PLGA NPs have been used in tumor-targeted drug delivery, hyperthermia, photodynamic therapy, and ultrasound with contrast agents [145]. They have also been used to encapsulate various anticancer drugs, including paclitaxel, doxorubicin, curcumin, and cisplatin, among others. In the case of delivery cancer drugs, PLGA NPs accumulate in the tumor

by take advantage of EPR effect [148]. Upon reaching the target site, PLGA NPs suffer endocytosis and are internalize by cancer cells. Within the acidic environment of the tumor microenvironment, the PLGA NPs undergo hydrolysis. Alternatively, enzymes such as esterases and proteases present in the tumor microenvironment can also trigger the degradation of PLGA. These enzymes break the bonds between the lactic acid and glycolic acid monomers, leading to the degradation of the polymer chain resulting in drug release [149], [150].

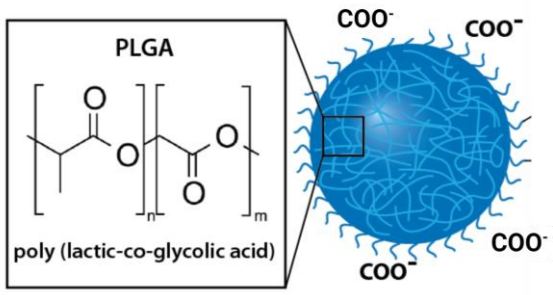

Figure 9: Schematic representation of a PLGA NPs. Adapted from [150] and modified with BioRender.com.

The encapsulation of cancer drugs in PLGA NPs has shown to decrease side effects and cytotoxicity, and increase the bioavailability, efficacy, and solubility of the drugs. Several studies demonstrated the enhanced bioavailability achieved through PLGA encapsulation and a prolonged circulation time associated with less side effects [151], [152]. One crucial aspect that makes PLGA NPs so tempting is the possibility to alter physical features like size and drug-loaded efficiency, through the manipulation of synthesis methods parameters. There are several methods to form PLGA NPs well established in the literature [153].

1.4.2.2. Virus-like particles as Drug Delivery Systems

Virus-like particles (VLPs) are self-assembling NPs that closely mimic the structural features of their parental viruses, typically ranging in size from 20 to 200 nm. Due to the absence of genetic material, VLPs are incapable of replication, contrarily to viruses, making them safer to use. While VLPs are well-established for their immunogenicity, primarily in the context of vaccination, emerging reports highlight their potential application as efficient DDSs, offering advantages over other delivery platforms. The DDSs approved for the delivery of anti-cancer drugs are mostly passive delivery [154], [155]. Active counterparts face greater challenges in progressing to clinical trials. Biological barriers hinder drug penetration to the tumor, while regulatory impediments and complex manufacturing processes present additional obstacles to the clinical translation of actively targeted DDSs [156], [157]. VLPs could potentially serve as vehicles that bypass biological barriers more easily.

The inherent advantages of VLPs in drug delivery include self-assembly, easy manufacture, robust stability, modifiability, biocompatibility, immunogenicity, good size distribution, and the ability to traverse cellular membranes for targeted cargo delivery. To harness these favorable characteristics effectively, it is imperative to address challenges such as potential

clearance through phagocytosis and the elicitation of strong immune reactions [155]. To ensure that VLPs can efficiently reach target cells and deliver cargo, the modification of their surfaces with diverse functional ligands is crucial to circumvent the challenges associated with phagocytosis clearance and immune response triggers. Additionally, due to the inherent structural characteristics of VLPs, it is possible to modify them for the loading of proteins, peptides, nucleic acids, imaging agents, drugs, quantum dots, or various other forms of NPs [158].

VLPs drug delivery relies primarily on endocytosis by targeted cells. Once the engineered VLPs bind to specific receptors on the cell surface, they are internalized via endocytic pathways. Within the endosomes, VLPs may undergo pH-dependent conformational changes, leading to their escape from the endosomal compartment into the cytoplasm. This process allows the release of encapsulated drugs or therapeutic cargo into the cellular interior, where they can exert their intended effects. By exploiting endocytosis, VLPs enable targeted delivery of drugs to specific cell types, enhancing therapeutic efficacy while minimizing off-target effects [158], [159].

VLPs could be enveloped or non-enveloped and have a single or multiple protein layers. One crucial aspect of producing VLPs is the choice of the correct expression system. Various systems, including prokaryotic (bacterial), eukaryotic (yeast, mammalian, insect and plant cells), and cell-free, are used. Choosing a system capable of expressing the necessary genes, with adequate post-translational modifications (PTMs) and guaranteeing the appropriate protein folding is essential to produce effective VLPs. For instance, prokaryotic systems, exemplified by *Escherichia coli*, prove to be efficient to produce recombinant proteins and assembling VLPs but they exhibit limitations in PTMs. Contrarily mammalian expression systems, are proficient in PTMs, but encounter hurdles related to production yields, time, cost, and scalability. After expression, VLPs undergo purification steps involving cell lysis, clarification, concentration in order to enhance VLPs properties [158].

1.4.3. Methods for Polymer NPs Formulation

Several methods could be used for PLGA NPs production. All methods have advantages and disadvantages. Emulsion-solvent evaporation, nanoprecipitation, salting out and microfluidic are between the methods most used to prepare PLGA NPs. The choice of the corrected method will depend on the hydrophobic or hydrophilic nature of the encapsulated drug and on the desire features of the final NPs. Different methods originate NPs with different size, morphology and charge (Table 1).

Table 1: Different PLGA NPs synthesis methods with different solvents and surfactants. Diameter range, advantages and disadvantages associated with each method. Adapted from [160].

Method	Diameter range	Solvent	Surfactant	Disadvantages	Advantages
Double emulsion solvent-evaporation	0.1-10 µm	DCM Chloroform Ethyl acetate	PVA Pluronic F68 Sodium cholate	Shear stress Size affected by cargo	Suitable for hydrophilic compounds Non-toxic solvents
Single-emulsion solvent-evaporation	≈50-700 nm	DCM Chloroform Ethyl acetate	PVA Tween-80 Pluronic F68	Size affected by cargo Size affected by polymer	Suitable for lipophilic compounds Solvent evaporation
Nanoprecipitation	80-700 nm	Acetonitrile Acetone Ethanol	PVA Poloxamer Poloxamines	Size affected by polymer concentration	Low energy consumption No high share forces
Emulsification/salting-out	100-500 nm	Acetone THF DMSO	PVA Poly (vinyl Pyrrolidone)	Poor encapsulation efficiency Low yield High polydispersity	Minimizes stress to protein cargo Good for heat sensitive substances
Microfluidics	200-1000 nm	DCM DMSO	PVA Tween-20/80	Slow diffusive mixing	Monodisperse droplets

The single emulsion-solvent evaporation method and nanoprecipitation method are two of the most employed techniques for encapsulating hydrophobic drugs making them promising methods for attempting to encapsulate THEDES [160], [161].

1.4.3.1. Emulsion method

The emulsion-evaporation method is a fundamental technique to formulate PLGA NPs. The single emulsion is employed when encapsulating hydrophobic drugs, while the double emulsion is utilized for hydrophilic drugs. In the first case, PLGA is dissolved in an organic solvent and emulsified with an aqueous phase containing a surfactant. The surfactant stabilizes the resulting water-in-oil emulsion, preventing coalescence of droplets. Stirring or sonication homogenizes the emulsion, and subsequent stirring allows the organic solvent to evaporate. The evaporation process leads to the formation of PLGA NPs within the aqueous phase. After complete evaporation, PLGA NPs are collected through methods like centrifugation, with additional washes to remove residual surfactant or solvent (Figure 10) [160].

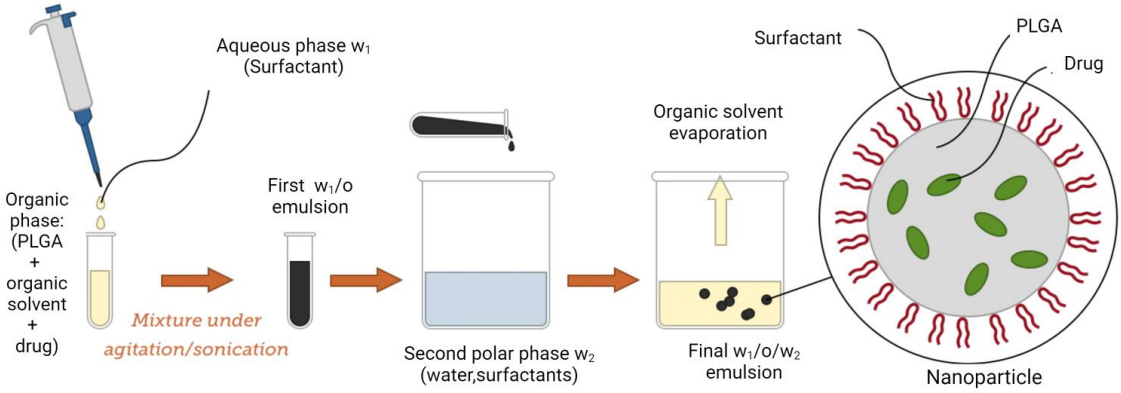

Figure 10: Doble Emulsion-Evaporation method for the formation of polymeric NPs. Adapted from [162] and modified with BioRender.com

Factors such as the choice of surfactant, polymer concentration, and evaporation rate influence the size, morphology and others characteristics of the NPs. The surfactant selection not only stabilizes the emulsion but also impacts NPs surface properties. Varying surfactants can result in different sizes and charges, affecting interactions with biological systems. Polysorbate 80, vitamin E-TPGS, and polyvinyl alcohol (PVA) are surfactants commonly used [163]. The concentration of PLGA in the organic phase influences NPs size, with higher concentrations leading to larger particles, influences drug-loading and drug release kinetics. Additionally, the evaporation rate during particle formation is critical; rapid evaporation yields smaller and more homogeneous particles, while slower evaporation may result in larger and polydisperse NPs. Careful manipulation of these parameters allows for tailored adjustments in PLGA NPs characteristics, ensuring precise control over NPs properties, making it a versatile and reproducible approach for specific biomedical applications, particularly in drug delivery systems. [164]. However, it requires optimization and customization for each drug, as different drugs may influence the NPs formation process differently.

1.4.3.2. Nanoprecipitation method

Nanoprecipitation is an attractive method, due to be simple, conducted in a single step, exhibits good reproducibility, and does not demand high energy input, resulting in small NPs. In this method the polymer is dissolve in an organic phase and dropwise in aqueous phase under stirring. A separation phase will occur and the organic solvent will evaporate allowing the formation of the NPs (Figure 11) [165], [166].

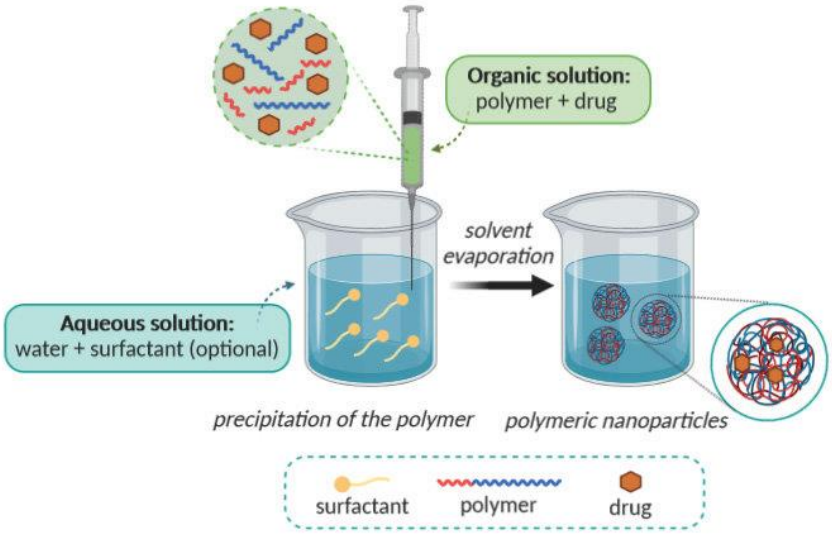

Figure 11: Nanoprecipitation method for polymeric NPs synthesis [166].

Acetone and acetonitrile are frequently employed as solvents in the organic phase due to their immiscibility with water. The inclusion of surfactants is not mandatory for NPs formulation, yet they can serve to stabilize the NPs, enhance their dispersion, or regulate their size and shape. However, there are some protocols in literature that have reported stable NPs formed by nanoprecipitation without using a surfactant [167], [168] . The polymer and surfactant concentration, the speed of rotation and evaporation could impact the size of the NPs. Typically, a decrease on the concentration of both polymer and surfactant leads to small NPs [169].

1.4.4. VLPs Loading methods

Loading substances into VLPs necessitates a comprehensive understanding of their structure and composition. Different strategies to load cargo into VLPs could be applied (Figure 12).

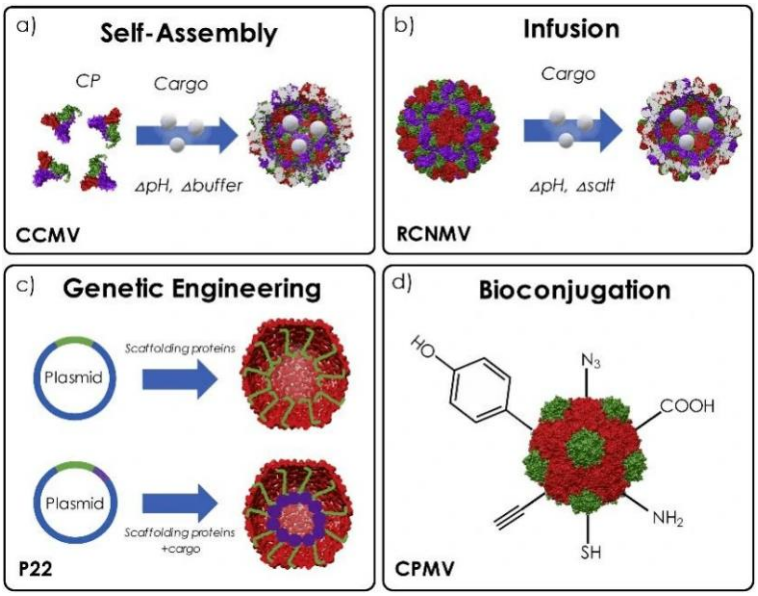

Figure 12: Different strategies for loading cargo into VLPs: a) Self-assembly-disassembly of the capsid induce by variation on pH or buffer. b) Infusion c) Genetic engineering d) Bioconjugation. Adapted from [170].

The self-assembly strategy consists of inducing changes in pH ionic strength and buffer conditions, affecting the interaction of the capsid proteins, which are responsible for maintaining the VLP structure. This results in capsid disassembling. Next, using buffer exchange methods, it is possible to assemble the VLP and loaded the desired cargo. The infusion technique takes advantage of the fact that VLPs have small spaces and could work as channels for small molecules to be incorporated inside them. This technique is based on the fact that these spaces could increase in size with changes in the pH or ionic strength through the application of chelators to remove ions. In cases where the cargo consists of proteins or peptides, an alternative approach involves genetic engineering. This involves inserting the genetic code of the cargo into the vector alongside the genetic code of the capsid. Moreover, conjugating the cargo outside of the VLP using functionalized groups of amino acid chains could be a good approach for small molecules [171].

The strategy used to load the cargo will depend on the type of cargo and the VLP structure [170]. For instance, a study developed DOX-FA-VLPs, conjugating doxorubicin to the external surface of Hepatitis B VLPs functionalized with folic acid for active delivery. This innovative DDS exhibited increased cellular uptake in breast and CRC cells, showcasing its potential for targeted and effective cancer treatments [172]. Additionally, Physalis mottle virus (PhMV) VLPs have been used as carriers to deliver DOX and cisplatin, showing an increase in therapeutic efficiency. In this case, DOX loading in the interior of PhMV VLPs was made by covalent and non-covalent reactions, and cisplatin was conjugated to the cysteines present in the interior of the VLP [173], [174].

DDs such as NPs and VPLs, have emerged as promising strategies to enhance drug bioavailability and minimize side effects. However, to achieve successful therapeutic outcomes, these DDS must possess optimal characteristics, including precise size, charge, morphology,

and surface chemistry, which can be tuned by selecting appropriate methods and varying formulation parameters. These factors are crucial for ensuring that the delivery system effectively targets the desired site and maximizes the therapeutic efficacy of the drug.

2. AIM

The primary objective of this thesis was to directly load THEDES, which have already demonstrated antiproliferative and anti-inflammatory actions against CRC, into VLPs. However, this approach faced a significant challenge due to the hydrophobic nature of THEDES, which was incompatible with the hydrophilic interior of the VLPs, thereby complicating direct encapsulation. To overcome this obstacle, we shifted our strategy to first encapsulate THEDES within polymeric NPs composed of PLGA.

For the formulation of stable, small, and monodisperse NPs, various parameters were optimized, including concentrations of PLGA and surfactants, organic solvent used, surfactant type, and organic/aqueous phase ratios. The DDSs obtained were characterized using different techniques such as Scanning Electron Microscopy (SEM), Transmission Electron Microscopy (TEM), Dynamic Light Scattering (DLS) and Attenuated Total Reflectance-Fourier Transform Infrared Spectroscopy (ATR-FTIR).

To quantify the encapsulation efficiency of THEDES within the PLGA NPs, both direct and indirect quantification methods were employed using High-Performance Liquid Chromatography (HPLC).

To assess the cytotoxicity and therapeutic action of both empty and THEDES-loaded NPs on normal colorectal cells and CRC cells, cytotoxicity and antiproliferative assays were performed, using Caco-2 and HT29 cell lines, respectively. Direct and indirect contact between NPs and cells was tested. Direct contact was established through the direct addition of NPs, while indirect contact was mediated by employing NPs leachables. Additionally, NPs encapsulating hydrophobic and hydrophilic fluorescent probes were synthesized and exposed to cells to assess their cellular internalization.

Part of the work herein described has been internationally presented at the 3rd Annual Nanoseries Conference at Instituto Superior Técnico, Lisboa and was awarded a best poster presentation.

3. Materials and Methods

3.1. Preparation of THEDES

Menthol (Me; Sigma, Cat. No. W266507-1000) and ibuprofen (IBU; Alfa Aesar, Cat. No. B20989) were combined in a 3:1 molar ratio to form a therapeutic deep eutectic system. The mixture was heated to 50 °C and stirred continuously until a homogeneous phase was achieved (5-10 minutes). After THEDES formation, the eutectic mixture was allowed to cool down at room temperature.

3.2. PLGA NPs synthesis

Two methods were tested for the preparation of NPs, the single emulsion solvent-evaporation method and the nanoprecipitation method.

3.2.1. Single emulsion solvent-evaporation method

Me:IBU (3:1)-loaded PLGA NPs were prepared adapting the method reported by McCall R *et al.*, (Figure 13) [175]. Briefly, various concentrations (25, 50, and 100 mg/L) of PLGA (50:50, 40000 – 75000 g/mol, Sigma, Cat. No. P2066-0001S) and 14.5 mg of THEDES were dissolved in 2 mL of dichloromethane (DCM) (Honeywell, Cat. No 32222-1000), and allowed to dissolve completely overnight. The emulsion was formed under vortex mixing by adding the PLGA + THEDES solution into 10 mL of distilled water containing PVA (wt 30.000 - 70.000 g/mol, Sigma, Cat. No. P8136-0250) at concentrations of 3 % and 5 %. The sample was then sonicated three times using Sonics Vibracell VCX 750 with 1/4 probe (40 % amplitude, 10 seconds on, 10 seconds off, operating at 750 W, for 30 seconds). Then, the emulsion was added to 37 mL of distilled water containing 0.5 % or 0.3 % PVA, and DCM was evaporated for 3 hours. After solvent evaporation, the NPs were collected by ultracentrifugation at 30,000 rpm for 20 minutes and washed 2-4 times to remove residual surfactant. Empty NPs were prepared using the same protocol without the addition of THEDES. The resulting NPs were lyophilized with trehalose (using half of the PLGA mass of trehalose) and stored at -20 °C.

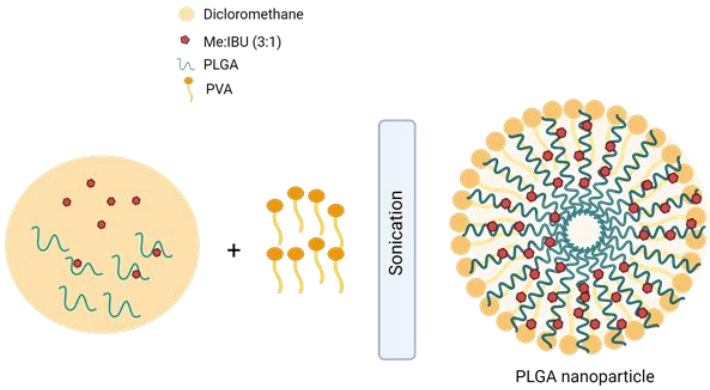

Figure 13: Schematic representation of the behavior of all the molecules involved in PLGA NPs formulation via single emulsion-solvent evaporation. Created with BioRender.com.

3.2.2 Nanoprecipitation method

In this case, THEDES-loaded PLGA NPs were prepared using a modified method inspired by Hernández-Giottonini *et al.*, (Figure 14) [176]. Initially, PLGA at concentrations ranging from 12.5 to 50 mg/mL were dissolved in 4 mL of acetone (AC) and left overnight for complete dissolution, and the amount of THEDES corresponding to 2 times the EC_{50} (14.5 mg) was added to the completely solubilized PLGA solution. Afterwards, the amount of THEDES was increased to 100 µL. The polymer solution was then added slowly drop by drop to 12 mL of distilled water or PBS (phosphate buffered saline) under stirring at 400 rpm, and AC was left to evaporate for 3 hours. Subsequently, the NPs solution underwent dialysis against 50 mL of distilled water for 3 days, with a medium change after the initial 24 hours. The dialysis supernatant was saved for further HPLC analysis. Finally, some NPs were lyophilized and stored at 4 °C, while others were not lyophilized for optimization purposes. Empty NPs were synthesized using the same protocol, but THEDES was excluded from the formulation. Furthermore, NPs loaded with hydrophobic fluorescent probes or hydrophilic fluorescent probes were synthesized using the method described above. The hydrophobic probes were incorporated into the organic phase, while the hydrophilic probes were introduced into the aqueous phase.

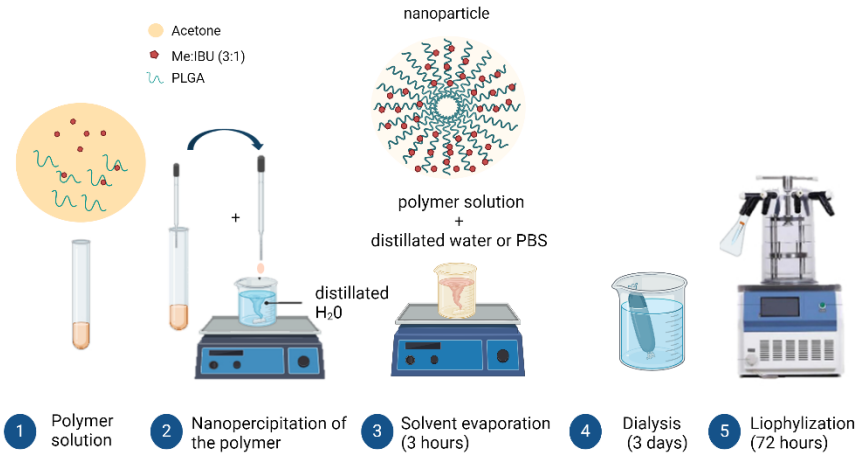

Figure 14: Schematic representation of the behavior and methodology of PLGA NPs prepared using the nanoprecipitation technique. Created with Biorender.com.

3.3. PLGA NPs characterization

In order to characterize and evaluate the produced NPs, different characterization techniques were used, such as SEM, TEM, FTIR and DLS.

3.3.1. Scanning Electron Microscopy

Free and loaded Me:IBU (3:1) PLGA NPs were characterized by SEM using a Regulus 8220 (Tokyo, Japan), operating at 5 and 15 kV. Dry PLGA NPs were carefully positioned on conductive carbon tape applied to a SEM sample holder. To enhance conductivity and minimize charging effects during imaging, a sputtered thin gold layer was added to the NPs. Various magnifications were used to capture images that provided insights into the morphology, size distribution, and surface characteristics of the PLGA NPs.

3.3.2. Transmission Electron Microscopy

The samples were analyzed by TEM using a Hitachi 8100 microscope (Tokyo, Japan) and were directly applied to the TEM grid for imaging. Samples that were not lyophilized were air-dried prior to application. TEM provides high-resolution images to analyze the structure and size of NPs, while SEM offers detailed surface morphology and also size information, making them complementary techniques for comprehensive NPs characterization.

3.3.3. Dynamic Light Scattering

DLS was employed to measure the hydrodynamic diameter, size distribution, and charge of NPs in suspension using a Malvern Nano ZS Zetasizer (Worcestershire, United Kingdom) with a 633 nm laser diode from PROTEOMASS Scientific Society (Caparica, Portugal) facility. The NPs solution was directly placed into the cuvette, and measurements were conducted by analyzing fluctuations in scattered light induced by Brownian motion. This motion arises from

collisions with rapidly moving fluid molecules. Each measurement were performed in triplicate to ensure reproducibility.

3.4. Fourier Transform Infrared Spectroscopy

ATR-FTIR was used to analyze the presence of chemical interactions on loaded NPs between PLGA and THEDES components (Me:IBU (3:1)), as well as to assess the interaction between PVA and PLGA in the empty NPs. Infrared spectra were obtained using a Spectrum Two spectrometer for Perkin Elmer (Madrid, Spain) in Attenuated Total Reflectance mode, scanning samples from 4000 to 450 cm^{-1} with a resolution of 16 cm^{-1} under ambient conditions.

3.5. Osmolarity

The osmolarity of the various NPs samples was measured to assess their compatibility for cell culture experiments. Osmolarity was determined using a KNAUER E0006XC osmometer (Berlin, Germany), which was calibrated according to the manufacturer's instructions before each measurement. Each sample, along with its corresponding dispersion medium, was prepared in triplicate, and the osmolarity values were recorded in milliosmoles per liter (mOsm/L). All measurements were performed in triplicate and at room temperature to ensure consistency.

3.6. Determination of encapsulation efficiency

The encapsulation efficiency for loaded Me:IBU (3:1) PLGA NPs formulated by nanoprecipitation was determined by HPLC using both direct and indirect methods. The direct method involved calculating the ratio of the amount of encapsulated THEDES divided by the total amount of THEDES used for the NPs formulation, as presented on Eq. 2.

$$Encapulation\ efficiency\ (\%) = \frac{Encapsulated\ THEDES\ (mg)}{Total\ amount\ THEDES\ (mg)} \times 100$$

Eq. 1

For direct determination, the NPs were dissolved in acetone and subjected to an ultrasonic bath for 30 minutes to ensure complete degradation. The samples were then filtered using a non-sterile hydrophilic PTFE syringe filter with a 0.22 µm pore size and 13 mm diameter (Filter Lab, Barcelona, Spain) and analyzed by HPLC. HPLC analysis was performed according to Ascar L *et al.*, with some modifications [178]. A Thermo Scientific Finnigan Surveyor system (Thermo Scientific, Waltham, MA, USA) was used, featuring a quaternary pump, solvent degasser, autosampler, and column oven, paired with an Accela UV-Vis detector (Thermo Scientific, USA). Each sample injection volume was 10 µL, with a flow rate of 1 mL/min, into an Agilent Eclipse XDB-C18 column, which has a 5 µm particle size, 100 Å pore size, and dimensions of

250 mm × 4.6 mm. The column temperature was maintained at 30 °C. Chromatographic separation was achieved using a mobile phase of 50 mM KH_2PO_4 (pH 4.2) and acetonitrile in a 65:35 (v/v) ratio. IBU quantification in the samples was achieved by measuring absorbance at 220 nm and comparing the results with a calibration curve of Me:IBU (3:1) prepared in the mobile phase.

For indirect determination, the supernatant resulting from dialysis was analyzed by HPLC using the same method described above. The encapsulation efficiency was calculated by the ratio of the difference between the total amount of THEDES and the amount of THEDES present in the dialysis supernatant (free THEDES that was not encapsulated) divided by the total amount of THEDES, as shown on Eq. 3.

$$Encapsulation\ efficiency\ (\%) = \frac{Total\ amount\ THEDES\ (mg) - Free\ THEDES\ (mg)}{Total\ amount\ THEDES\ (mg)} \times 100$$

Eq. 2

3.7. Cell viability analysis

3.7.1. Cell line

The HT29 cell line, obtained from the Deutsche Sammlung von Mikroorganismen und Zellkulturen (DSMZ), Germany, was originated from a primary tumor of colorectal adenocarcinoma removed from a 44-year-old Caucasian female patient (Figure 15 A). These adherent epithelial cells are an invaluable model for studying CRC, replicating key features of the disease such as high proliferative capacity and genetic mutations commonly found in CRC.

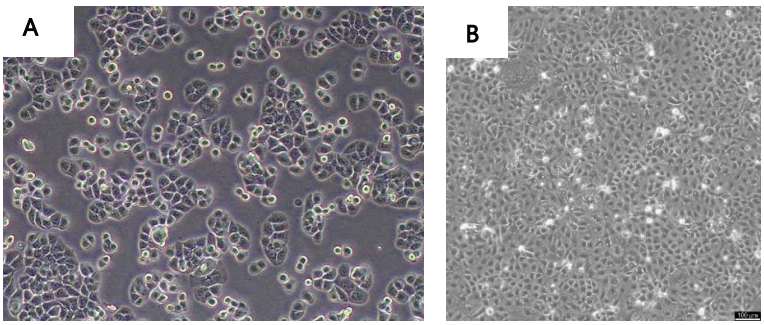

Figure 15: Microscope images of the cellular lines A) HT29 and B) Caco-2.

The Caco-2 cell line was also obtained from DSMZ, Germany. Caco-2 cells originate from the colon tissue of a 72-year-old Caucasian male diagnosed with colorectal adenocarcinoma. This cell line has the capability to differentiate and establish a polarized monolayer, characterized by tight junctions and microvilli that closely replicate the intestinal epithelium (Figure 15 B). Utilized extensively in research, Caco-2 cells are indispensable for assessing how different compounds impact colorectal cells [177].

3.7.2. Cell culturing and sub-culturing

The HT29 cells were cultured using Gibco Roswell Park Memorial Institute (RPMI, Corning, USA) 1640 medium with phenol red, supplemented with 10 % (v/v) heat-inactivated fetal bovine serum (FBS, Corning, USA) and 1 % (v/v) penicillin-streptomycin (PS, Corning, USA).

Cell culture was maintained as a monolayer in 75 cm^2 culture flasks (Falcon, Corning, USA) until it reaches 80-90 % of confluence, in a humidified environment at 37 °C with 5 % CO_2. Then, cells were sub-cultured. For that, medium was removed, and the cells were washed with 5 ml of PBS to ensure the total removal of supplemented culture medium. After that, 3 mL of trypsin (Corning, USA) was added for approximately 10 minutes at 37 °C, in order to break cell-cell and cell-surface connections. Following this, the trypsin enzyme activity was neutralized by adding 7 mL of supplemented culture medium. Subsequently, cells were transferred to new culture flasks at an appropriate dilution to continue growth.

Caco-2 cells were cultured in the same conditions of HT29 and using the same supplemented culture medium. Additionally, the subculturing process was also similar, with the exception that Caco-2 cells were detached using accutase (Millipore, Germany) instead of trypsin.

3.7.3. Antiproliferative assay

The impact of empty and Me:IBU (3:1)-loaded NPs on CRC cells viability was evaluated by Methyltetrazolium Salt (MTS) assay. For this purpose, HT29 cells were collected from culture flasks as described on Chapter 3.6.2, and from the 10 mL of cells suspension, 100 µL were used to count cells and determine cell concentration.

Cells were counted using a Neubauer hemocytometer. Cells were diluted in trypan blue reagent and counted under a microscope at low magnification. Trypan blue will allow to differentiate live cells form death cells, since cells colored blue are dead (Figure 16). The viability of the culture should be at least 95 % in the log phase.

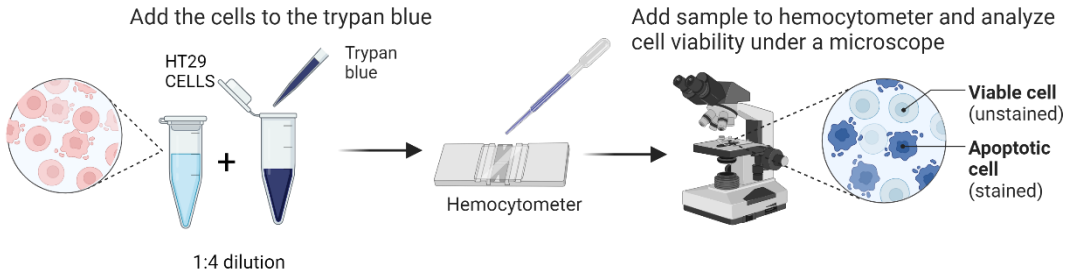

Figure 16: Cell counting using trypan blue. Created with BioRender.com.

The concentration of cells was determined as follows on Eq.1.

$$Cell\ concentration\ (cell/ml) = \frac{number\ of\ cells\ counted}{number\ of\ squares} \times dilution\ factor \times 10^4$$

Eq. 3

The cells solution was prepared at a concentration of 1×10^5 cells/ml, with 100 µl added to each of the central 60 wells, being the surrounding wells filled with water. Following preparation, cells were incubated for 24 hours in a humidified environment at 37 °C with 5 % CO_2.

Following the 24 hours incubation period, the cell culture medium was removed from the plate, and two different approaches were used to evaluate the antiproliferative activity of empty and THEDES-loaded NPs. Direct contact experiments were conducted using both lyophilized and non-lyophilized NPs. For the lyophilized NPs, concentrations ranging from 0 to 20 mg/mL were prepared. For the non-lyophilized NPs, which were formulated in water and PBS, the samples obtained after dialysis were diluted in several ratios: 1:1.5, 1:2, 1:3, 1:4, and 1:8. Each concentration was applied to cells in triplicate wells, with additional wells serving as controls. The NPs-cell contact was maintained for 24 hours.

For indirect contact experiments, leachables from the lyophilized NPs (empty and loaded) were prepared in concentrations ranging from 0 to 20 mg/mL and left 24 hours in a 37 °C bath under agitation. The leachabels were just done for the lyophilized NPs. After incubation, the NPs solutions were filtered and placed in contact with cells, in triplicate wells, leaving control wells.

After 24 hours of exposer, the solutions containing NPs and leachables were removed, and cells were washed at least twice with PBS. Subsequently, cells viability was analyzed using MTS reagent with a concentration of 16 %, diluted 1:10 in RPMI medium supplemented with 0.5 % FBS, and incubated between 2:30 hours and 3 hours at 37 °C with 5 % CO_2. Absorbance was then measured at 490 nm using a spectrophotometer (Perkin Elmer, Victor Nivo 3S) to assess cell viability. The results present were obtained from at least duplicate experiments.

3.7.4- Cytotoxicity assay

The viability of normal colorectal cells in response to both empty and Me:IBU (3:1)-loaded NPs was evaluated using the MTS assay. Caco-2 cells were subcultured upon reaching 80-90 % confluence, following the previously described protocol. Cell concentration was determined using a Neubauer hemocytometer, with cells stained with trypan blue and counted under a low magnification microscope. Cell concentration was subsequently calculated using Eq. 1.

A cell solution was prepared at a concentration of 2×10^5 cells/mL, and 100 µL was added to each of the central 60 wells, being the surrounding wells filled with water. The cells were incubated for 7 days in a humidified atmosphere at 37 °C with 5 % CO_2. After a 7-day incubation period, during which the medium was replaced after 2-3 days, the culture medium was

removed from the plate. The cytotoxic effects of empty and THEDES-loaded NPs on Caco-2 cells were then evaluated using the same two approaches that was used in proliferation assay for HT29. Briefly, the direct contact experiments were done using lyophilized and non-lyophilized NPs. The lyophilized NPs were prepared with concertation range of 0 to 20 mg/mL and the non-lyophilized NPs, prepared in water and PBS, were diluted in several ratios: 1:1.5, 1:2, 1:3, 1:4, and 1:8. The NPs solutions were applied to cells in triplicate wells, with control wells included for comparison. The NPs-cell contact lasted for 24 hours.

For the indirect contact assays executed just for the lyophilized NPs, the same range of concentrations from 10 to 20 mg of NPs were prepared and agitated at 37 °C for 24 hours. Post-incubation, the NPs solutions were applied to cells in triplicate wells, with control wells maintained separately. After 24 hours, the solutions were removed, and the cells were washed with PBS. Subsequently, cells were exposed to MTS reagent, and cell viability was measured at 490 nm using a spectrophotometer. The results reported were derived from at least two experimental replicates.

3.8. PLGA NPs cellular uptake

For the evaluation of NP cellular uptake, NPs were formulated using the previously described nanoprecipitation technique, incorporating FITC, a hydrophilic dye, and Nile Red, an hydrophobic dye. Specifically, FITC was incorporated into the aqueous phase containing PBS, while Nile Red was incorporated into the aqueous phase containing water. After NP formulation, we assessed cellular uptake in the HT29 cell line. To do this, HT29 cells were exposed to NPs containing the dyes for 24 hours, then the media was removed from the cells, and washed once with PBS. The cells were fixed by adding 10% formalin and incubated at room temperature for 30 minutes. Following fixation, the formalin was removed and the cells were washed 2-3 times with PBS. A staining solution was prepared by combining 0.13 µL of phalloidin (from a 0.1 mg/mL stock) and 0.1 µL of the fluorescent dye DAPI (from a 1 mg/mL stock) in 80 µL of PBS. This solution was added to each well (80 µL per well) and incubated in the dark for 20-30 minutes. After incubation, the staining solution was removed and the cells were washed 2-3 times with PBS. The cells were then observed under a microscope to analyze NP uptake.

4.

RESULTS AND DISCUSSION

4.1. Emulsion Solvent Evaporation Method

4.1.1. Preparation of Empty and Me:IBU (3:1)-loaded PLGA NPs formulated by Emulsion Solvent Evaporation Method

In this study, both empty and Me:IBU (3:1)-loaded PLGA NPs were prepared using the single emulsion solvent evaporation method. This technique was chosen for its efficacy in encapsulating hydrophobic drugs, offering a cost-effective and adaptable approach to NPs production. The single emulsion solvent evaporation method is particularly advantageous because it enables the fine-tuning of NPs properties through adjustments in formulation parameters [179]. In this study, the objective was to produce spherical, stable NPs with a diameter ideally less than 200 nm, optimizing the EPR effect and increasing the likelihood of successful incorporation of PLGA NPs into VPLS, ultimately enhancing targeted drug delivery efficacy. For that purpose, two critical factors, known to influence size and morphology, were selected as variables to refine and reduce NPs size: polymer and surfactant concentrations [180].

For the synthesis of PLGA NPs, PLGA solution, dissolved in DCM, was added to an aqueous phase containing PVA, creating an emulsion under vigorous vortex mixing. PVA was selected as the surfactant due to its non-toxicity, hydrophilicity, chemical resistance, and high biocompatibility [181]. PVA has also been shown to promote the production of smaller, spherical NPs with a narrow size distribution [182]. PVA concentrations of 3 % (v/v) and 5 % (v/v) were selected based on evidence that these percentages are optimal for producing NPs with the desirable characteristics [183], [184]. Hernández-Giottonini *et al.*, demonstrated that increasing PVA concentration from 1 % to 5 % results in a decrease in NPs size and a more uniform morphology [176]. After emulsion, NPs are sonicated, to reduce their size, and then centrifugated to wash the surfactant and the THEDES that do not enter in the NPs. Finally, trehalose is added to the solution, to avoid crystals formation, and the NPs are lyophilized to be stored and used on further studies [185]. Empty NPs were first formulated to optimized these steps, and only after optimizations Me:IBU (3:1)-loaded NPs were synthetized.

4.1.1.1. Effect of PLGA Concentration

The formulation process involved dissolving PLGA at two different concentrations, 25 mg/mL and 50 mg/mL, in the organic solvent DCM. For the THEDES-loaded PLGA NPs, Me:IBU (3:1) was also dissolved in DCM in a concentration corresponding to two times the EC_{50}. PLGA (50:50) was selected due to its extensive use in the biomedical field, attributed to its biocompatibility, biodegradability, and non-toxicity, as well as its regulatory approval by both the FDA and EMA [186]. The 50:50 ratio of lactic acid to glycolic acid in PLGA facilitates a faster hydrolytic degradation compared to other ratios, providing a predictable and controlled drug release profile while reducing the risk of polymer accumulation and associated toxicity [187]. DCM was chosen as the solvent because of its immiscibility with water and its rapid evaporation properties, which are crucial for achieving smaller NPs, a key factor in optimizing drug delivery systems [188].

The choice of PLGA concentrations (25 mg/mL and 50 mg/mL) was based on published research indicating that higher polymer concentrations typically result in larger NPs size and enhanced encapsulation efficiency [189], [190], [191].

In this study, SEM analysis was used to evaluate the size and shape of polymeric NPs formulated with variable concentrations of PLGA while the other parameters are kept constant. The results suggest that an increase in polymer concentration from 25 mg/mL to 50 mg/mL led to an increase in the size diameter of the NPs. Specifically, NPs prepared with 25 mg/mL of PLGA and 5 % PVA showed a size distribution ranging from 88 to 185 nm. When the PLGA concentration was increased to 50 mg/mL, while keeping the PVA concentration at 5 %, the resulting NPs exhibited a higher size diameter, ranging from 108 to 193 nm. Additionally, aggregation is equally visible in both conditions (Figure 17).

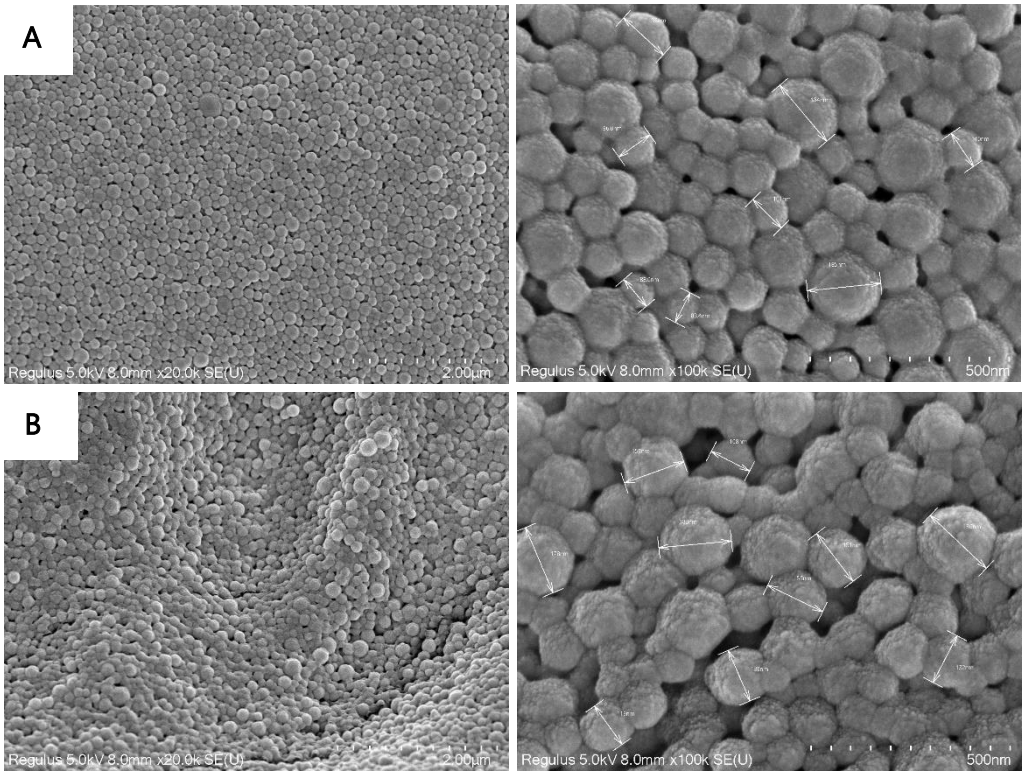

Figure 17: SEM photomicrograph of empty PLGA NPs. A) PLGA NPs formulated with 25 mg/ml of PLGA and 5 % of PVA; B) PLGA NPs formulated with 50 mg/ml of PLGA and 5 % of PVA.

The direct correlation between PLGA concentration and NPs size observed in previous studies aligns with our results, confirming that within this concentration range, higher polymer concentrations generally lead to larger NPs [191], [192], [193], [194], [195]. Budhian *et al.*, investigated the impact of PLGA concentrations on both particle size and drug loading efficiency and demonstrated that PLGA NPs formulated with concentrations ranging from 5 mg/mL to 66 mg/mL exhibit an increase in size from approximately 190 nm to 250 nm, accompanied by improved drug loading efficiency from about 1 % to 2.5 % [193]. Rana Bakhaidar *et al.*, reported a significant increase in the size of PLGA-polyethylene glycol (PEG) NPs as the polymer concentration increased from 10 mg/mL to 100 mg/mL, resulting in a size increase from 111.55 nm to 576.19 nm [192]. Similarly, Sayantan Ray *et al.*, demonstrated a direct correlation between increased PLGA concentration and NPs size, showing that a gradual increase in polymer concentration from 20 mg/mL to 60 mg/mL led to a size increase from 140 nm to 300 nm [194]. These could be due to the increase of viscosity of the organic phase as reported by Wei Huang *et al.*, that saw an exponential increase in viscosity when the PLGA concentration increases from 0.1 mg/mL to 10 mg/mL reflected in the decreasing of the organic solvent coefficient diffusion [191]. Furthermore, D. Cun *et al.*, also reported an increased in viscosity when increasing PLGA concentration from 20 to 60 mg/mL [195]. This increase of viscosity in the organic solution impairs the formation of small droplets due to the higher internal friction between the liquid molecules. This restricts the solution's ability to flow and disperse effectively. As a result, the thicker, more viscous solution resists breaking into finer droplets during

the formulation process. Consequently, this resistance leads to the formation of larger droplets, which results in larger NPs after solvent evaporation [196].

Furthermore, this thesis aims to develop a DDS specifically for the targeted delivery of a THEDES formulation to CRC cells. To achieve this, the DDS must ensure controlled and sustained release of the drug to maintain a sufficiently high concentration of THEDES within the tumor microenvironment. Additionally, the system must facilitate efficient cellular uptake to maximize therapeutic efficacy while minimizing off-target effects. These factors are heavily influenced by the size of the NPs. NPs within the size range of 100 nm to 200 nm are generally considered optimal for controlled and sustained release, as well as for efficient tumor accumulation [197]. This is supported by Schädlich *et al.*, who found that PEG-PLA NPs sized between 111 nm and 141 nm accumulated efficiently in tumors, whereas slightly larger particles (166 nm) were rapidly cleared by the liver [198]. In contrast, Sudhir *et al.*, demonstrated that larger PLGA microparticles (1-10 μm) improved the efficacy of paclitaxel against breast tumors compared to smaller NPs (315 nm) [199]. Our findings, with NPs ranging between 88 nm and 193 nm, suggest that both conditions fall within a size range conducive to achieving effective tumor targeting and sustained drug release.

SEM results also demonstrate that the NPs have similar spherical morphology independent on PLGA concentrations. The ideal shape of the NPs to achieved a good therapeutic outcome is not straightforward. Kaplan *et al.*, found no significant differences in tumor accumulation among spherical, rod-shaped and elliptical disk-shaped NPs in non-small cell lung cancer, although spherical particles showed higher drug release [200]. In CRC, Tchoryk *et al.*, found that smaller spherical NPs (30-50 nm) penetrated tumor spheroids more efficiently than larger ones (100 nm) [201].

An important observation to notice is that although these measurements provide a preliminary indication of the size distribution and visual insights of NPs stabilization, it is important to acknowledge that the size data were obtained by measuring the diameters of only 7-9 NPs, which is a relatively small sample size that may not fully capture the variability within the population of NPs. Further studies and programs that offer a more comprehensive and statistically robust analysis of NPs size distribution were not pursued here because the NPs were aggregated and, therefore, not suitable for future applications.

4.1.1.2. Effect of PVA Concentration

To achieve stable and small NPs, surfactants play a key role by reducing surface tension between the organic and aqueous phases, thereby enhancing particle solubility. We tested PVA concentrations of 3 % (w/v) and 5 % (w/v) while maintaining a constant PLGA concentration. Interestingly, SEM analysis of empty PLGA NPs revealed that varying the PVA concentration within this range did not significantly impact NPs size, suggesting that within these levels, PVA concentration is not a critical factor in controlling NPs dimensions (Figure 18 A and Figure 18 B). Moreover, the NPs in this study are not stable demonstrating a tendency to aggregate.

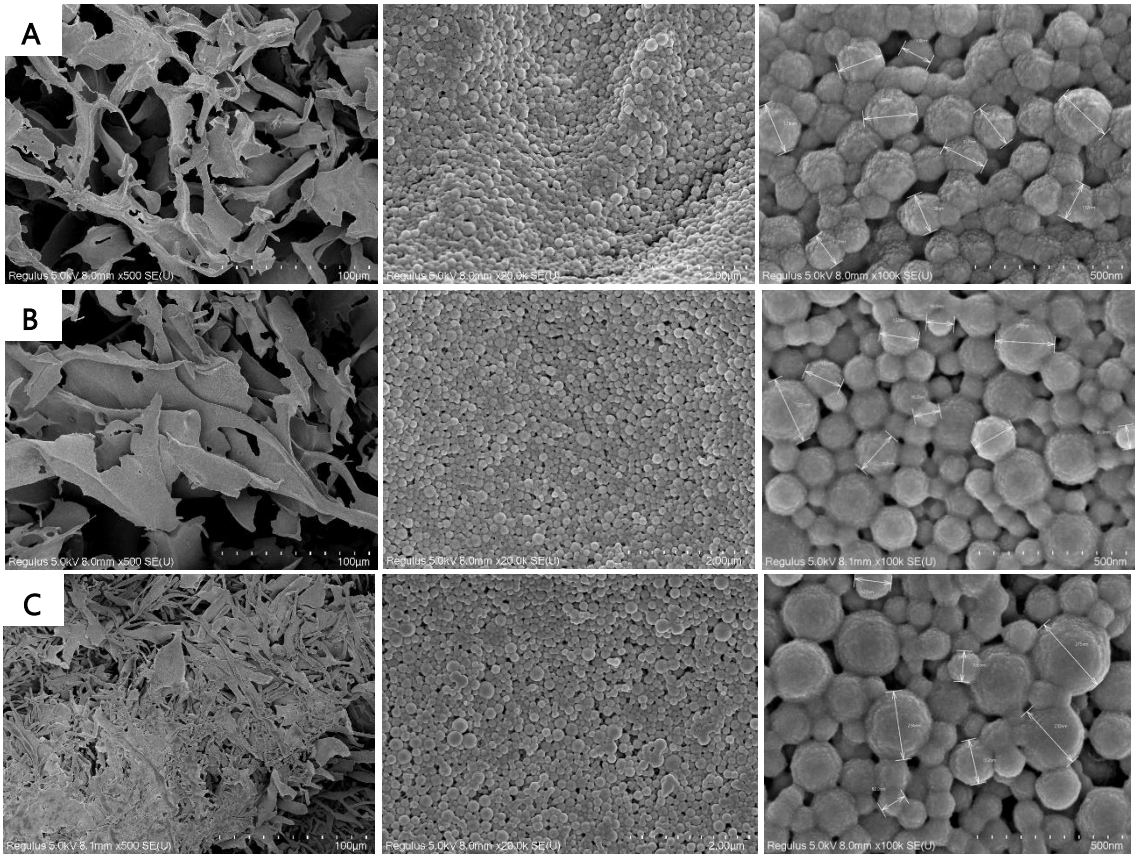

Figure 18: SEM photomicrograph of PLGA NPs formulated with different PVA concentrations A) Empty PLGA NPs with 50 mg/ml of PLGA and 5 % PVA; B) Empty PLGA NPs with 50 mg/ml PLGA and 3 % PVA; C) PLGA NPs formulated in the presence of Me:IBU (3:1) with 50 mg/ml PLGA and 3 % PVA.

Although these early results do not give a clear picture of NPs size, and more characterization studies, like DLS, are needed for precise size measurement, it is surprising that changing the PVA concentration did not significantly affect NPs size. Instead, increasing PVA concentration led to aggregation, which was not anticipated, since increased surfactant concentration is typically associated with improved stabilization and reduced aggregation. Higher surfactant concentrations stabilize smaller NPs by further reducing surface tension during their formation. For instance, Song X *et al.*, observed a decrease in PLGA NPs size from 522 nm to 380 nm as PVA concentration increased from 0.5 % (w/v) to 5 % (w/v) [202]. Similarly, Sawasdee *et al.*, found that increasing PVA concentration from 1 % to 5 % led to a reduction in NPs size from 259 nm to 179 nm, with further increases up to 10% showing no significant size reduction [203]. Conversely, Ozturk K *et al.*, achieved smaller NPs with 2 % (w/v) and 3 % (w/v) PVA compared to higher concentrations [204].

Surfactant molecules interact with NPs surfaces by adsorbing to them, which reduces surface energy. This reduction in surface energy minimizes the overall free energy of the system, stabilizing the particles at a size that achieves the lowest energy state. Consequently, the particles tend to attain a uniform size as the surfactant helps balance and stabilize them. At high surfactant concentrations, there is enough surfactant to effectively cover the particle sur-

faces, leading to a decrease in average particle size and a narrower size distribution. Additionally, the surfactant reduces surface tension and prevents aggregation, resulting in smaller and more uniformly sized NPs [205]. A possible explanation for the aggregation observed and lack of significant change in NPs size with increasing PVA concentration is the occurrence of surfactant oversaturation. When PVA becomes oversaturated, it can increase the solution's viscosity, leading to the clumping and aggregation of particles. Rather than producing a uniform size, this can result in a bimodal or even polymodal size distribution. In such cases, the NPs may vary widely in size and form clusters due to the excessive surfactant disrupting the stabilization process [206].

Furthermore, NPs loaded with Me:IBU (3:1) using 50 mg/mL of PLGA and 3 % PVA also exhibited similar aggregation behavior (Figure 18 C). However, a comparison between empty NPs and Me:IBU (3:1)-loaded NPs, both formulated with 50 mg/mL of PLGA and 3% PVA, seems to reveal an increase in overall NPs size for the loaded formulation. This could suggest some level of encapsulation. However, these results are not sufficient to confirm this, and further drug encapsulation efficiency quantification is needed. However, if the encapsulation of Me:IBU (3:1) was successful, the encapsulation did not affect NPs morphology.

TEM characterization was also conducted, nonetheless, the analysis was unsuccessful because the NPs degraded upon exposure to light during the imaging process (Figure 19).

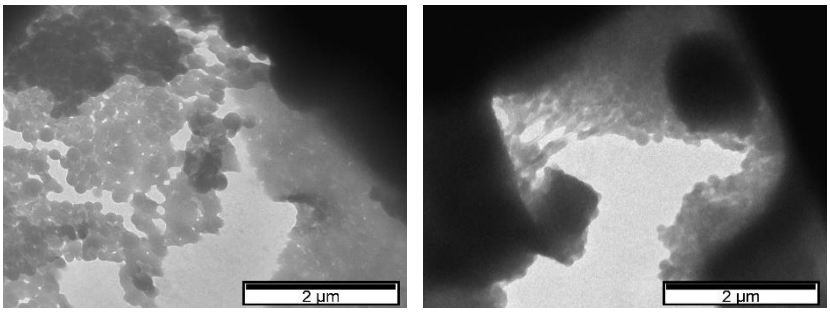

Figure 19: TEM results of empty NPs synthesized with 25 mg/mL PLGA and 5 % PVA.

4.1.2. Chemical Characterization of NPs

With the aim to elucidate the fundamental composition of the formulation and verify the successful incorporation of these polymers into the NPs matrix, FTIR reveal key interactions between PLGA and PVA, evident from the characteristic shifts in peak positions. The PLGA spectrum is marked by a prominent absorption band around 1738 cm^{-1}, corresponding to C=O stretching of ester groups, a signature feature of the PLGA backbone. In the PVA spectrum, the broad band observed between 3383 cm^{-1}, attributed to O-H stretching, is indicative of hydroxyl groups. In the spectra corresponding to 25 mg/mL and 50 mg/mL PLGA NPs, a noticeable shift in the O-H stretching band occurs, suggesting hydrogen bonding or other forms of molecular interaction between the PVA and the PLGA. The C=O stretching band also displays minor shifts, suggesting an interaction at the molecular level, possibly through hydrogen bonding. Furthermore, the absence of the O-H stretching band in the 50 mg/mL PLGA

formulation indicates more pronounced interactions between PLGA and PVA, likely due to hydrogen bonding. This interaction effectively masks the O-H groups, leading to the attenuation of their signal in the FTIR spectrum (Figure 20).

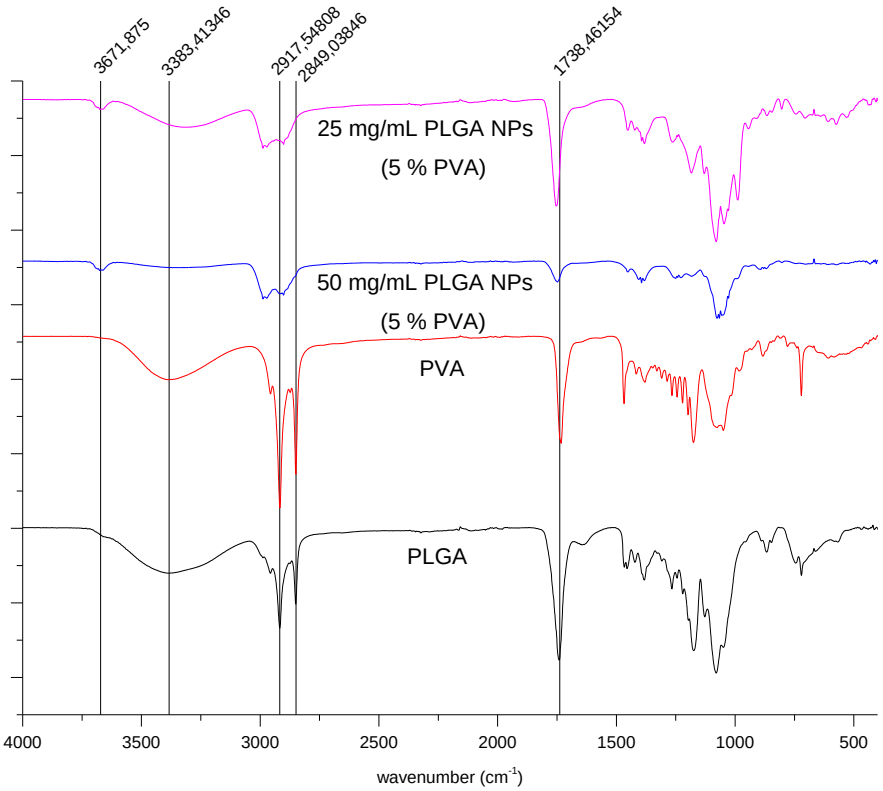

Figure 20: ATR-FTIR analysis of the PLGA NPs with 25 mg/mL (5 % PVA) and 50mg/mL of PLGA (5 % PVA), PLGA and PVA.

4.1.3. Optimization of Emulsion Solvent Evaporation Method to Avoid Aggregation

Our primary goal was to obtain small and stable NPs, so before conducting detailed characterization to validate our findings and for further formulation of NPs with the desire features, it was crucial to first address the aggregation issue. We encountered significant difficulties in resuspending NPs after ultracentrifugation, which was often nearly impossible. In an attempt to address these issues, we reduced the ultracentrifugation speed to 20,000 rpm, hypothesizing that a gentler force might prevent the NPs from packing too tightly, thereby easing resuspension. However, after this change the aggregation still occurred and the NPs still did not fully deposit, suggesting that surfactant residues and centrifugation likely played a significant role in particle aggregation. Vauthier C *et al.*, reported the aggregation of NPs after ultracentrifugation, leading to a solid and compact pellet impossible to be completely resuspended [207].

Furthermore, we also suspected that residual surfactant, which is difficult to remove during ultracentrifugation, was causing aggregation. To address this, we increased the number of washes from 3 washes to 6 washes to remove excess PVA, but the issue persisted, as PVA continued to remain in the solution. Menon J *et al.*, mentioned the especially challenging step to fully remove PVA. This could be to the fact that PVA binds strongly to the hydrophobic regions of PLGA [208]. Achieving stable and colloidal NPs requires a precise balance in PVA concentration, too low may not stabilize the particles effectively, while too high can lead to aggregation. Uskoković V. *et al.*, observed PLGA aggregation even with PVA concentrations of 1 %, 2 %, and 3 % [209]. The ideal concentration is influenced by multiple factors, such as the type of organic phase, the organic-to-aqueous phase ratio, and polymer concentration, making it difficult to generalize. Additionally, some studies have reported *in vivo* toxicity linked to residual PVA, further emphasizing the need for surfactant removal [210]. Furthermore, PVA influences NPs cellular uptake, once the NPs are more hydrophilic [211].

Given the persistent challenges associated with PVA, including its difficult removal, potential cytotoxicity, and its tendency to cause NPs aggregation, it became clear that continuing to optimize PVA concentrations would likely be time-consuming and may not yield the desired results. Attempts to reduce PVA concentration still resulted in aggregation, while increasing the number of washes proved ineffective in fully eliminating residual surfactant. Instead of continuing to experiment with minor adjustments, we recognized that a more efficient approach would be eliminating the surfactant of the equation. Switching to a nanoprecipitation method that uses a partially miscible organic phase, eliminating the need for surfactants, emerged as a promising alternative solution. Our hypothesis is that using this surfactant-free method we will eliminate the need for extensive purification steps like ultracentrifugation, reduce the risk of aggregation due to excess surfactant, and avoid potential cytotoxicity issues associated with residual PVA. Moreover, the nanoprecipitation process is more streamlined and can produce smaller and more uniform NPs without the complications introduced by surfactants. By adopting this method, we can focus on producing stable and consistent NPs, ensuring better reproducibility and ultimately achieving our goal of obtaining small and well-dispersed particles for our intended applications [212], [213].

4.2. Lyophilized PLGA NPs formulated by Nanoprecipitation

4.2.1. Preparation of Empty and Me:IBU (3:1)-loaded PLGA NPs formulated in water

Surfactant free nanoprecipitation method is a technique recognized for its simplicity, minimal energy requirements, and capacity to produce stable and small NPs without surfactants, potentially resolving the problems of aggregation and enhancing the effectiveness of the DDS [214].

In this study, both Me:IBU (3:1)-loaded and empty NPs were formulated using the nanoprecipitation method, with acetone and water serving as co-solvents. Initially, 25 mg/mL of PLGA were dissolved in acetone, since, based on our prior findings, the reduction of polymer concentration suggests the production of smaller NPs. This is because the viscosity of the organic phase, influenced by PLGA concentration, plays a significant role in NPs size. The organic phase was then gradually added dropwise into an aqueous phase containing distilled water. The partial miscibility of acetone with water reduces surface tension and helps it diffuse into the aqueous phase. This diffusion enhances the distribution of the polymer, creating a stable environment for polymer precipitation. As acetone slowly evaporates, the polymer concentration in the organic phase increases, resulting in controlled and consistent polymer precipitation and the formation of NPs.

The primary challenge encountered with the nanoprecipitation technique was the aggregation of PLGA during the solvent evaporation process (Figure 21).

To address the issue of polymer aggregation during the nanoprecipitation process, we reduced the PLGA concentration to 12.5 mg/mL. Higher polymer concentrations increase the viscosity of the organic phase, so lowering the concentration aimed to reduce polymer content in the solution, thereby minimizing aggregation and improving yield. An interestingly observation was the fact that during the evaporation process, we observed that the solution of empty NPs exhibited significantly more PLGA precipitation compared to the solution containing the THEDES.

This observation suggests that THEDES may influence the stabilization of PLGA NPs, potentially reducing precipitation. Additionally, empty NPs did not form effectively when only water was used as the aqueous phase, indicating a greater instability in this solvent environment than anticipated. The aggregation of PLGA when producing empty NPs could be due to the absence of surfactant agents in the formulation. In contrast, the Me:IBU (3:1)-loaded NPs benefit from the encapsulated material, which contributes to a more stable core. Without stabilizing components, PLGA are, hence, more susceptible to aggregation.

Furthermore, the lyophilization process appears to exacerbate aggregation. This could be due to the fact that pre-existing aggregates in the solution may promote the adhesion of

additional NPs to these filamentous polymer clusters. Despite these challenges, we proceeded with the characterization of the NPs. This analysis is expected to provide valuable insights into their physical properties and elucidate the effects of lyophilization and various formulation parameters. Understanding these factors, as well as the differences between empty and loaded NPs, will be crucial for optimizing the final characteristics of the NPs.

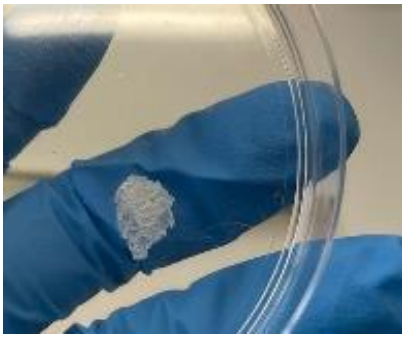

Figure 21: PLGA aggregates after acetone evaporation.

4.2.2. Characterization of lyophilized PLGA NPs formulated by nano-precipitation

4.2.2.1 SEM

SEM analysis of the empty NPs confirm the macroscopic observations of NPs aggregation during the nanoprecipitation technique (Figure 22 A). The images reveal a lamellar, sheet-like structure typical of lyophilized polymer material, rather than distinct nanoparticles. This suggests weak structural integrity and a higher tendency for aggregation or collapse during lyophilization due to the absence of stabilizing agents.

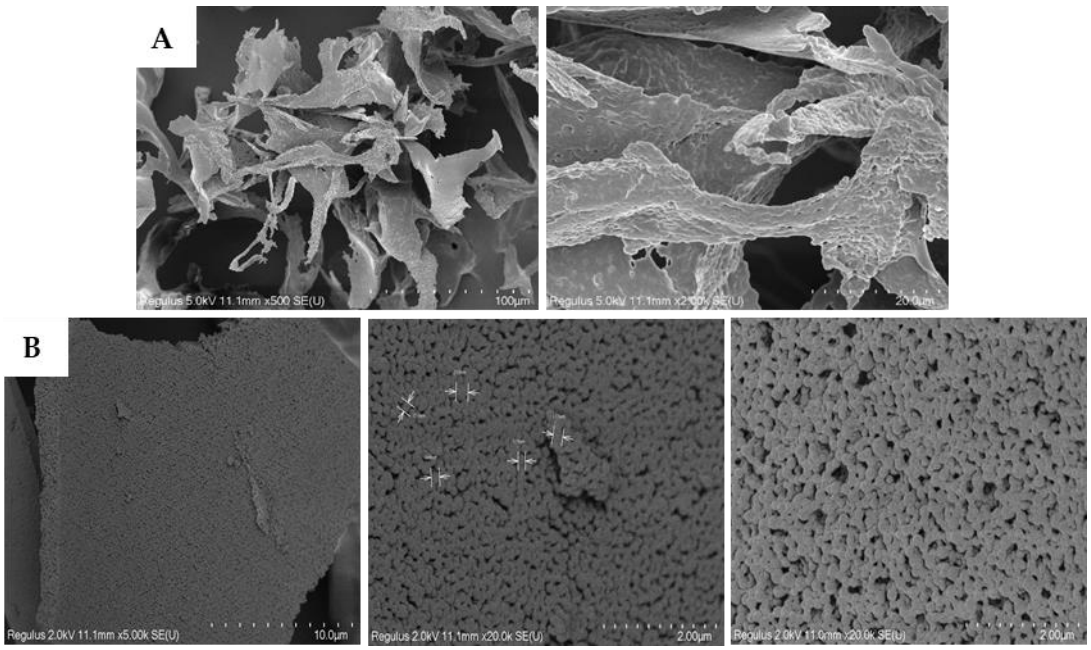

Figure 22: SEM photomicrograph of A) empty lyophilized PLGA NPs and B) lyophilized PLGA NPs formulated in the presence of Me:IBU (3:1) by nanoprecipitation method.

SEM results of lyophilized Me:IBU (3:1)-loaded NPs also reveals a higher degree of aggregation (Figure 22 B). However, in contrast to the empty NPs, discrete NPs are clearly visible. These particles appear embedded within polymeric aggregates, highlighting the challenges inherent to the lyophilization process. While lyophilization was necessary to dry the particles for SEM imaging, it induced aggregation that likely does not represent the original state of the NPs. Despite this, the presence of discrete NPs suggests that without lyophilization, the particles may have remained separate and well-defined, unlike the empty NPs. E. Trenkenschuh *et al.*, reported that several factors during lyophilization could lead to NP aggregation. These include a decrease in the distance between particles and a reduction in surface charge, which may result in a predominance of attractive forces over repulsive forces due to the increased NP concentration caused by rapid freezing [215].

These findings suggest that in the absence of THEDES, NPs are more susceptible to deformation and aggregation, leading to structural collapse during lyophilization. In contrast, THEDES appears to positively impact NPs stabilization. However, additional analyses as DLS or FTIR would be required to confirm this effect.

The fate of NPs in the human body and their effectiveness as drug delivery systems are influenced not only by size but also by their surface charge [216], [217]. Therefore, DLS analysis is a key technique for characterizing NPs, in terms of surface charge, but also in terms of size distribution and stability. It provides the hydrodynamic diameter of a population of NPs, which includes not only the core particle size but also the surrounding, as water and/or any other adsorbed molecules [218].

4.2.2.2. DLS

The DLS analysis of lyophilized Me:IBU (3:1)-loaded NPs yielded a mean hydrodynamic diameter of 362.4 ± 113.7 nm, a PDI of 0.83 ± 0.14 and zeta potential of -11.6 ± 0.4 mV, for one representative batch (

Table 2). This size is notably larger than the typical range reported for PLGA NPs, which is between 100 and 250 nm [219]. However, as highlight before, the ideal size for this application would be between 100 nm and 200 nm for tumor accumulation [197]. Bigger NPs are more likely to be accumulated in liver and spleen, reducing the percentage of NPs that effectively reach the target [220]. Consequently, the larger size of these NPs may affect their cellular uptake and overall behavior in biological systems. Additionally, the ideal size for VLPs encapsulation is also between 100 nm and 200 nm.

Table 2: DLS results of the lyophilized Me:IBU (3:1)-loaded PLGA NPs and the respective standard deviations (SD).

	Size (nm)	PDI	Zeta potential (mV)
Lyophilized Me:IBU (3:1) loaded PLGA NPs	362.4 ± 113.7	0.83 ± 0.14	-11.6 ± 0.4

In summary, while the DLS results for the lyophilized Me:IBU (3:1)-loaded NPs indicate a larger size and higher variability than typically desired, and the zeta potential suggests moderate colloidal stability, the negative surface charge may still confer advantages for biological applications. Therefore, antiproliferative activity was evaluated in colorectal cancer cells.

4.2.3. Antiproliferative and cytotoxic activity of Lyophilized Empty and Me:IBU (3:1)-loaded PLGA NPs

The first studies were done with lyophilized empty and Me:IBU (3:1)-loaded NPs, and were tested on HT29 cells, the CRC model, to assess their antiproliferative effects. The MTS assay was used to evaluate cell viability by measuring metabolic activity, where metabolically active cells reduce MTS to formazan. An increase in formazan production indicates that the cells remain viable and metabolically active [221].

In the initial studies, a concentration between 0 and 20 mg/mL of both empty and Me:IBU (3:1)-loaded NPs previous lyophilized were directly exposed to HT29 cells for 24 hours, followed by further incubation for up to 96 hours. This time was chosen to ensure that the NPs have time to enter the cells.

Results from the initial 24-hour viability assays showed no significant reduction in cell viability for either formulation, indicating that neither the empty NPs nor the drug-loaded NPs caused noticeable metabolic disruption (Figure 23 A). The concentrations between 10 and 20 mg/mL relative to Me:IBU (3:1)-loaded NPs are excluded from the graphic because the NPs

interfered with absorbance measurements, leading to inaccurate values. The observation that the empty NPs did not impact cell viability suggests that the NPs themselves are non-toxic to HT29 cells. Similarly, in the 96-hour exposure assay, no significant impact on cell viability and consequently non-significant antiproliferation effect, was observed for either condition (Figure 23 B). The decrease in viability seen in the graph is likely due to NPs sedimentation at the bottom of the wells, which could inhibit nutrient exchange and thereby affect cell growth (Figure 24).

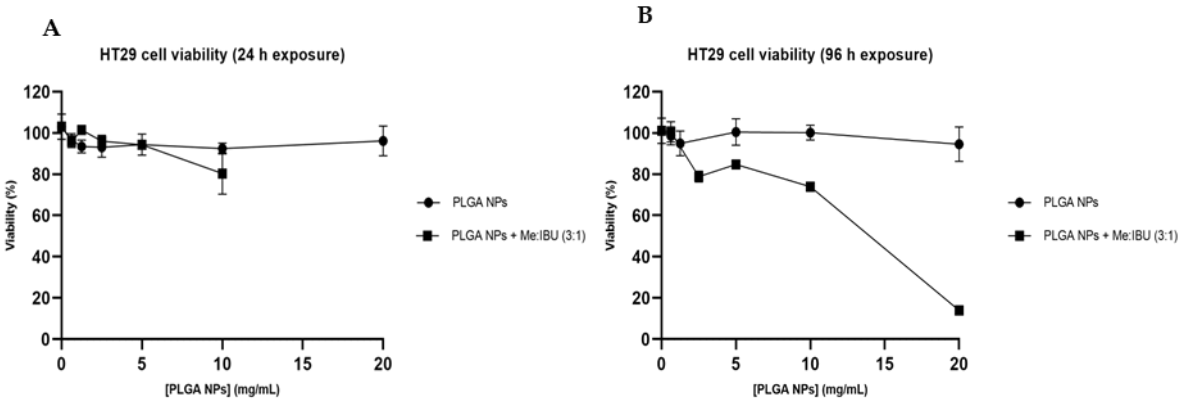

Figure 23: HT29 Cells Viability upon 24 hours (A) and 96 hours (B) of exposure to the lipolyzed empty and Me:IBU (3:1)-loaded PLGA NPs.

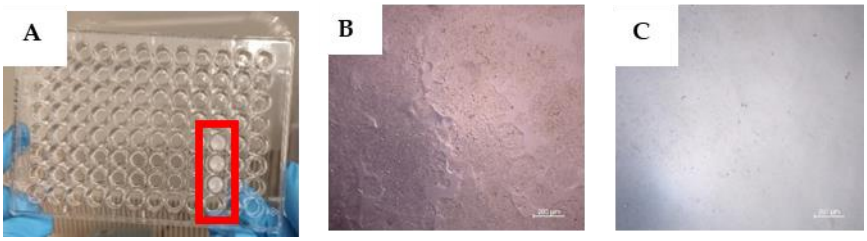

Figure 24: HT29 after 96 hours exposure of 20 mg/mL of Me:IBU loaded PLGA NPs. A) Visual observation of the sedimentation at the bottom of the wells; B) Microscopic image of HT29 control; C) Microscopic image of the well corresponding to 20 mg/mL of Me:IBU (3:1)-loaded PLGA NPs exposer in the end of the MTS assay.

Given that no significant differences in cell viability were observed between the two exposure timelines, if we look just until the 10 mg/mL of NPs, we streamlined our analysis to focus on a 24-hour exposure period. Since the viability seem to decrease only at 10 mg/mL, a concentration range of 10 to 20 mg/mL of both empty and drug-loaded NPs was evaluated.

To mitigate potential issues caused by NPs sedimentation in the wells, which could hinder respiratory and nutrient exchange, leachables of the empty NPs were also assessed. These serve as a control to assess whether the PLGA matrix or any excipients used in the formulation are responsible for any of the observed cytotoxicity. The study comprehensively investigated

both the direct contact and leachable effects of empty and Me:IBU (3:1)-loaded NPs on cells viability (Figure 25 A).

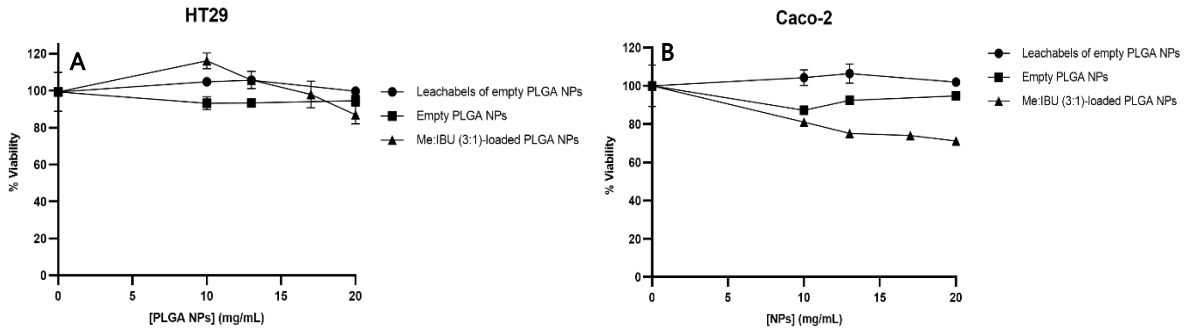

Figure 25: A) HT29 cells viability upon 24 hours of exposure to the lyophilized empty and Me:IBU (3:1)-loaded PLGA NPs and to the leachables of the empty PLGA NPs B).Caco-2 cells viability upon 24 hours of exposure to the lyophilized empty and Me:IBU (3:1)-loaded PLGA NPs and to the leachables of the empty PLGA NPs.

Lyophilized empty and THEDES-loaded NPs in the concentration range of 10 to 20 mg/mL did not negatively impact the metabolism of HT29 cells. The range of concentration used was chosen in order to see how the PLGA NPs impact cellular viability. PLGA NPs are biocompatible and several studies demonstrate that it is safe to use PLGA NPs with concentrations until 2.5 mg/mL with the better concentration being 1 mg/mL [222]. However, we do not see any negative impact on cells viability using up to 20 mg/mL. The viability values exceeding 100% are likely due to errors in the controls, possibly linked to pipetting inconsistencies. This could also be due to the fact that NPs were not monodisperse and stable, but instead showed significant aggregation, as observed on SEM and DLS analysis. Given these findings, these initial results are inconclusive regarding the true biological impact of the NPs, as the aggregation could have influenced the observed outcomes.

To assess the cytotoxicity of the PLGA NPs in normal colorectal cells, the Caco-2 cell model was employed. Three conditions of lyophilized NPs were tested: leachables from the empty PLGA NPs, empty PLGA NPs, and PLGA NPs loaded with Me:IBU (3:1), being the last two directly exposed to the cells. The results suggest that none of the three PLGA NPs conditions significantly impacted cell viability (Figure 25 B). Across the different concentrations tested, cell viability remained relatively stable for empty NPs. This could suggest that the PLGA NPs are generally biocompatible with Caco-2 cells, showing minimal cytotoxicity under the conditions tested. In the case of Me:IBU (3:1)-loaded NPs a viability decrease is observed at higher concentrations. This can be related to the fact that these NPs are not stable and monodispersed, being almost completely aggregated according to SEM and DLS results, and that can

influence cells viability independent of the presence of the THEDES. Therefore, it is not possible to take any conclusion and further optimization and characterization was needed to enhanced the properties of NPs for effective tumor target and accumulation.

4.3. Non lyophilized PLGA NPs formulated by Nanoprecipitation

4.3.1. Preparation of Empty and Me:IBU (3:1)-loaded PLGA NPs formulated in water or PBS

Efforts to understand and mitigate the behavior of NPs post-lyophilization, which seemed to cause aggregation due to suboptimal nanoprecipitation conditions, led us to hypothesize that lyophilization negatively impacts NPs stability. Consequently, we decided to eliminate lyophilization from our process and maintained the NPs formulation in water. Additionally, previous observations suggested that empty NPs in water exhibited instability and difficult formation compared to the NPs when Me:IBU (3:1) was present. Moreover, optimizing a formulation that is suitable for human delivery is imperative for these NPs to be considered strong candidates for a THEDES delivery system. We attempted centrifugation to concentrate the NPs solution, but this lead to similar aggregation issues as observed with the NPs produced by the emulsion method and also are in accordance with the aggregation problem observed by Vauthier C *et al.*, in use this method for concentrate the NPs [207]. We then explored evaporating the water, first using a rotary evaporator and subsequently by heating the sample under stirring at 60°C, considering that PLGA degradation occurs at temperatures higher than this threshold. Unfortunately, both approaches resulted in the formation of a film adhering to the glass surface, rendering them impractical and time-consuming. A possible explanation for that could be the high concentration of PLGA that increases during the water evaporation, leading to increased viscosity and subsequent precipitation [223]. This concentrated PLGA may become sticky and adhere to the glass, forming a film. Additionally, the interaction between the PLGA and the glass surface might further contribute to this issue, especially under the high temperatures and conditions used during the evaporation process. The rapid concentration of PLGA, combined with its adhesive properties and the glass surface potential affinity for the polymer, once both are hydrophobic, makes the process inefficient and problematic. This highlighted the need for further optimization to ensure that NPs remain stable and applicable for cell-based assays.

Given the challenge of drying the NPs, delivering them in a liquid form became necessary. Since a water-based solution was unsuitable, formulating the NPs in PBS emerged as the logical alternative. PBS was selected not only for its osmolarity, which closely matches that of

the cells (~250 mOsm), but also for its buffering capacity, ensuring NPs stability and compatibility with the cellular environment for subsequent biological assays [224]. This adjustment aimed to maintain NPs stability while ensuring compatibility with the cell environment. Both empty and Me:IBU (3:1)-loaded NPs were formulated following exactly the same nanoprecipitation protocol, only changing water by PBS.

Interestingly, the results of formulating NPs in PBS revealed some unexpected findings. Empty NPs formed in PBS (Figure 26 A) appeared to be more stable and uniform compared to those prepared in water (Figure 26 B). Conversely, the THEDES-loaded NPs did not form in PBS (Figure 26 C and Figure 26 D), which contrasts with their successful formation in water (Figure 26 E).

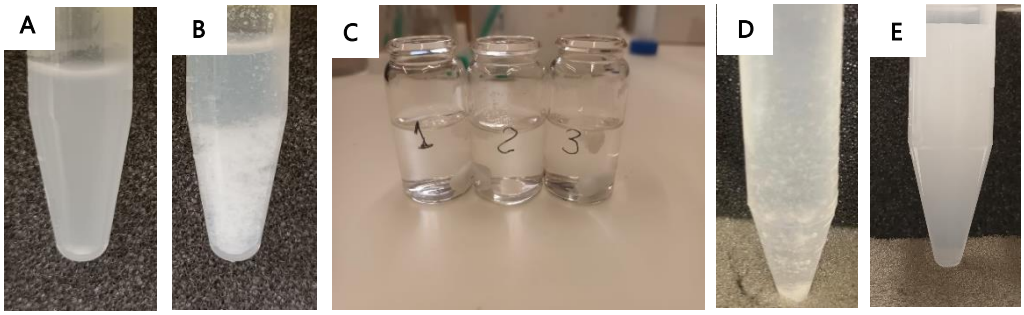

Figure 26: Visual observation after nanoprecipitation protocol of: A) Empty PLGA NPs formulated in PBS b) Empty PLGA NPs formulated in water; C) Visual result obtained after nanoprecipitation protocol in the presence of Me:IBU (3:1) in PBS; D) Me:IBU (3:1)-loaded PLGA NPs formulated in water and posterior addition of PBS salts; E) Me:IBU (3:1)-loaded PLGA NPs formulated in water.

These findings suggest that the ionic strength and osmolarity of PBS play a stabilizing role, potentially by reducing electrostatic repulsion between particles and promoting a more uniform size distribution. The failure of THEDES-loaded NPs to form in PBS could be attributed to specific interactions between the THEDES components and the ionic constituents of PBS, which may interfere with encapsulation or destabilize the NPs structure.

Intrigued by this discrepancy, we attempted to formulate Me:IBU (3:1)-loaded NPs in water, followed by the addition of PBS salts post-formation (Figure 26 C). This approach resulted in significant NPs aggregation, further supporting the hypothesis that the ionic environment in PBS adversely affects the stability of THEDES-loaded NPs.

In water, the successful formation of THEDES-loaded NPs, despite the challenges faced with empty NPs, indicates that the encapsulated THEDES plays a crucial role in stabilizing the particles. The presence of THEDES likely contributes to a more robust core, enhancing stability and preventing aggregation. Conversely, the failure of empty NPs to form effectively in water could be due to the absence of internal stabilizing agents, leaving them more susceptible to aggregation. For empty NPs, the stabilization appears to rely primarily on the ionic components provided by PBS.

4.3.2. Characterization of Empty and Me:IBU (3:1)-loaded PLGA NPs formulated by Nanoprecipitation in water or in PBS

4.3.2.1 SEM

SEM results for the 3 batchs also confirm the successful formation of PLGA NPs in PBS, showing the presence of spherical NPs (Figure 27). However, some of the NPs appear to be fused together, indicating a degree of aggregation. Additionally, the NPs observed in SEM images are less monodisperse compared to the DLS results.

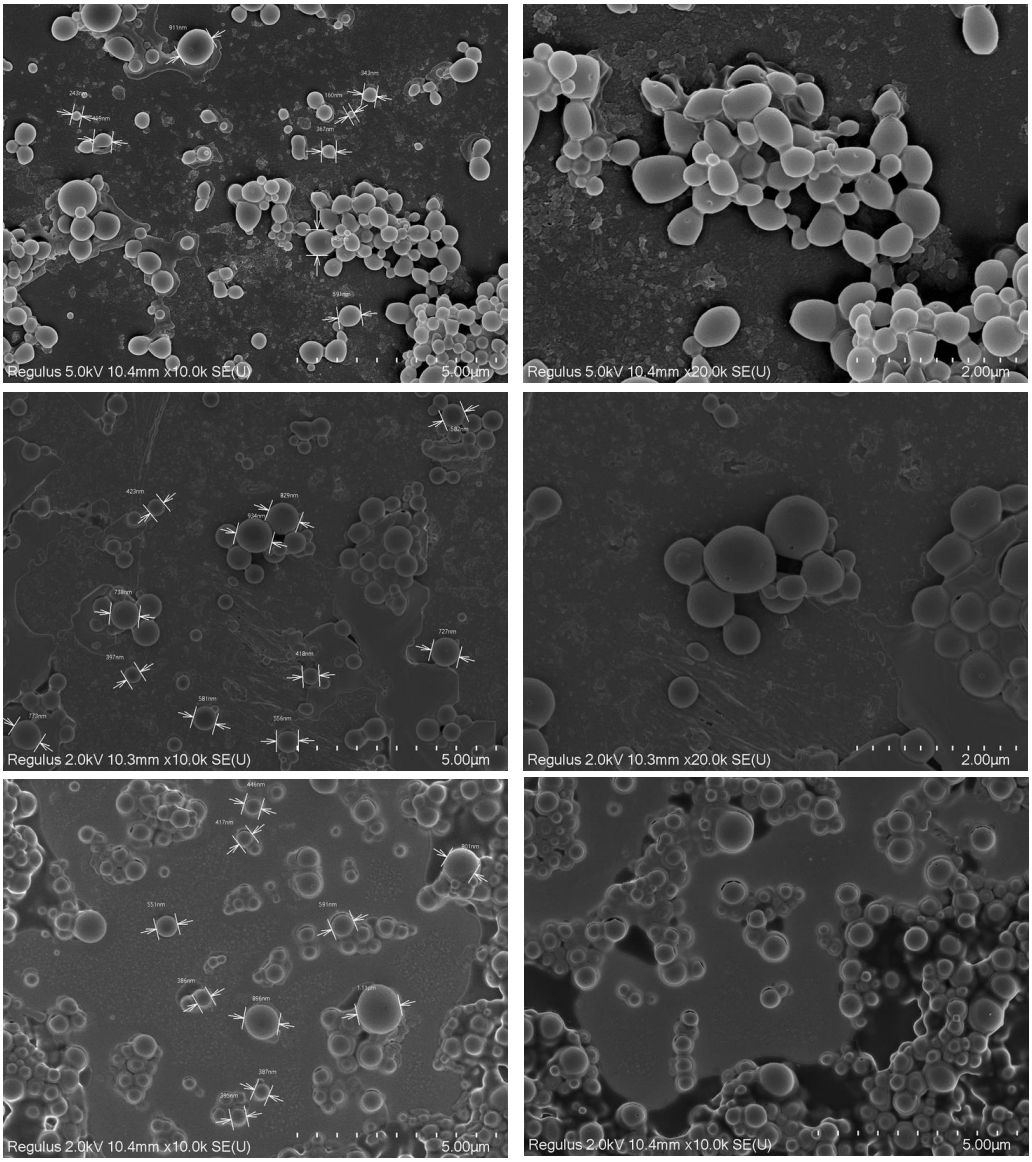

Figure 27: SEM photomicrographs of empty PLGA NPs formulated in PBS.

The discrepancy observed could be attributed to the sample preparation processes required for SEM analysis. Unlike DLS, SEM necessitates drying the samples, followed by gold coating, which involves exposure to elevated temperatures. Additionally, the intense SEM laser

may have induced morphological changes in the NPs, potentially altering their observed characteristics. Ghomrasni *et al.*, also observed that air drying, adversely affect NPs morphology by causing agglomeration. The study suggested spin-coating, as an alternative method, which consists in the deposition of the liquid NPs suspension onto a rotating substrate. The centrifugal force from spinning spreads the liquid evenly, helping to preserve NPs morphology and reduce aggregation [225].

NPs containing THEDES in PBS were also characterized by SEM (Figure 28). As anticipated, Me:IBU (3:1)-loaded NPs did not form in PBS. This supports the hypothesis that PBS may interact with THEDES, destabilizing NP formation. Typically, NPs are formulated in water, with PBS commonly used to assess drug release and mimic biological environments. However, there are successful examples of stable formulations in PBS. For instance, Mohanty *et al.*, demonstrated the stability of curcumin-loaded PLGA NPs in PBS [226].

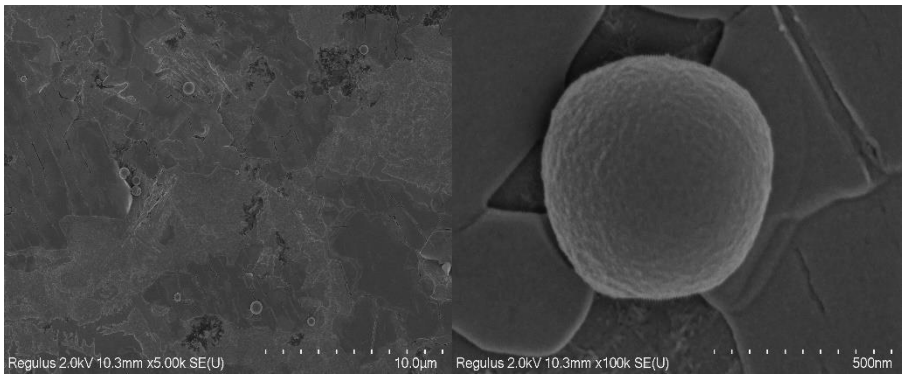

Figure 28: SEM photomicrographs of Me:IBU (3:1)-loaded PLGA NPs formulated in PBS.

These contrasting behaviors highlight the critical influence of the medium on NPs formation and stability. The results suggest that while PBS can be advantageous for the formation of empty NPs, it may not be suitable for all types of NPs formulations, particularly those involving sensitive or reactive payloads like THEDES. This finding emphasizes the need for a tailored approach to NPs formulation, where the choice of solvent and medium is carefully optimized based on the specific requirements of the NPs and their intended applications. Since the intended application is within the human body, incorporating this formulation in its aqueous form containing water is not feasible. The water has a different osmolarity compared to the biological environment, which could lead to cell death due to osmotic imbalance.

4.3.2.2. TEM

The Me:IBU (3:1)-loaded PLGA NPs were also characterized by TEM, revealing key insights into their morphology and distribution (Figure 29). The images show that the NPs exhibit a predominantly spherical shape, presenting size uniformity. Notably, some regions exhibit well-dispersed particles, while others show closer proximity, likely due to the sample preparation process. The drying of the sample before TEM analysis may have led to this apparent

clustering, as particles can become more closely packed during the drying process. Additionally, the surface of the NPs appears relatively smooth, although minor roughness and irregularities are observed, which might be linked to the encapsulation process or the effects of drying during sample preparation. However, once more, the confirmation of THEDES encapsulation its necessary to confirm this.

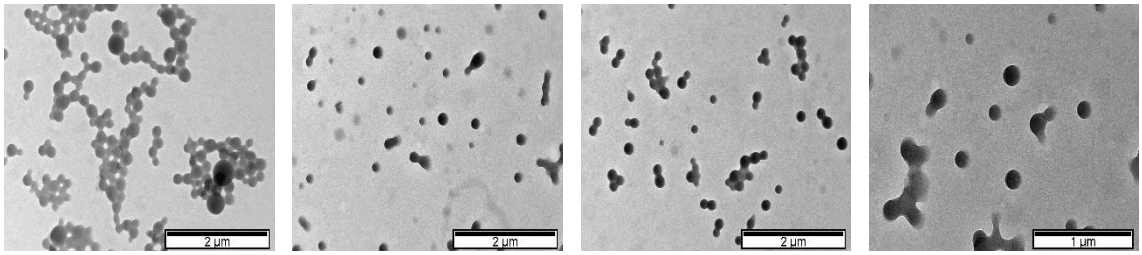

Figure 29: TEM photomicrographs of the Me:IBU (3:1)-loaded NPs formulated in water.

4.3.2.3. DLS

DLS measurements were conducted on three different batches of empty NPs in PBS and on three batches of Me:IBU (3:1)-loaded NPs in water. Additionally, a DLS analysis was performed on a sample of Me:IBU (3:1)-loaded NPs after two months of storage to evaluate their long-term stability (Table 3 and Figure 30).

Table 3: DLS results for the NPS formulated in PBS, water + Me: IBU (3:1) and water + Me: IBU (3:1) with 2 months, and the respective standard deviations (SD).

	Aqueous phase	Size (nm)	PDI	zeta potential (mV)
Empty PLGA NPs	PBS	509.9 ± 4.4	0.081 ±0.003	-59.5 ± 2.6
Me:IBU (3:1)-loaded NPs	water	246.9 ± 2.6	0.066 ± 0.019	-32.6 ± 2.2
Me:IBU (3:1)-loaded NPs (w/ 2 months)	water	369.0 ± 4.3	0.095 ± 0.01	-32.7 ± 0.9

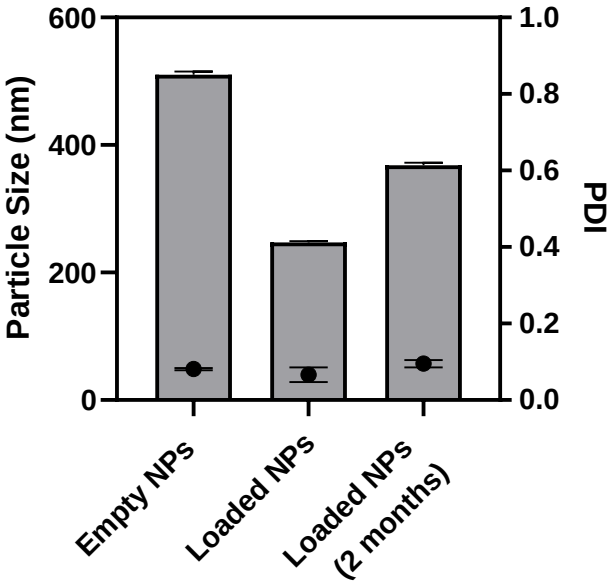

Figure 30: Graphical representation of DLS results for the NPS formulated in PBS, water + Me: IBU (3:1) and water + Me: IBU (3:1) with 2 months.

Empty PLGA NPs formulated in PBS exhibited relatively large hydrodynamic sizes, ranging from 505 to 514 nm across three batches. This increase in size can be attributed to the hydration and swelling of the PLGA matrix in the isotonic PBS environment. Rapier C. *et al.*, suggested that PBS salts could interact with the hydrophilic PLGA polymer, leading to increased water absorption and subsequent swelling of the NPs. The absence of a stabilizing core, in this case loaded Me:IBU (3:1), allows the PLGA matrix to expand more freely in response to the hydrating conditions of PBS, resulting in larger particles [227].

Despite their increased hydrodynamic size, the PLGA NPs in PSB exhibited excellent stability. This stability is evidenced by a highly negative zeta potential, -59.5 ± 2.6 mV, which indicates strong electrostatic repulsion between the particles. This repulsion effectively prevents aggregation and maintains a well-dispersed system. Furthermore, the low PDI values, ranging from 0.078 to 0.084, confirm that the NPs form a uniform and monodisperse population with consistent size distribution.

The high ionic strength and osmolarity of PBS likely play a role in this stability [228]. It seems to suggest that, although PBS does increase the hydrodynamic size of the NPs due to ionic interactions and hydration effects, the ionic strength helps stabilize the dispersion by mitigating potential aggregation through electrostatic repulsion. Despite that, literature presents some contradictions on the impact of ionic strength on NPs stability. Some studies indicate that the ionic strength of PBS can diminish repulsive interactions among NPs, potentially leading to agglomeration. For example, Vuković *et al.*, reported that gold NPs exhibited agglomeration in PBS, underscoring the impact of ionic strength on stability [229]. Similary,

Stromberg Z *et al.*, formulated PLGA NPs with comparable molecular weights and ratios and showed a dramatic increase in size when dispersed in PBS, ranging from 233.6 nm to 4126 nm, accompanied by an increase in PDI from 0.01 to 0.42 and a shift in zeta potential from -47 mV to -67 mV. This significant change in size and variability underscores the complex interactions between PLGA, PBS and other formulation components. Additionally, the study also observed that variations in the ratio of lactic to glycolic acid and mass of PLGA influence stability, highlighting the crucial roles of hydrophilicity and ionic forces [230]. In contrast, our study found that PLGA NPs remained stable in PBS due to their high negative zeta potential, which ensures strong electrostatic repulsion and prevents aggregation despite the increased size. This suggests that the effect of ionic strength on NPs stability is highly dependent on the specific properties of the NPs and the experimental conditions.

The Me:IBU (3:1)-loaded NPs are smaller than the empty NPs formulated in PBS. PDI values, which varied from 0.047 to 0.088, indicate that the loaded NPs are still monodisperse, being an optimal PDI for PLGA NPs often less than 0.2 [226]. The zeta potential for these drug-loaded NPs ranged from -30.4 to -34.8 mV, which suggests high stability, even though it is less robust than the empty NPs in PBS. This difference in zeta potential, and thus stability, may be due to the reduced surface charge resulting from the drug incorporation and the absence of the ionic strength provided by PBS [231]. An hypothesis for this is that the Me:IBU (3:1), a THEDES, could interact with the PLGA matrix in ways that affect hydration and stabilization properties. These findings support the hypothesis that THEDES might act as stabilizers or surfactants within the NPs formulations. The observed enhanced stability of PLGA NPs in the presence of THEDES, as indicated by consistent size distribution and a high negative zeta potential, suggests that THEDES effectively interact with the NPs to prevent aggregation. This stabilization effect is similar to that of surfactants, which stabilize colloidal systems by modifying surface interactions and reducing aggregation. Additionally, this aligns with what Martins M. *et al.*, reported, suggesting the NADES potential as plasticizing agents in the supercritical foaming of natural-based polymers [232]. Furthermore, M. Pu *et al.*, demonstrate that DES can play a stabilizing role in emulsion-based systems, as they successfully prepared microparticles and microcapsules of PLGA-IBU by using solvent evaporation extraction of oil-in-deep eutectic solvent (O/DES) emulsions [233]. If THEDES could function effectively as plasticizers, their underlying mechanism might also contribute to stabilizing NPs. However, to confirm these hypotheses the first step is confirm that the Me:IBU (3:1) was successfully loaded in the PLGA NPs.

Upon assessing the stability of Me:IBU (3:1)-loaded NPs over two months, a notable increase in particle size to 368 nm was observed. This size increase suggests a change in the NPs, which could be attributed to either aggregation or the gradual release of THEDES [234], [235]. However, the consistently low PDI (below 0.1) indicates a narrow size distribution, while the strongly negative zeta potential (below -30 mV) demonstrates that the particles remain

well-dispersed and stable. These stability indicators effectively eliminate aggregation as a possible cause, making the gradual release of THEDES during storage the most plausible explanation for the observed increase in particle size. This suggests a controlled process likely driven by THEDES release. Furthermore, confirming whether THEDES is encapsulated within the NPs or at least present on their surface is essential to validate this hypothesis.

4.3.3. ATR-FTIR Analysis

In order to evaluate if Me:IBU (3:1) is present in loaded NPs, ATR-FTIR analyses was conducted (Figure 31). In the PLGA spectrum the carbonyl (C=O) stretch is found at 1750 cm^{-1}, while the CH, CH_2, and CH_3 stretching vibrations are detected between 2850 cm^{-1} and 3000 cm^{-1}. The OH stretching band appears around 3378 cm^{-1} for PLGA spectrum, but it is no longer detectable on the empty NPs spectrum. This disappearance suggests that hydroxyl groups are likely engaged in new interactions with other PLGA molecules. Additionally the only feature in the FTIR results that could indicate the presence of Me:IBU (3:1) in NPs is the peak near 1513 cm^{-1}, which corresponds to C=C and C=O vibrations and is also present in the Me:IBU (3:1) (Figure 31). These suggest potential interactions between Me:IBU (3:1) and the NPs, either on the surface or within the NPs. Furthermore, confirming the encapsulation of Me:IBU (3:1) recurring to other methods as HPLC is necessary to confirm successful encapsulation.

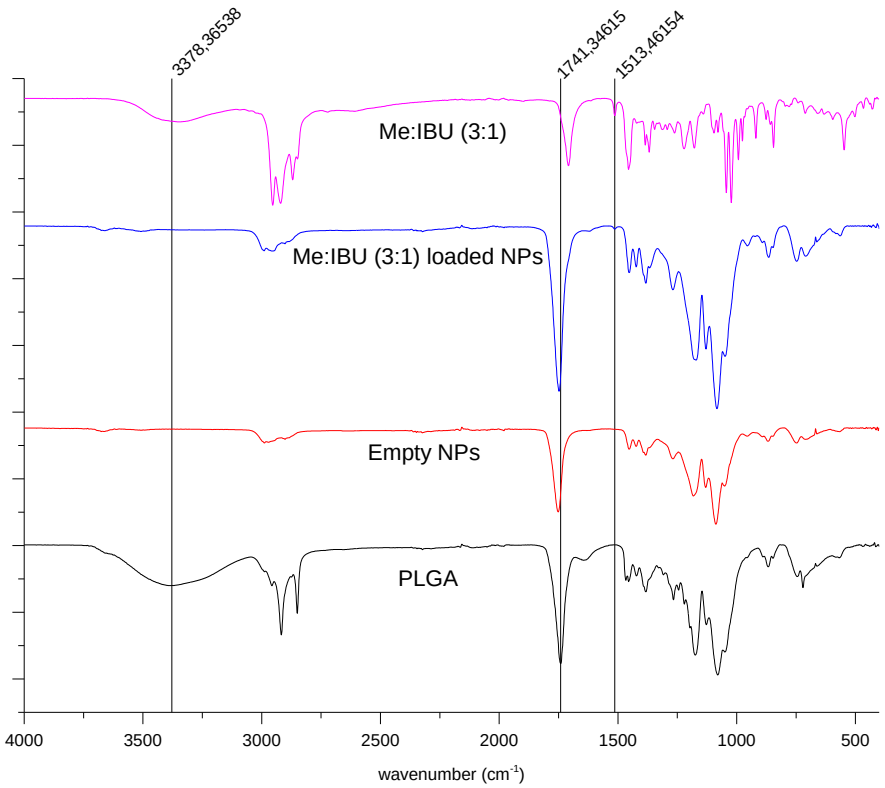

Figure 31: ATR-FTIR analysis of the lyophilized empty and Me:IBU (3:1)-loaded PLGA NPs formulated by nanoprecipitation.

4.3.4. Osmolarity

Additionally, since some of the NPs were in water, it is important to measure the osmolarity of the samples that came into contact with the cells. This ensures that any observed changes in cell viability are due to alterations in osmolarity or water flux, which could otherwise affect cell health independently of the treatment (Table 4).

Table 4: Osmolarities of the PLGA NPs formulated in PBS and water, and the respective standard deviations (SD).

Samples	Osmolarity (mOsm/kg)
Me:IBU (3:1)-loaded NPs in water	0.004 ± 0.001
Me:IBU (3:1)-loaded NPs in water + RPMI (1:1)	132.000 ± 29.513
Empty NPs in PBS	1228.000 ± 10.149
Empty NPs in PBS + RPMI (1:1)	642.000 ± 9.539
PBS	281.666 ± 1.528
RPMI	260.000 ± 1.000

It would be expected that the low osmolarity Me:IBU (3:1)-loaded NPs in water + RPMI (132 mOsmol/kg) would cause hypotonic stress, leading to potential cell swelling and lysis, and the high osmolarity of empty NPs in PBS diluted with RPMI (642 mOsmol/kg) would induce hypertonic stress, leading to dehydration and reduced viability at least for the two more concentrated samples, when the dilution is 1:1.5 and 1:1. Both conditions deviate significantly from the physiological range (280-320 mOsmol/Kg), even though, antiproliferative and cytotoxic tests were carried out [236].

4.3.5. Antiproliferative Activity of Non-Lyophilized Empty and Me:IBU (3:1)-loaded PLGA NPs formulated in PBS and water

The antiproliferative activity of Me:IBU (3:1)-loaded PLGA NPs formulated in water and PBS, and of the empty PLGA NPs formulated in PBS were also study using MTS and assessing the impact on cells viability. In this case concentrations were not used as unit because the NPs were not lyophilized, and we could not dry our samples despite our efforts. So, several dilutions were done using RPMI to see the impact of the different dilution on cells viability.

The MTS results in HT29 do not suggest any impact on cell viability for the three different NPs tested (Figure 32 A). The MTS assay results indicate that both empty and Me:IBU (3:1)-loaded PLGA NPs are non-toxic to HT29 cells, as cell viability remains consistently above 90 %

across all dilutions. Similar viability trends are observed whether the NPs are prepared in water or PBS, suggesting that neither PBS or water adversely affect the formulations.

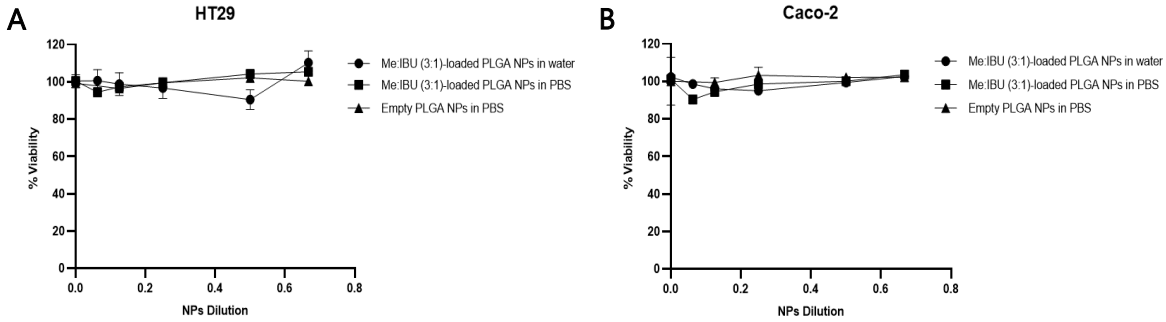

Figure 32: A) HT29 cells viability upon 24 hours of exposure to the non-lyophilized empty and Me:IBU (3:1)-loaded PLGA NPs formulated in PBS and water; B) Caco-2 cells viability upon 24 hours of exposure to the non-lyophilized empty and Me:IBU (3:1)-loaded PLGA NPs formulated in PBS and water.

The maintenance of cell viability after exposer to empty NPs suggests that the NPs carrier itself are non-toxic to HT29 cells. M. M. El-Hammadi *et al.*, reported low toxicity of PLGA NPs in HT29 cell line, proving PLGA NPs biocompatibility [237]. However, the lack of a significant effect with the loaded NPs raises several possibilities: the concentration of NPs used may have been insufficient to reach the EC_{50} of the Me:IBU (3:1), the drug may not have been successfully encapsulated, or the PLGA NPs may have failed to enter the cells and release the THEDES, assuming that successful encapsulation was achieved.

The cytotoxicity of PLGA NPs in Caco-2 cells of empty PLGA NPs in PBS, Me:IBU (3:1)-loaded PLGA NPs in PBS and Me:IBU (3:1)-loaded PLGA NPs formulated in water were also evaluated (Figure 32 B). The results indicate that cell viability remained above 90 % across all dilutions and conditions, suggesting minimal cytotoxic effects. Interestingly, while there were slight fluctuations in cell viability, none of the conditions caused a significant decrease, with viability generally around 100 %. This outcome suggests that both empty and Me:IBU (3:1)-loaded PLGA NPs are well-tolerated by Caco-2 cells, whether prepared in PBS or water. Therefore, these PLGA formulations appear to be biocompatible and do not adversely affect the viability of colorectal cells, supporting their potential use in therapeutic applications. However, as previously pointed out, the absence of a significant impact on cell viability could be due to an insufficient concentration of NPs.

To evaluate if the nanoparticles could be internalized by the cells further studies were conducted.

4.4. Cellular Uptake of FITC-dextran and Nile Red-loaded PLGA NPs

The cellular uptake of the NPs is a key to predict the therapeutic efficacy of the NPs as DDS. To study if cells can incorporate the NPs, two fluorescent dyes were encapsulated in PLGA

NPs: FITC and Nile Red. The FITC and Nile Red-loaded NPs were formulated in PBS and water, respectively, using the same nanoprecipitation method as the empty NPs and the Me:IBU (3:1)-loaded NPs. FITC-dextran, a hydrophilic dye, is commonly used to assess NPs uptake [238]. Nile Red, on the other hand, is a hydrophobic dye often employed for similar purposes, that was used to simulate our hydrophobic THEDES [239], [240].

The successful encapsulation of both FITC-dextran and Nile Red in PLGA NPs, was confirmed through fluorescence microscopy, with distinct green and red fluorescence, respectively (Figure 33). The FITC-dextran-loaded NPs showed uniform green fluorescence, indicating effective encapsulation. This suggests that the hydrophilic FITC-dextran helped maintain even distribution of the NPs in the aqueous environment, minimizing aggregation. The encapsulation of Nile Red was successful in water, similar to what we observed with non-lyophilized Me:IBU-loaded PLGA NPs formulated in water.

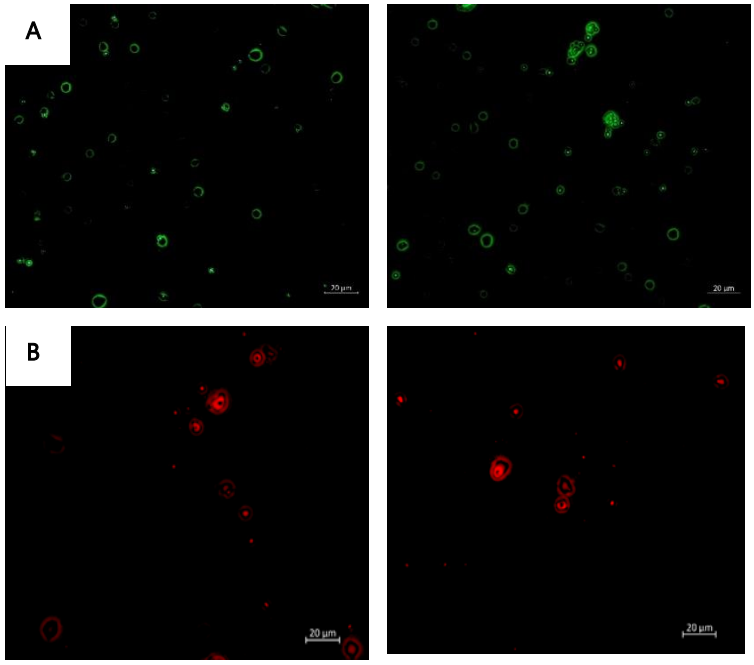

Figure 33: Fluorescent microscopy images of A) FITC-dextran-loaded PLGA NPs; B) Nile Red-loaded PLGA NPs.

Furthermore, HT29 cells were exposed to loaded FITC-dextran during 24 hours (Figure 34). Fluorescent microscopy images clearly demonstrate the successful internalization of the FITC-dextran-loaded NPs by the cells. The green fluorescence observed within the cytoplasm confirms that the NPs were taken up by the cells and are distributed throughout the intracellular environment. The PLGA NPs uptake by HT29 are in accordance with literature. Sasaki K *et al.*, reported the same phenomena [241]. The presence of localized clusters of fluorescence suggests potential aggregation or sequestration of the NPs within specific organelles or vesicular compartments. The co-localization of these signals with the cellular structures stained, nucleus (blue) and actin filamentous (yellow/orange), further validates their intracellular pres-

ence. This suggests that, despite of the challenges encounter in this path, the nanoprecipitation method is efficiently in producing NPs that are capable of being internalized by cells, making them promising candidates for further studies in drug delivery.

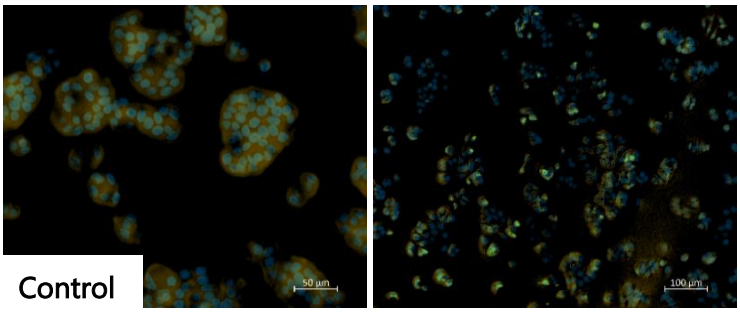

Figure 34: Fluorescent microscopy images of cellular uptake of FITC-dextran-loaded PLGA NPs by HT29 cells.

The next step is to evaluate the incorporation of Nile Red-loaded PLGA into cells. Testing these NPs would have been crucial, as they mimic the Me:IBU (3:1)-loaded PLGA NPs, given that both the dye and THEDES are hydrophobic. Evaluating their cellular uptake would provide insights into how well these particles can deliver hydrophobic compounds.

The mechanism of cellular uptake for NPs is influenced by several factors, including the size, surface charge, and morphology of the NPs. NPs within this size range are generally too large for passive diffusion and instead enter cells through active uptake processes. The primary mechanism for the cellular uptake of PLGA NPs is clathrin-mediated endocytosis, as reported by Malinovskaya *et al.* Despite that, Oliveira *et al.*, described cellular uptake though caveolae-mediated endocytosis [242]. However, Xu *et al.*, observed that PLGA NPs may not always be efficiently internalized by cells, potentially delivering their drug outside the cells [243]. Once inside the cell, Malinovskaya *et al.*, highlight that PLGA NPs are typically localized within the endo-lysosomal compartment, where the encapsulated drug is released to reach its intended target site [244].

4.5. Me:IBU (3:1) Encapsulation Efficiency

The encapsulation efficiency of Me:IBU (3:1) within PLGA NPs is a critical parameter to continue with cell assays and further evaluate the success of the formulation and its potential therapeutic application. In this study, attempts were made to quantify the encapsulation efficiency, through IBU detection, using HPLC via both direct and indirect methods. The direct method involved measuring the amount of Me:IBU (3:1) encapsulated within the NPs after the formulation process by degradation of the PLGA, while the indirect method calculated the encapsulation efficiency by quantifying the unencapsulated drug remaining in the supernatant of the dialysis.

Despite multiple trials, accurate quantification of the encapsulation efficiency proved to be challenging. It was not possible to determinate the Me:IBU (3:1) encapsulation efficiency (Table 5). Ibuprofen was chosen for HPLC quantification because there is a well-established,

validated method for this compound, and its sensitivity is sufficient to accurately detect the concentrations used. Furthermore, quantifying just one of the components of the THEDES simplifies the analysis, making it easier to assess drug content, encapsulation efficiency, and overall formulation quality.

Table 5: Direct and indirect quantification of Me:IBU (3:1) in PLGA NPs formulated by nanoprecipitation by HPLC.

	IBU (mg)	Total amount of IBU quantified by HPLC (mg)	IBU used to formulate NPs (mg)	Me:IBU (3:1) used to formulate NPs (mg)
Indirect quantification of sample 1	0.087	1.249	22.72	74.5
Direct quantification of sample 1	1.162			
Indirect quantification of sample 2	0.514	1.696		
Direct quantification of sample 2	1.181			

The HPLC analysis of the dialysate supernatant and the Me:IBU (3:1) encapsulated in the NPs, revealed that the total amount of THEDES detected was significantly lower than the initial quantity added. Several factors may account for this discrepancy. One potential explanation is the incomplete extraction of Me:IBU (3:1) from the PLGA matrix during direct analysis. Additionally, the precipitation of PLGA during NPs formation may have led to some THEDES binding to the polymer due to their hydrophobic properties.

The indirect method also faced limitations, particularly due to the low solubility of Me:IBU (3:1) in the aqueous medium used for NPs formulation, which led to unreliable measurements of the unencapsulated drug. As a result, the HPLC readings of Me:IBU (3:1) may not accurately represent the total content in the sample.

Interestingly, when combining the results from both the direct and indirect methods, the total amount of THEDES detected was approximately more than ten times lower than what was initially added. Initially, we targeted a concentration of two times the EC_{50}, but due to these encapsulation challenges, we increased the concentration to approximately five times the EC_{50} (≈74.5 mg of Me:IBU (3:1)) that corresponds to 22.72 mg of IBU, to enhance the likelihood of successful loading and to investigate this phenomenon more precisely.

These difficulties show the complexity of encapsulating a hydrophobic DES like Me:IBU (3:1) within PLGA NPs. The unique physicochemical properties of THEDES, particularly its ability

to interact strongly with the PLGA matrix, may have led to partial encapsulation, irregular drug distribution, or even drug-polymer interactions that do not allow an effective encapsulation.

4.6. Conclusion and Futures Perspectives

To successfully deliver THEDES to CRC cells using PLGA NPs, it is essential that these NPs demonstrate stability, monodispersity, high encapsulation efficiency, and appropriate size and morphology. These critical attributes can be tailored by carefully selecting the preparation methods and fine-tuning key parameters.

Despite efforts using the emulsion-solvent evaporation method, achieving consistent and stable formulations of both empty and Me:IBU (3:1)-loaded PLGA NPs remains challenging. However, it was possible to conclude that an increase in polymer concentration correlates with a larger NPs size. However, varying the PVA concentration within the tested range did not result in significant differences. Additionally, NPs aggregation was observed after centrifugation and lyophilization, that was likely due to surfactant effects. Attempts to resolve this issue by increasing the number of washes and decreasing centrifugation speed were unsuccessful. Consequently, a surfactant-free nanoprecipitation method was employed, though some aggregation persisted due to lyophilization.

Eliminating the lyophilization step improved the stability of the NPs formulated by nanoprecipitation, yet stability remained highly dependent on the dispersion medium. Specifically, empty PLGA NPs were stable only in PBS, while Me:IBU (3:1)-loaded NPs were stable only in water, suggesting that THEDES plays a role in stabilizing PLGA NPs in water. The antiproliferative and cytotoxicity assays were inconclusive, possibly due to the range of non-lyophilized NPs concentrations used. Additionally, it was not possible to assess the encapsulation efficiency of THEDES.

The cellular uptake assay demonstrated successful encapsulation of FITC-dextran-loaded PLGA NPs in HT29 cells. However, the results for Nile Red encapsulated NPs were not possible to be evaluated during this work.

Several key areas require attention to enhance the development of these NPs. First, the optimization of the formation of stable and small NPs as well the improvement of encapsulation efficiency is critical. The current inability to accurately determine encapsulation efficiency has impeded progress in evaluating the biological effects of the formulations. Without precise concentration data, drawing reliable conclusions from antiproliferative and cytotoxicity assays is challenging. Future work could involve exploring alternative methodologies such as microfluidics or supercritical CO_2 techniques, both of which offer finer control over NP size, stability, and encapsulation efficiency [245], [246].

Second, the exploration of advanced characterization techniques, such as NMR and MS, could provide deeper insights into the encapsulation process and drug-polymer interactions.

These techniques could complement traditional methods, like HPLC, by offering a more detailed understanding of the physicochemical properties of the NPs, thus guiding further optimization [247], [248].

Third, while the initial goal of incorporating the NPs into 130 nm HIV VLPs for targeted delivery was not achievable due to size limitations, alternative strategies could be explored for PLGA NPs. For instance, surface modifications, such as PEG coating, can improve circulation time and reduce immunogenicity [249]. Incorporating targeting molecules, such as CD44, could enhance specificity for colorectal cancer cells [250]. Although these larger NPs might not fully benefit from the EPR effect, targeted delivery mechanisms, such as ligand-mediated targeting could still be effective [251].

Finally, further investigation into the drug release kinetics and the long-term stability of the NPs in various physiological conditions is necessary. This includes studying the behavior of the NPs in complex biological environments, such as blood plasma, to ensure that the formulations maintain their integrity and efficacy over time. Additionally, exploring the use of stimuli-responsive polymers or coatings could offer controlled drug release in response to specific triggers within the target tissue, further enhancing therapeutic outcomes [252].

BIBLIOGRAPHY

[1] "Oldest descriptions of cancer q." Acessed: Mar. 09, 24. [Online]. Available: www.cancer.org/cancer/understanding-cancer/what-is-cancer.html

[2] "Cancer Today." Accessed: Mar. 09, 2024. [Online]. Available: https://gco.iarc.fr/today/en/dataviz/tables?mode=population&age_end=17&types=1&group_populations=0&multiple_populations=1

[3] H. Sung *et al.*, "Global Cancer Statistics 2020: GLOBOCAN Estimates of Incidence and Mortality Worldwide for 36 Cancers in 185 Countries," *CA Cancer J Clin*, vol. 71, no. 3, pp. 209–249, May 2021, doi: 10.3322/caac.21660.

[4] "Statistics at a glance, 2022 Top 5 most frequent cancers." Accessed Mar. 09, 2024. [Online]. Available: https://gco.iarc.who.int/media/globocan/factsheets/populations/620-portugal-fact-sheet.pdf

[5] C. Mattiuzzi and G. Lippi, "Current Cancer Epidemiology," *J Epidemiol Glob Health*, vol. 9, no. 4, p. 217, 2019, doi: 10.2991/jegh.k.191008.001.

[6] Cancer (WHO)." Accessed: Mar.15, 2024. [Online]. Available: www.who.int/health-topics/cancer#tab=tab_1.

[7] M. S. Lawrence *et al.*, "Mutational heterogeneity in cancer and the search for new cancer-associated genes," *Nature*, vol. 499, no. 7457, pp. 214–218, Jul. 2013, doi: 10.1038/nature12213.

[8] A. Z. Ayob and T. S. Ramasamy, "Cancer stem cells as key drivers of tumour progression," *J Biomed Sci*, vol. 25, no. 1, p. 20, Dec. 2018, doi: 10.1186/s12929-018-0426-4.

[9] *Cancer and the Environment*. Washington, D.C.: National Academies Press, 2002. doi: 10.17226/10464.

[10] Y. Wen *et al.*, "Chronic inflammation, cancer development and immunotherapy," *Front Pharmacol*, vol. 13, Oct. 2022, doi: 10.3389/fphar.2022.1040163.

[11] K. J. Barnum and M. J. O'Connell, "Cell Cycle Regulation by Checkpoints," 2014, pp. 29–40. doi: 10.1007/978-1-4939-0888-2_2.

[12] E. Y. H. P. Lee and W. J. Muller, "Oncogenes and Tumor Suppressor Genes," *Cold Spring Harb Perspect Biol*, vol. 2, no. 10, pp. a003236–a003236, Oct. 2010, doi: 10.1101/cshperspect.a003236.

[13] A. Karagiannakos *et al.*, "Targeting Oncogenic Pathways in the Era of Personalized Oncology: A Systemic Analysis Reveals Highly Mutated Signaling Pathways in Cancer Patients and Potential Therapeutic Targets," *Cancers (Basel)*, vol. 14, no. 3, p. 664, Jan. 2022, doi: 10.3390/cancers14030664.

[14] N. Datta, S. Chakraborty, M. Basu, and M. K. Ghosh, "Tumor Suppressors Having Oncogenic Functions: The Double Agents," *Cells*, vol. 10, no. 1, p. 46, Dec. 2020, doi: 10.3390/cells10010046.

[15] F. Grizzi *et al.*, "Cancer initiation and progression: an unsimplifiable complexity," *Theor Biol Med Model*, vol. 3, no. 1, p. 37, Dec. 2006, doi: 10.1186/1742-4682-3-37.

[16] G.-S. Chaudhry, A. Md Akim, Y. Y. Sung, and T. M. T. Sifzizul, "Cancer and apoptosis: The apoptotic activity of plant and marine natural products and their potential as targeted cancer therapeutics," *Front Pharmacol*, vol. 13, Aug. 2022, doi: 10.3389/fphar.2022.842376.

[17] A. Patel, "Benign vs Malignant Tumors," *JAMA Oncol*, vol. 6, no. 9, p. 1488, Sep. 2020, doi: 10.1001/jamaoncol.2020.2592.

[18] S. Guo and C.-X. Deng, "Effect of Stromal Cells in Tumor Microenvironment on Metastasis Initiation," *Int J Biol Sci*, vol. 14, no. 14, pp. 2083–2093, 2018, doi: 10.7150/ijbs.25720.

[19] F. R. Greten and S. I. Grivennikov, "Inflammation and Cancer: Triggers, Mechanisms, and Consequences," *Immunity*, vol. 51, no. 1, pp. 27–41, Jul. 2019, doi: 10.1016/j.immuni.2019.06.025.

[20] E. Aboud-Pirak, E. Hurwitz, M. E. Pirak, F. Bellot, J. Schlessinger, and M. Sela, "Efficacy of Antibodies to Epidermal Growth Factor Receptor Against KB Carcinoma In Vitro and in Nude Mice," *JNCI Journal of the National Cancer Institute*, vol. 80, no. 20, pp. 1605–1611, Dec. 1988, doi: 10.1093/jnci/80.20.1605.

[21] M. Greaves and C. C. Maley, "Clonal evolution in cancer," *Nature*, vol. 481, no. 7381, pp. 306–313, Jan. 2012, doi: 10.1038/nature10762.

[22] X. Pan and L. Zheng, "Epigenetics in modulating immune functions of stromal and immune cells in the tumor microenvironment," *Cell Mol Immunol*, vol. 17, no. 9, pp. 940–953, Sep. 2020, doi: 10.1038/s41423-020-0505-9.

[23] N. Nishida, H. Yano, T. Nishida, T. Kamura, and M. Kojiro, "Angiogenesis in cancer," *Vasc Health Risk Manag*, vol. 2, no. 3, pp. 213–219, Aug. 2006, doi: 10.2147/vhrm.2006.2.3.213.

[24] R. Baghban *et al.*, "Tumor microenvironment complexity and therapeutic implications at a glance," *Cell Communication and Signaling*, vol. 18, no. 1, p. 59, Dec. 2020, doi: 10.1186/s12964-020-0530-4.

[25] C. M. Neophytou, M. Panagi, T. Stylianopoulos, and P. Papageorgis, "The Role of Tumor Microenvironment in Cancer Metastasis: Molecular Mechanisms and Therapeutic Opportunities," *Cancers (Basel)*, vol. 13, no. 9, p. 2053, Apr. 2021, doi: 10.3390/cancers13092053.

[26] P. Nistico, M. J. Bissell, and D. C. Radisky, "Epithelial-Mesenchymal Transition: General Principles and Pathological Relevance with Special Emphasis on the Role of Matrix Metalloproteinases," *Cold Spring Harb Perspect Biol*, vol. 4, no. 2, pp. a011908–a011908, Feb. 2012, doi: 10.1101/cshperspect.a011908.

[27] G. Manfioletti and M. Fedele, "Epithelial–Mesenchymal Transition (EMT) 2021," *Int J Mol Sci*, vol. 23, no. 10, p. 5848, May 2022, doi: 10.3390/ijms23105848.

[28] H. Zhao *et al.*, "Inflammation and tumor progression: signaling pathways and targeted intervention," *Signal Transduct Target Ther*, vol. 6, no. 1, p. 263, Jul. 2021, doi: 10.1038/s41392-021-00658-5.

[29] R. J. Birch *et al.*, "Inflammatory Bowel Disease-Associated Colorectal Cancer Epidemiology and Outcomes: An English Population-Based Study," *American Journal of Gastroenterology*, vol. 117, no. 11, pp. 1858–1870, Nov. 2022, doi: 10.14309/ajg.0000000000001941.

[30] "Colorectal cancer." Accessed: Mar. 16, 2024. [Online]. Available: https://www.who.int/news-room/fact-sheets/detail/colorectal-cancer

[31] "In just ten years, colorectal cancer cases have doubled in people under 50 | Champalimaud Foundation." Accessed: Mar. 16, 2024. [Online]. Available: https://fchampalimaud.org/news/just-ten-years-colorectal-cancer-cases-have-doubled-people-under-50-0

[32] T. Sawicki, M. Ruszkowska, A. Danielewicz, E. Niedźwiedzka, T. Arłukowicz, and K. E. Przybyłowicz, "A Review of Colorectal Cancer in Terms of Epidemiology, Risk Factors, Development, Symptoms and Diagnosis," *Cancers (Basel)*, vol. 13, no. 9, p. 2025, Apr. 2021, doi: 10.3390/cancers13092025.

[33] R. L. Siegel, N. S. Wagle, A. Cercek, R. A. Smith, and A. Jemal, "Colorectal cancer statistics, 2023," *CA Cancer J Clin*, vol. 73, no. 3, pp. 233–254, May 2023, doi: 10.3322/caac.21772.

[34] A. K. Lofters *et al.*, "Cancer Screening Disparities Before and After the COVID-19 Pandemic," *JAMA Netw Open*, vol. 6, no. 11, p. e2343796, Nov. 2023, doi: 10.1001/jamanetworkopen.2023.43796.

[35] K. Szymańska, "Cancers of the Colorectum. Diagnosis and Treatment," in *Reference Module in Biomedical Sciences*, Elsevier, 2018. doi: 10.1016/B978-0-12-801238-3.65304-7.

[36] H. Yamagishi, H. Kuroda, Y. Imai, and H. Hiraishi, "Molecular pathogenesis of sporadic colorectal cancers," *Chin J Cancer*, vol. 35, no. 1, p. 4, Dec. 2016, doi: 10.1186/s40880-015-0066-y.

[37] K. W. Jasperson, T. M. Tuohy, D. W. Neklason, and R. W. Burt, "Hereditary and Familial Colon Cancer," *Gastroenterology*, vol. 138, no. 6, pp. 2044–2058, May 2010, doi: 10.1053/j.gastro.2010.01.054.

[38] S. C. Shah and S. H. Itzkowitz, "Colorectal Cancer in Inflammatory Bowel Disease: Mechanisms and Management," *Gastroenterology*, vol. 162, no. 3, pp. 715-730.e3, Mar. 2022, doi: 10.1053/j.gastro.2021.10.035.

[39] W.-Y. Dan, G.-Z. Zhou, L.-H. Peng, and F. Pan, "Update and latest advances in mechanisms and management of colitis-associated colorectal cancer," *World J Gastrointest Oncol*, vol. 15, no. 8, pp. 1317–1331, Aug. 2023, doi: 10.4251/wjgo.v15.i8.1317.

[40] C. Lengauer, K. W. Kinzler, and B. Vogelstein, "Genetic instabilities in human cancers," *Nature*, vol. 396, no. 6712, pp. 643–649, Dec. 1998, doi: 10.1038/25292.

[41] M. S. Pino and D. C. Chung, "The Chromosomal Instability Pathway in Colon Cancer," *Gastroenterology*, vol. 138, no. 6, pp. 2059–2072, May 2010, doi: 10.1053/j.gastro.2009.12.065.

[42] W. Hankey, W. L. Frankel, and J. Groden, "Functions of the APC tumor suppressor protein dependent and independent of canonical WNT signaling: implications for therapeutic targeting," *Cancer and Metastasis Reviews*, vol. 37, no. 1, pp. 159–172, Mar. 2018, doi: 10.1007/s10555-017-9725-6.

[43] Y. Zhou, Y. Kuang, C. Wang, Y. Yu, L. Pan, and X. Hu, "Impact of KRAS mutation on the tumor microenvironment in colorectal cancer," *Int J Biol Sci*, vol. 20, no. 5, pp. 1947–1964, 2024, doi: 10.7150/ijbs.88779.

[44] J. N. Nojadeh, S. Behrouz Sharif, and E. Sakhinia, "Microsatellite instability in colorectal cancer.," *EXCLI J*, vol. 17, pp. 159–168, 2018, doi: 10.17179/excli2017-948.

[45] F. Jasmine *et al.*, "Interaction between Microsatellite Instability (MSI) and Tumor DNA Methylation in the Pathogenesis of Colorectal Carcinoma," *Cancers (Basel)*, vol. 13, no. 19, p. 4956, Oct. 2021, doi: 10.3390/cancers13194956.

[46] Caputo *et al.*, "BRAF-Mutated Colorectal Cancer: Clinical and Molecular Insights," *Int J Mol Sci*, vol. 20, no. 21, p. 5369, Oct. 2019, doi: 10.3390/ijms20215369.

[47] N. Rampino *et al.*, "Somatic Frameshift Mutations in the *BAX* Gene in Colon Cancers of the Microsatellite Mutator Phenotype," *Science (1979)*, vol. 275, no. 5302, pp. 967–969, Feb. 1997, doi: 10.1126/science.275.5302.967.

[48] J. Borowczak *et al.*, "The Role of Inflammatory Cytokines in the Pathogenesis of Colorectal Carcinoma—Recent Findings and Review," *Biomedicines*, vol. 10, no. 7, p. 1670, Jul. 2022, doi: 10.3390/biomedicines10071670.

[49] M. Yashiro, K. Hirakawa, and C. R. Boland, "Mutations in TGFbeta-RII and BAXmediate tumor progression in the later stages of colorectal cancer with microsatellite instability," *BMC Cancer*, vol. 10, no. 1, p. 303, Dec. 2010, doi: 10.1186/1471-2407-10-303.

[50] F. De Palma, V. D'Argenio, J. Pol, G. Kroemer, M. Maiuri, and F. Salvatore, "The Molecular Hallmarks of the Serrated Pathway in Colorectal Cancer," *Cancers (Basel)*, vol. 11, no. 7, p. 1017, Jul. 2019, doi: 10.3390/cancers11071017.

[51] R. W. Zhou, N. Harpaz, S. H. Itzkowitz, and R. E. Parsons, "Molecular mechanisms in colitis-associated colorectal cancer," *Oncogenesis*, vol. 12, no. 1, p. 48, Oct. 2023, doi: 10.1038/s41389-023-00492-0.

[52] A. I. Robles *et al.*, "Whole-Exome Sequencing Analyses of Inflammatory Bowel Disease–Associated Colorectal Cancers," *Gastroenterology*, vol. 150, no. 4, pp. 931–943, Apr. 2016, doi: 10.1053/j.gastro.2015.12.036.

[53] Y. Lin *et al.*, " Progress in Understanding the IL-6/STAT3 Pathway in Colorectal Cancer ," *Onco Targets Ther*, vol. Volume 13, pp. 13023–13032, Dec. 2020, doi: 10.2147/OTT.S278013.

[54] T. V. Velikova, L. Miteva, N. Stanilov, Z. Spassova, and S. A. Stanilova, "Interleukin-6 compared to the other Th17/Treg related cytokines in inflammatory bowel disease and colorectal cancer," *World J Gastroenterol*, vol. 26, no. 16, pp. 1912–1925, Apr. 2020, doi: 10.3748/wjg.v26.i16.1912.

[55] J. I Young, J. E. Hooper, K. C. Lu, D. O. Herzig, and V. L. Tsikitis, "Serrated polyposis syndrome," *Colorectal Cancer*, vol. 3, no. 4, pp. 375–386, Aug. 2014, doi: 10.2217/crc.14.23.

[56] W. H. Liggett and D. Sidransky, "Role of the p16 tumor suppressor gene in cancer.," *Journal of Clinical Oncology*, vol. 16, no. 3, pp. 1197–1206, Mar. 1998, doi: 10.1200/JCO.1998.16.3.1197.

[57] Ł. Szylberg, M. Janiczek, A. Popiel, and A. Marszałek, "Expression of COX-2, IL-1β, TNF-α and IL-4 in epithelium of serrated adenoma, adenoma and hyperplastic polyp," *Archives of Medical Science*, vol. 1, pp. 172–178, 2016, doi: 10.5114/aoms.2016.57594.

[58] T. Zhang, C. Ma, Z. Zhang, H. Zhang, and H. Hu, "NF-κB signaling in inflammation and cancer," *MedComm (Beijing)*, vol. 2, no. 4, pp. 618–653, Dec. 2021, doi: 10.1002/mco2.104.

[59] J. Borowczak *et al.*, "The Role of Inflammatory Cytokines in the Pathogenesis of Colorectal Carcinoma—Recent Findings and Review," *Biomedicines*, vol. 10, no. 7, p. 1670, Jul. 2022, doi: 10.3390/biomedicines10071670.

[60] A. A. Bhat *et al.*, "Cytokine- and chemokine-induced inflammatory colorectal tumor microenvironment: Emerging avenue for targeted therapy," *Cancer Commun*, vol. 42, no. 8, pp. 689–715, Aug. 2022, doi: 10.1002/cac2.12295.

[61] A. G. Vaiopoulos, K. Ch. Athanasoula, and A. G. Papavassiliou, "NF-κB in colorectal cancer," *J Mol Med*, vol. 91, no. 9, pp. 1029–1037, Sep. 2013, doi: 10.1007/s00109-013-1045-x.

[62] C. Disoma, Y. Zhou, S. Li, J. Peng, and Z. Xia, "Wnt/β-catenin signaling in colorectal cancer: Is therapeutic targeting even possible?," *Biochimie*, vol. 195, pp. 39–53, Apr. 2022, doi: 10.1016/j.biochi.2022.01.009.

[63] N. Nada, "Role of Cyclooxygenase-2 in colorectal cancer patients," *Frontiers in Bioscience*, vol. 26, no. 4, p. 4914, 2021, doi: 10.2741/4914.

[64] S. Nakatsugi *et al.*, "Suppression of Intestinal Polyp Development by Nimesulide, a Selective Cyclooxygenase-2 Inhibitor, in Min Mice," *Japanese Journal of Cancer Research*, vol. 88, no. 12, pp. 1117–1120, Dec. 1997, doi: 10.1111/j.1349-7006.1997.tb00337.x.

[65] J. F. Evans, "Rofecoxib (Vioxx), a Specific Cyclooxygenase-2 Inhibitor, Is Chemopreventive in a Mouse Model of Colon Cancer," *Am J Clin Oncol*, vol. 26, no. Supplement 2, pp. S62–S65, Aug. 2003, doi: 10.1097/01.COC.0000074159.05087.50.

[66] G. Rashid *et al.*, "Non-steroidal anti-inflammatory drugs and biomarkers: A new paradigm in colorectal cancer," *Front Med (Lausanne)*, vol. 10, Mar. 2023, doi: 10.3389/fmed.2023.1130710.

[67] C. Stolfi, V. De Simone, F. Pallone, and G. Monteleone, "Mechanisms of Action of Non-Steroidal Anti-Inflammatory Drugs (NSAIDs) and Mesalazine in the Chemoprevention of Colorectal Cancer," *Int J Mol Sci*, vol. 14, no. 9, pp. 17972–17985, Sep. 2013, doi: 10.3390/ijms140917972.

[68] V. Grossi, "p38α MAPK pathway: A key factor in colorectal cancer therapy and chemoresistance," *World J Gastroenterol*, vol. 20, no. 29, p. 9744, 2014, doi: 10.3748/wjg.v20.i29.9744.

[69] A. Kumar, V. Gautam, A. Sandhu, K. Rawat, A. Sharma, and L. Saha, "Current and emerging therapeutic approaches for colorectal cancer: A comprehensive review," *World J Gastrointest Surg*, vol. 15, no. 4, pp. 495–519, Apr. 2023, doi: 10.4240/wjgs.v15.i4.495.

[70] C. J. H. van de Velde *et al.*, "EURECCA colorectal: Multidisciplinary management: European consensus conference colon & rectum," *Eur J Cancer*, vol. 50, no. 1, pp. 1.e1-1.e34, Jan. 2014, doi: 10.1016/j.ejca.2013.06.048.

[71] M. Pahwa, A. R. Pahwa, M. Girotra, R. R. Abrahm, S. Kathuria, and A. Sharma, "Defining the Pros and Cons of Open, Conventional Laparoscopy, and Robot-Assisted Pyeloplasty in a Developing Nation," *Adv Urol*, vol. 2014, pp. 1–6, 2014, doi: 10.1155/2014/850156.

[72] PDQ Screening and Prevention Editorial Board, *Colorectal Cancer Screening (PDQ®): Patient Version*. 2002.

[73] A. M. Gonzalez-Angulo and J. Fuloria, "The role of chemotherapy in colon cancer.," *Ochsner journal*, vol. 4, no. 3, pp. 163–7, 2002.

[74] M. Koopman *et al.*, "Sequential versus combination chemotherapy with capecitabine, irinotecan, and oxaliplatin in advanced colorectal cancer (CAIRO): a phase III randomised controlled trial," *The Lancet*, vol. 370, no. 9582, pp. 135–142, Jul. 2007, doi: 10.1016/S0140-6736(07)61086-1.

[75] K. Hwang, J. H. Yoon, J. H. Lee, and S. Lee, "Recent Advances in Monoclonal Antibody Therapy for Colorectal Cancers," *Biomedicines*, vol. 9, no. 1, p. 39, Jan. 2021, doi: 10.3390/biomedicines9010039.

[76] W. Sun, "Angiogenesis in metastatic colorectal cancer and the benefits of targeted therapy," *J Hematol Oncol*, vol. 5, no. 1, p. 63, Dec. 2012, doi: 10.1186/1756-8722-5-63.

[77] M. García-Aranda and M. Redondo, "Targeting Receptor Kinases in Colorectal Cancer," *Cancers (Basel)*, vol. 11, no. 4, p. 433, Mar. 2019, doi: 10.3390/cancers11040433.

[78] G. Golshani and Y. Zhang, "Advances in immunotherapy for colorectal cancer: a review," *Therap Adv Gastroenterol*, vol. 13, p. 175628482091752, Jan. 2020, doi: 10.1177/1756284820917527.

[79] P. Muthukutty and S. Y. Yoo, "Oncolytic Virus Engineering and Utilizations: Cancer Immunotherapy Perspective," *Viruses*, vol. 15, no. 8, p. 1645, Jul. 2023, doi: 10.3390/v15081645.

[80] M. Xu *et al.*, "Cancer Nanomedicine: Emerging Strategies and Therapeutic Potentials," *Molecules*, vol. 28, no. 13, p. 5145, Jun. 2023, doi: 10.3390/molecules28135145.

[81] R. M Singh, R. Pramanik, and S. Hazra, "Role of green chemistry in pharmaceutical industry: a review," *Journal of University of Shanghai for Science and Technology*, vol. 23, no. 12, pp. 291–299, Dec. 2021, doi: 10.51201/JUSST/21/121018.

[82] C. Castiello *et al.*, "GreenMedChem: the challenge in the next decade toward eco-friendly compounds and processes in drug design," *Green Chemistry*, vol. 25, no. 6, pp. 2109–2169, 2023, doi: 10.1039/D2GC03772F.

[83] T. Welton, "Solvents and sustainable chemistry," *Proceedings of the Royal Society A: Mathematical, Physical and Engineering Sciences*, vol. 471, no. 2183, p. 20150502, Nov. 2015, doi: 10.1098/rspa.2015.0502.

[84] A. Prabhune and R. Dey, "Green and sustainable solvents of the future: Deep eutectic solvents," *J Mol Liq*, vol. 379, p. 121676, Jun. 2023, doi: 10.1016/j.molliq.2023.121676.

[85] N. M. Stephens and E. A. Smith, "Structure of Deep Eutectic Solvents (DESs): What We Know, What We Want to Know, and Why We Need to Know It," *Langmuir*, vol. 38, no. 46, pp. 14017–14024, Nov. 2022, doi: 10.1021/acs.langmuir.2c02116.

[86] A. T. N. Fajar, T. Hanada, A. D. Hartono, and M. Goto, "Estimating the phase diagrams of deep eutectic solvents within an extensive chemical space," *Commun Chem*, vol. 7, no. 1, p. 27, Feb. 2024, doi: 10.1038/s42004-024-01116-3.

[87] E. Scelsi, A. Angelini, and C. Pastore, "Deep Eutectic Solvents for the Valorisation of Lignocellulosic Biomasses towards Fine Chemicals," *Biomass*, vol. 1, no. 1, pp. 29–59, Jul. 2021, doi: 10.3390/biomass1010003.

[88] Q. Zhang, K. De Oliveira Vigier, S. Royer, and F. Jérôme, "Deep eutectic solvents: syntheses, properties and applications," *Chem Soc Rev*, vol. 41, no. 21, p. 7108, 2012, doi: 10.1039/c2cs35178a.

[89] S. P. Ijardar, V. Singh, and R. L. Gardas, "Revisiting the Physicochemical Properties and Applications of Deep Eutectic Solvents," *Molecules*, vol. 27, no. 4, p. 1368, Feb. 2022, doi: 10.3390/molecules27041368.

[90] "Deep Eutectic Solvents: An Overview of its Application as a 'Green' Extractant," *International Journal of Advanced Research in Chemical Science*, vol. 4, no. 6, 2017, doi: 10.20431/2349-0403.0406003.

[91] M. Zdanowicz, K. Wilpiszewska, and T. Spychaj, "Deep eutectic solvents for polysaccharides processing. A review," *Carbohydr Polym*, vol. 200, pp. 361–380, Nov. 2018, doi: 10.1016/j.carbpol.2018.07.078.

[92] C. Ferreira and M. Sarraguça, "A Comprehensive Review on Deep Eutectic Solvents and Its Use to Extract Bioactive Compounds of Pharmaceutical Interest," *Pharmaceuticals*, vol. 17, no. 1, p. 124, Jan. 2024, doi: 10.3390/ph17010124.

[93] P. Suthar *et al.*, "Deep eutectic solvents (DES): An update on the applications in food sectors," *J Agric Food Res*, vol. 14, p. 100678, Dec. 2023, doi: 10.1016/j.jafr.2023.100678.

[94] M. M. Abdelquader, S. Li, G. P. Andrews, and D. S. Jones, "Therapeutic deep eutectic solvents: A comprehensive review of their thermodynamics, microstructure and drug delivery applications," *European Journal of Pharmaceutics and Biopharmaceutics*, vol. 186, pp. 85–104, May 2023, doi: 10.1016/j.ejpb.2023.03.002.

[95] H. Kaur, S. S. Siwal, V. Kumar, and V. K. Thakur, "Deep Eutectic Solvents toward the Detection and Extraction of Neurotransmitters: An Emerging Paradigm for Biomedical Applications," *Ind Eng Chem Res*, May 2023, doi: 10.1021/acs.iecr.3c00410.

[96] T. Swebocki *et al.*, "Comparison of the Antibacterial Activity of Selected Deep Eutectic Solvents (DESs) and Deep Eutectic Solvents Comprising Organic Acids (OA-DESs) Towards Gram-positive and Gram-negative Species," *Adv Healthc Mater*, Feb. 2024, doi: 10.1002/adhm.202303475.

[97] I. Bashir *et al.*, "Deep eutectic solvents for extraction of functional components from plant-based products: A promising approach," *Sustain Chem Pharm*, vol. 33, p. 101102, Jun. 2023, doi: 10.1016/j.scp.2023.101102.

[98] S. N. Pedro, C. S. R. Freire, A. J. D. Silvestre, and M. G. Freire, "Deep Eutectic Solvents and Pharmaceuticals," *Encyclopedia*, vol. 1, no. 3, pp. 942–963, Sep. 2021, doi: 10.3390/encyclopedia1030072.

[99] M. Hayyan, "Versatile applications of deep eutectic solvents in drug discovery and drug delivery systems: Perspectives and opportunities," *Asian J Pharm Sci*, vol. 18, no. 2, p. 100780, Mar. 2023, doi: 10.1016/j.ajps.2023.100780.

[100] M. H. Zainal-Abidin, M. Hayyan, G. C. Ngoh, W. F. Wong, and T. T. Tok, "Derivation of an anti-cancer drug nanocarrier using a malonic acid-based deep eutectic solvent as a functionalization agent," *J Drug Deliv Sci Technol*, vol. 75, p. 103657, Sep. 2022, doi: 10.1016/j.jddst.2022.103657.

[101] M. Q. Farooq, N. M. Abbasi, E. A. Smith, J. W. Petrich, and J. L. Anderson, "Characterizing the Solvation Characteristics of Deep Eutectic Solvents Composed of Active Pharmaceutical Ingredients as a Hydrogen Bond Donor and/or Acceptor," *ACS Sustain Chem Eng*, vol. 10, no. 9, pp. 3066–3078, Mar. 2022, doi: 10.1021/acssuschemeng.1c08675.

[102] A. Paiva, R. Craveiro, I. Aroso, M. Martins, R. L. Reis, and A. R. C. Duarte, "Natural Deep Eutectic Solvents – Solvents for the 21st Century," *ACS Sustain Chem Eng*, vol. 2, no. 5, pp. 1063–1071, May 2014, doi: 10.1021/sc500096j.

[103] I. M. Aroso *et al.*, "Design of controlled release systems for THEDES—Therapeutic deep eutectic solvents, using supercritical fluid technology," *Int J Pharm*, vol. 492, no. 1–2, pp. 73–79, Aug. 2015, doi: 10.1016/j.ijpharm.2015.06.038.

[104] Y. Cha *et al.*, "Drug repurposing from the perspective of pharmaceutical companies," *Br J Pharmacol*, vol. 175, no. 2, pp. 168–180, Jan. 2018, doi: 10.1111/bph.13798.

[105] L. H. Ng, J. K. U. Ling, and K. Hadinoto, "Formulation Strategies to Improve the Stability and Handling of Oral Solid Dosage Forms of Highly Hygroscopic Pharmaceuticals and Nutraceuticals," *Pharmaceutics*, vol. 14, no. 10, p. 2015, Sep. 2022, doi: 10.3390/pharmaceutics14102015.

[106] P. A. Shah, V. Chavda, D. Hirpara, V. S. Sharma, P. S. Shrivastav, and S. Kumar, "Exploring the potential of deep eutectic solvents in pharmaceuticals: Challenges and opportunities," *J Mol Liq*, vol. 390, p. 123171, Nov. 2023, doi: 10.1016/j.molliq.2023.123171.

[107] C. Lu, J. Cao, N. Wang, and E. Su, "Significantly improving the solubility of non-steroidal anti-inflammatory drugs in deep eutectic solvents for potential non-aqueous liquid administration," *Medchemcomm*, vol. 7, no. 5, pp. 955–959, 2016, doi: 10.1039/C5MD00551E.

[108] C. V. Pereira *et al.*, "Unveil the Anticancer Potential of Limomene Based Therapeutic Deep Eutectic Solvents," *Sci Rep*, vol. 9, no. 1, p. 14926, Oct. 2019, doi: 10.1038/s41598-019-51472-7.

[109] E. Silva, F. Oliveira, J. M. Silva, A. Matias, R. L. Reis, and A. R. C. Duarte, "Optimal Design of THEDES Based on Perillyl Alcohol and Ibuprofen," *Pharmaceutics*, vol. 12, no. 11, p. 1121, Nov. 2020, doi: 10.3390/pharmaceutics12111121.

[110] J. Pereira *et al.*, "Selective terpene based therapeutic deep eutectic systems against colorectal cancer," *European Journal of Pharmaceutics and Biopharmaceutics*, vol. 175, pp. 13–26, Jun. 2022, doi: 10.1016/j.ejpb.2022.04.008.

[111] E. Silva, F. Oliveira, J. M. Silva, R. L. Reis, and A. R. C. Duarte, "Untangling the bioactive properties of therapeutic deep eutectic solvents based on natural terpenes," *Current Research in Chemical Biology*, vol. 1, p. 100003, 2021, doi: 10.1016/j.crchbi.2021.100003.

[112] J. Wang *et al.*, "Deep Eutectic Systems as Novel Vehicles for Assisting Drug Transdermal Delivery," *Pharmaceutics*, vol. 14, no. 11, p. 2265, Oct. 2022, doi: 10.3390/pharmaceutics14112265.

[113] G. Tiwari *et al.*, "Drug delivery systems: An updated review," *Int J Pharm Investig*, vol. 2, no. 1, p. 2, 2012, doi: 10.4103/2230-973X.96920.

[114] J. B. Stenlake, "Bioavailability from pharmaceutical dosage forms," *Analyst*, vol. 99, no. 1185, p. 824, 1974, doi: 10.1039/an9749900824.

[115] S. Øie and J. Huang, "Influence of Administration Route on Drug Delivery to a Target Organ," *J Pharm Sci*, vol. 70, no. 12, pp. 1344–1347, Dec. 1981, doi: 10.1002/jps.2600701214.

[116] S. Adepu and S. Ramakrishna, "Controlled Drug Delivery Systems: Current Status and Future Directions," *Molecules*, vol. 26, no. 19, p. 5905, Sep. 2021, doi: 10.3390/molecules26195905.

[117] T. C. Ezike *et al.*, "Advances in drug delivery systems, challenges and future directions," *Heliyon*, vol. 9, no. 6, p. e17488, Jun. 2023, doi: 10.1016/j.heliyon.2023.e17488.

[118] K. H. Bae, H. J. Chung, and T. G. Park, "Nanomaterials for Cancer Therapy and Imaging," *Mol Cells*, vol. 31, no. 4, pp. 295–302, Apr. 2011, doi: 10.1007/s10059-011-0051-5.

[119] P. Kumari, B. Ghosh, and S. Biswas, "Nanocarriers for cancer-targeted drug delivery," *J Drug Target*, vol. 24, no. 3, pp. 179–191, Mar. 2016, doi: 10.3109/1061186X.2015.1051049.

[120] J. K. Patra *et al.*, "Nano based drug delivery systems: recent developments and future prospects," *J Nanobiotechnology*, vol. 16, no. 1, p. 71, Dec. 2018, doi: 10.1186/s12951-018-0392-8.

[121] J. Nicolas, S. Mura, D. Brambilla, N. Mackiewicz, and P. Couvreur, "Design, functionalization strategies and biomedical applications of targeted biodegradable/biocompatible polymer-based nanocarriers for drug delivery," *Chem. Soc. Rev.*, vol. 42, no. 3, pp. 1147–1235, 2013, doi: 10.1039/C2CS35265F.

[122] J. Fang, H. Nakamura, and H. Maeda, "The EPR effect: Unique features of tumor blood vessels for drug delivery, factors involved, and limitations and augmentation of the effect," *Adv Drug Deliv Rev*, vol. 63, no. 3, pp. 136–151, Mar. 2011, doi: 10.1016/j.addr.2010.04.009.

[123] V. P. Torchilin, "Passive and Active Drug Targeting: Drug Delivery to Tumors as an Example," 2010, pp. 3–53. doi: 10.1007/978-3-642-00477-3_1.

[124] A. Tewabe, A. Abate, M. Tamrie, A. Seyfu, and E. Abdela Siraj, "Targeted Drug Delivery — From Magic Bullet to Nanomedicine: Principles, Challenges, and Future Perspectives," *J Multidiscip Healthc*, vol. Volume 14, pp. 1711–1724, Jul. 2021, doi: 10.2147/JMDH.S313968.

[125] N. Hoshyar, S. Gray, H. Han, and G. Bao, "The Effect of Nanoparticle Size on *In Vivo* Pharmacokinetics and Cellular Interaction," *Nanomedicine*, vol. 11, no. 6, pp. 673–692, Mar. 2016, doi: 10.2217/nnm.16.5.

[126] Y. Yao *et al.*, "Nanoparticle-Based Drug Delivery in Cancer Therapy and Its Role in Overcoming Drug Resistance," *Front Mol Biosci*, vol. 7, Aug. 2020, doi: 10.3389/fmolb.2020.00193.

[127] D. Mishra, J. R. Hubenak, and A. B. Mathur, "Nanoparticle systems as tools to improve drug delivery and therapeutic efficacy," *J Biomed Mater Res A*, vol. 101, no. 12, pp. 3646–3660, Dec. 2013, doi: 10.1002/jbm.a.34642.

[128] L. Cabeza *et al.*, "Nanoparticles in Colorectal Cancer Therapy: Latest In Vivo Assays, Clinical Trials, and Patents," *AAPS PharmSciTech*, vol. 21, no. 5, p. 178, Jul. 2020, doi: 10.1208/s12249-020-01731-y.

[129] Y. H. Yun, B. K. Lee, and K. Park, "Controlled Drug Delivery: Historical perspective for the next generation," *Journal of Controlled Release*, vol. 219, pp. 2–7, Dec. 2015, doi: 10.1016/j.jconrel.2015.10.005.

[130] R. Kashapov *et al.*, "Nanocarriers for Biomedicine: From Lipid Formulations to Inorganic and Hybrid Nanoparticles," *Int J Mol Sci*, vol. 22, no. 13, p. 7055, Jun. 2021, doi: 10.3390/ijms22137055.

[131] P. Siafaka, N. Üstündağ Okur, E. Karavas, and D. Bikiaris, "Surface Modified Multifunctional and Stimuli Responsive Nanoparticles for Drug Targeting: Current Status and Uses," *Int J Mol Sci*, vol. 17, no. 9, p. 1440, Aug. 2016, doi: 10.3390/ijms17091440.

[132] K. Wang, R. Shen, T. Meng, F. Hu, and H. Yuan, "Nano-Drug Delivery Systems Based on Different Targeting Mechanisms in the Targeted Therapy of Colorectal Cancer," *Molecules*, vol. 27, no. 9, p. 2981, May 2022, doi: 10.3390/molecules27092981.

[133] S. B. Lim, A. Banerjee, and H. Önyüksel, "Improvement of drug safety by the use of lipid-based nanocarriers," *Journal of Controlled Release*, vol. 163, no. 1, pp. 34–45, Oct. 2012, doi: 10.1016/j.jconrel.2012.06.002.

[134] J. E. Frampton, "Liposomal Irinotecan: A Review in Metastatic Pancreatic Adenocarcinoma," *Drugs*, vol. 80, no. 10, pp. 1007–1018, Jul. 2020, doi: 10.1007/s40265-020-01336-6.

[135] W. Paul and C. P. Sharma, "Inorganic nanoparticles for targeted drug delivery," in *Biointegration of Medical Implant Materials*, Elsevier, 2010, pp. 204–235. doi: 10.1533/9781845699802.2.204.

[136] F. Danhier, E. Ansorena, J. M. Silva, R. Coco, A. Le Breton, and V. Préat, "PLGA-based nanoparticles: An overview of biomedical applications," *Journal of Controlled Release*, vol. 161, no. 2, pp. 505–522, Jul. 2012, doi: 10.1016/j.jconrel.2012.01.043.

[137] Y. Wang, J. Ma, T. Qiu, M. Tang, X. Zhang, and W. Dong, "In vitro and in vivo combinatorial anticancer effects of oxaliplatin- and resveratrol-loaded N,O-carboxymethyl chitosan nanoparticles against colorectal cancer," *European Journal of Pharmaceutical Sciences*, vol. 163, p. 105864, Aug. 2021, doi: 10.1016/j.ejps.2021.105864.

[138] B. Zhang *et al.*, "Development and evaluation of oxaliplatin and irinotecan co-loaded liposomes for enhanced colorectal cancer therapy," *Journal of Controlled Release*, vol. 238, pp. 10–21, Sep. 2016, doi: 10.1016/j.jconrel.2016.07.022.

[139] A. Anitha, S. Maya, A. J. Sivaram, U. Mony, and R. Jayakumar, "Combinatorial nanomedicines for colon cancer therapy," *WIREs Nanomedicine and Nanobiotechnology*, vol. 8, no. 1, pp. 151–159, Jan. 2016, doi: 10.1002/wnan.1353.

[140] A. Seeber and G. Gastl, "Targeted Therapy of Colorectal Cancer," *Oncol Res Treat*, vol. 39, no. 12, pp. 796–802, 2016, doi: 10.1159/000453027.

[141] P. Kesharwani, R. Chadar, A. Sheikh, W. Y. Rizg, and A. Y. Safhi, "CD44-Targeted Nanocarrier for Cancer Therapy," *Front Pharmacol*, vol. 12, Mar. 2022, doi: 10.3389/fphar.2021.800481.

[142] S. Bhattacharya, "Anti-EGFR-mAb and 5-Fluorouracil Conjugated Polymeric Nanoparticles for Colorectal Cancer," *Recent Pat Anticancer Drug Discov*, vol. 16, no. 1, pp. 84–100, May 2021, doi: 10.2174/1574892815666201221121859.

[143] R. H. Fang and L. Zhang, "Dispersion-Based Methods for the Engineering and Manufacture of Polymeric Nanoparticles for Drug Delivery Applications," *Journal of Nanoengineering and Nanomanufacturing*, vol. 1, no. 1, pp. 106–112, Apr. 2011, doi: 10.1166/jnan.2011.1012.

[144] M. Haider, K. Z. Zaki, M. R. El Hamshary, Z. Hussain, G. Orive, and H. O. Ibrahim, "Polymeric nanocarriers: A promising tool for early diagnosis and efficient treatment of colorectal cancer," *J Adv Res*, vol. 39, pp. 237–255, Jul. 2022, doi: 10.1016/j.jare.2021.11.008.

[145] A. Agrawal, S. Rellegadla, and S. Jain, "Biomedical applications of PLGA particles," in *Materials for Biomedical Engineering*, Elsevier, 2019, pp. 87–129. doi: 10.1016/B978-0-12-816913-1.00004-0.

[146] H. K. Makadia and S. J. Siegel, "Poly Lactic-co-Glycolic Acid (PLGA) as Biodegradable Controlled Drug Delivery Carrier," *Polymers (Basel)*, vol. 3, no. 3, pp. 1377–1397, Aug. 2011, doi: 10.3390/polym3031377.

[147] C. M. Agrawal, D. Huang, J. P. Schmitz, and K. A. Athanasiou, "Elevated Temperature Degradation of a 50:50 Copolymer of PLA-PGA," *Tissue Eng*, vol. 3, no. 4, pp. 345–352, Dec. 1997, doi: 10.1089/ten.1997.3.345.

[148] A. Jasim, S. Abdelghany, and K. Greish, "Current Update on the Role of Enhanced Permeability and Retention Effect in Cancer Nanomedicine," in *Nanotechnology-Based Approaches for Targeting and Delivery of Drugs and Genes*, Elsevier, 2017, pp. 62–109. doi: 10.1016/B978-0-12-809717-5.00002-6.

[149] Q. Lu *et al.*, "Nanoparticles in tumor microenvironment remodeling and cancer immunotherapy," *J Hematol Oncol*, vol. 17, no. 1, p. 16, Apr. 2024, doi: 10.1186/s13045-024-01535-8.

[150] "PLGA Nanoparticles, Carboxyl, 20 mg - You Do Bio." Accessed: Jul. 01, 2024. [Online]. Available: https://www.youdobio.com/product/plga-nanoparticles-carboxyl-20-mg/

[151] X. Chen, L. Yi, Z. Yu, and L. Gao-wei, " Formulation, Characterization And Evaluation Of Curcumin- Loaded PLGA- TPGS Nanoparticles For Liver Cancer Treatment ," *Drug Des Devel Ther*, vol. Volume 13, pp. 3569–3578, Oct. 2019, doi: 10.2147/DDDT.S211748.

[152] X. Hu *et al.*, "Chitooligosaccharides-modified PLGA nanoparticles enhance the anti-tumor efficacy of AZD9291 (Osimertinib) by promoting apoptosis," *Int J Biol Macromol*, vol. 162, pp. 262–272, Nov. 2020, doi: 10.1016/j.ijbiomac.2020.06.154.

[153] C. E. Astete and C. M. Sabliov, "Synthesis and characterization of PLGA nanoparticles," *J Biomater Sci Polym Ed*, vol. 17, no. 3, pp. 247–289, Jan. 2006, doi: 10.1163/156856206775997322.

[154] B. Ikwuagwu and D. Tullman-Ercek, "Virus-like particles for drug delivery: a review of methods and applications," *Curr Opin Biotechnol*, vol. 78, p. 102785, Dec. 2022, doi: 10.1016/j.copbio.2022.102785.

[155] S. Nooraei *et al.*, "Virus-like particles: preparation, immunogenicity and their roles as nanovaccines and drug nanocarriers," *J Nanobiotechnology*, vol. 19, no. 1, p. 59, Feb. 2021, doi: 10.1186/s12951-021-00806-7.

[156] P. Kumari, B. Ghosh, and S. Biswas, "Nanocarriers for cancer-targeted drug delivery," *J Drug Target*, vol. 24, no. 3, pp. 179–191, Mar. 2016, doi: 10.3109/1061186X.2015.1051049.

[157] A. C. Anselmo and S. Mitragotri, "Nanoparticles in the clinic," *Bioeng Transl Med*, vol. 1, no. 1, pp. 10–29, Mar. 2016, doi: 10.1002/btm2.10003.

[158] B. Yuan *et al.*, "Virus-like particle-based nanocarriers as an emerging platform for drug delivery," *J Drug Target*, vol. 31, no. 5, pp. 433–455, May 2023, doi: 10.1080/1061186X.2023.2193358.

[159] J. He *et al.*, "Virus-like Particles as Nanocarriers for Intracellular Delivery of Biomolecules and Compounds," *Viruses*, vol. 14, no. 9, p. 1905, Aug. 2022, doi: 10.3390/v14091905.

[160] R. Jenjob, T. Phakkeeree, F. Seidi, M. Theerasilp, and D. Crespy, "Emulsion Techniques for the Production of Pharmacological Nanoparticles," *Macromol Biosci*, vol. 19, no. 6, Jun. 2019, doi: 10.1002/mabi.201900063.

[161] R. Paliwal, R. J. Babu, and S. Palakurthi, "Nanomedicine Scale-up Technologies: Feasibilities and Challenges," *AAPS PharmSciTech*, vol. 15, no. 6, pp. 1527–1534, Dec. 2014, doi: 10.1208/s12249-014-0177-9.

[162] F. Danhier, E. Ansorena, J. M. Silva, R. Coco, A. Le Breton, and V. Préat, "PLGA-based nanoparticles: An overview of biomedical applications," *Journal of Controlled Release*, vol. 161, no. 2, pp. 505–522, Jul. 2012, doi: 10.1016/J.JCONREL.2012.01.043.

[163] O. Esim, N. K. Bakirhan, M. Sarper, A. Savaser, S. A. Ozkan, and Y. Ozkan, "Influence of emulsifiers on the formation and in vitro anticancer activity of epirubicin loaded PLGA nanoparticles," *J Drug Deliv Sci Technol*, vol. 60, p. 102027, Dec. 2020, doi: 10.1016/j.jddst.2020.102027.

[164] D. Helal, "PREPARATION AND CHARACTERIZATION OF PLGA NANOPARTICLES," *Al-Azhar Journal of Pharmaceutical Sciences*, vol. 51, no. 1, pp. 1–17, Mar. 2015, doi: 10.21608/ajps.2015.12488.

[165] X. Guo *et al.*, "PLGA-Based Micro/Nanoparticles: An Overview of Their Applications in Respiratory Diseases," *Int J Mol Sci*, vol. 24, no. 5, p. 4333, Feb. 2023, doi: 10.3390/ijms24054333.

[166] A. Zielińska *et al.*, "Polymeric Nanoparticles: Production, Characterization, Toxicology and Ecotoxicology," *Molecules*, vol. 25, no. 16, p. 3731, Aug. 2020, doi: 10.3390/molecules25163731.

[167] Y.-C. Wang, Y.-T. Wu, H.-Y. Huang, and C.-S. Yang, "Surfactant-free Formulation of Poly(Lactic/Glycolic) Acid Nanoparticles Encapsulating Functional Polypeptide: A Technical Note," *AAPS PharmSciTech*, vol. 10, no. 4, p. 1263, Dec. 2009, doi: 10.1208/s12249-009-9330-2.

[168] C. Shi, F. Zeng, and D. Fu, "Surfactant-free poly(lactide-co-glycolide) nanoparticles for improving *in vitro* anticancer efficacy of tetrandrine," *J Microencapsul*, vol. 33, no. 3, pp. 249–256, Apr. 2016, doi: 10.3109/02652048.2016.1156175.

[169] K. Y. Hernández-Giottonini *et al.*, "PLGA nanoparticle preparations by emulsification and nanoprecipitation techniques: effects of formulation parameters," *RSC Adv*, vol. 10, no. 8, pp. 4218–4231, 2020, doi: 10.1039/C9RA10857B.

[170] Y. H. Chung, H. Cai, and N. F. Steinmetz, "Viral nanoparticles for drug delivery, imaging, immunotherapy, and theranostic applications," *Adv Drug Deliv Rev*, vol. 156, pp. 214–235, 2020, doi: 10.1016/j.addr.2020.06.024.

[171] D. T. Le and K. M. Müller, "In Vitro Assembly of Virus-Like Particles and Their Applications," *Life*, vol. 11, no. 4, p. 334, Apr. 2021, doi: 10.3390/life11040334.

[172] R. Biabanikhankahdani, K. Ho, N. Alitheen, and W. Tan, "A Dual Bioconjugated Virus-Like Nanoparticle as a Drug Delivery System and Comparison with a pH-Responsive Delivery System," *Nanomaterials*, vol. 8, no. 4, p. 236, Apr. 2018, doi: 10.3390/nano8040236.

[173] K. R. Kim, A. S. Lee, S. M. Kim, H. R. Heo, and C. S. Kim, "Virus-like nanoparticles as a theranostic platform for cancer," *Front Bioeng Biotechnol*, vol. 10, Jan. 2023, doi: 10.3389/fbioe.2022.1106767.

[174] H. Hu and N. F. Steinmetz, "Doxorubicin-Loaded Physalis Mottle Virus Particles Function as a pH-Responsive Prodrug Enabling Cancer Therapy," *Biotechnol J*, vol. 15, no. 12, Dec. 2020, doi: 10.1002/biot.202000077.

[175] R. L. McCall and R. W. Sirianni, "PLGA Nanoparticles Formed by Single- or Double-emulsion with Vitamin E-TPGS," *Journal of Visualized Experiments*, no. 82, Dec. 2013, doi: 10.3791/51015.

[176] K. Y. Hernández-Giottonini *et al.*, "PLGA nanoparticle preparations by emulsification and nanoprecipitation techniques: effects of formulation parameters," *RSC Adv*, vol. 10, no. 8, pp. 4218–4231, 2020, doi: 10.1039/C9RA10857B.

[177] T. Lea, "Caco-2 Cell Line," in *The Impact of Food Bioactives on Health*, Cham: Springer International Publishing, 2015, pp. 103–111. doi: 10.1007/978-3-319-16104-4_10.

[178] L. Ascar, I. Ahumada, A. López, F. Quintanilla, and K. Leiva, "Nonsteroidal Anti-Inflammatory Drug Determination in Water Samples by HPLC-DAD under Isocratic Conditions," *J Braz Chem Soc*, 2013, doi: 10.5935/0103-5053.20130150.

[179] E. Lagreca, V. Onesto, C. Di Natale, S. La Manna, P. A. Netti, and R. Vecchione, "Recent advances in the formulation of PLGA microparticles for controlled drug delivery," *Prog Biomater*, vol. 9, no. 4, pp. 153–174, Dec. 2020, doi: 10.1007/s40204-020-00139-y.

[180] M. G. Nava-Arzaluz, E. Pinon-Segundo, A. Ganem-Rondero, and D. Lechuga-Ballesteros, "Single Emulsion-Solvent Evaporation Technique and Modifications for the Preparation of Pharmaceutical Polymeric Nanoparticles," *Recent Pat Drug Deliv Formul*, vol. 6, no. 3, pp. 209–223, Aug. 2012, doi: 10.2174/187221112802652633.

[181] T. Gaaz, A. Sulong, M. Akhtar, A. Kadhum, A. Mohamad, and A. Al-Amiery, "Properties and Applications of Polyvinyl Alcohol, Halloysite Nanotubes and Their Nanocomposites," *Molecules*, vol. 20, no. 12, pp. 22833–22847, Dec. 2015, doi: 10.3390/molecules201219884.

[182] X. CHEN and T. Wang, "Preparation and characterization of atrazine-loaded biodegradable PLGA nanospheres," *J Integr Agric*, vol. 18, no. 5, pp. 1035–1041, May 2019, doi: 10.1016/S2095-3119(19)62613-4.

[183] C. K. Holley, S. Alkhalifah, and S. Majd, "Fabrication and Optimization of Dp44mT-Loaded Nanoparticles," in *2018 40th Annual International Conference of the IEEE Engineering in Medicine and Biology Society (EMBC)*, IEEE, Jul. 2018, pp. 5733–5736. doi: 10.1109/EMBC.2018.8513598.

[184] Y. Z. Zhou, R. G. Alany, V. Chuang, and J. Wen, "Optimization of PLGA nanoparticles formulation containing L-DOPA by applying the central composite design," *Drug Dev Ind Pharm*, vol. 39, no. 2, pp. 321–330, Feb. 2013, doi: 10.3109/03639045.2012.681054.

[185] P. V. Date, A. Samad, and P. V. Devarajan, "Freeze Thaw: A Simple Approach for Prediction of Optimal Cryoprotectant for Freeze Drying," *AAPS PharmSciTech*, vol. 11, no. 1, pp. 304–313, Mar. 2010, doi: 10.1208/s12249-010-9382-3.

[186] H. O. Alsaab *et al.*, "PLGA-Based Nanomedicine: History of Advancement and Development in Clinical Applications of Multiple Diseases," *Pharmaceutics*, vol. 14, no. 12, p. 2728, Dec. 2022, doi: 10.3390/pharmaceutics14122728.

[187] N. Surya and S. Bhattacharyya, "PLGA – THE SMART POLYMER FOR DRUG DELIVERY," *Pharmacy & Pharmacology*, vol. 9, no. 5, pp. 334–345, Oct. 2021, doi: 10.19163/2307-9266-2021-9-5-334-345.

[188] M. Alkholief, M. A. Kalam, M. K. Anwer, and A. Alshamsan, "Effect of Solvents, Stabilizers and the Concentration of Stabilizers on the Physical Properties of Poly(d,l-lactide-co-glycolide) Nanoparticles: Encapsulation, In Vitro Release of Indomethacin and Cytotoxicity against HepG2-Cell," *Pharmaceutics*, vol. 14, no. 4, p. 870, Apr. 2022, doi: 10.3390/pharmaceutics14040870.

[189] C. Draheim, F. de Crécy, S. Hansen, E.-M. Collnot, and C.-M. Lehr, "A Design of Experiment Study of Nanoprecipitation and Nano Spray Drying as Processes to Prepare PLGA Nano- and Microparticles with Defined Sizes and Size Distributions," *Pharm Res*, Feb. 2015, doi: 10.1007/s11095-015-1647-9.

[190] L. J. Mohan, L. McDonald, J. S. Daly, and Z. Ramtoola, "Optimising PLGA-PEG Nanoparticle Size and Distribution for Enhanced Drug Targeting to the Inflamed Intestinal Barrier," *Pharmaceutics*, vol. 12, no. 11, p. 1114, Nov. 2020, doi: 10.3390/pharmaceutics12111114.

[191] W. Huang and C. Zhang, "Tuning the Size of Poly(lactic-co-glycolic Acid) (PLGA) Nanoparticles Fabricated by Nanoprecipitation," *Biotechnol J*, vol. 13, no. 1, Jan. 2018, doi: 10.1002/biot.201700203.

[192] R. Bakhaidar *et al.*, "Effect of Size and Concentration of PLGA-PEG Nanoparticles on Activation and Aggregation of Washed Human Platelets," *Pharmaceutics*, vol. 11, no. 10, p. 514, Oct. 2019, doi: 10.3390/pharmaceutics11100514.

[193] A. Budhian, S. J. Siegel, and K. I. Winey, "Haloperidol-loaded PLGA nanoparticles: Systematic study of particle size and drug content," *Int J Pharm*, vol. 336, no. 2, pp. 367–375, May 2007, doi: 10.1016/j.ijpharm.2006.11.061.

[194] S. Ray, A. Mishra, T. K. Mandal, B. Sa, and J. Chakraborty, "Optimization of the process parameters for the fabrication of a polymer coated layered double hydroxide-methotrexate nanohybrid for the possible treatment of osteosarcoma," *RSC Adv*, vol. 5, no. 124, pp. 102574–102592, 2015, doi: 10.1039/C5RA15859A.

[195] D. Cun *et al.*, "High loading efficiency and sustained release of siRNA encapsulated in PLGA nanoparticles: Quality by design optimization and characterization," *European Journal of Pharmaceutics and Biopharmaceutics*, vol. 77, no. 1, pp. 26–35, Jan. 2011, doi: 10.1016/j.ejpb.2010.11.008.

[196] S. Desgouilles *et al.*, "The Design of Nanoparticles Obtained by Solvent Evaporation: A Comprehensive Study," *Langmuir*, vol. 19, no. 22, pp. 9504–9510, Oct. 2003, doi: 10.1021/la034999q.

[197] J. W. Hickey, J. L. Santos, J.-M. Williford, and H.-Q. Mao, "Control of polymeric nanoparticle size to improve therapeutic delivery," *Journal of Controlled Release*, vol. 219, pp. 536–547, Dec. 2015, doi: 10.1016/j.jconrel.2015.10.006.

[198] A. Schädlich *et al.*, "Tumor Accumulation of NIR Fluorescent PEG–PLA Nanoparticles: Impact of Particle Size and Human Xenograft Tumor Model," *ACS Nano*, vol. 5, no. 11, pp. 8710–8720, Nov. 2011, doi: 10.1021/nn2026353.

[199] S. S. Chakravarthi, S. De, D. W. Miller, and D. H. Robinson, "Comparison of anti-tumor efficacy of paclitaxel delivered in nano- and microparticles," *Int J Pharm*, vol. 383, no. 1–2, pp. 37–44, Jan. 2010, doi: 10.1016/j.ijpharm.2009.09.004.

[200] M. Kaplan, K. Öztürk, S. C. Öztürk, E. Tavukçuoğlu, G. Esendağlı, and S. Calis, "Effects of Particle Geometry for PLGA-Based Nanoparticles: Preparation and In Vitro/In Vivo Evaluation," *Pharmaceutics*, vol. 15, no. 1, p. 175, Jan. 2023, doi: 10.3390/pharmaceutics15010175.

[201] A. Tchoryk *et al.*, "Penetration and Uptake of Nanoparticles in 3D Tumor Spheroids," *Bioconjug Chem*, vol. 30, no. 5, pp. 1371–1384, May 2019, doi: 10.1021/acs.bioconjchem.9b00136.

[202] X. Song *et al.*, "Dual agents loaded PLGA nanoparticles: Systematic study of particle size and drug entrapment efficiency," *European Journal of Pharmaceutics and Biopharmaceutics*, vol. 69, no. 2, pp. 445–453, Jun. 2008, doi: 10.1016/j.ejpb.2008.01.013.

[203] K. Sawasdee, P. Choksawad, S. Pimcharoen, and K. Prapainop, "Development of size-tunable polymeric nanoparticles for drug delivery applications," *GHMJ (Global Health Management Journal)*, vol. 1, no. 2, p. 31, Oct. 2017, doi: 10.35898/ghmj-12113.

[204] K. Ozturk, S. Caban, S. Kozlu, E. Kadayifci, F. Yerlikaya, and Y. Capan, "The influence of technological parameters on the physicochemical properties of blank PLGA nanoparticles.," *Pharmazie*, vol. 65, no. 9, pp. 665–9, Sep. 2010.

[205] V. M. Burlakov and A. Goriely, "Reverse Coarsening and the Control of Particle Size Distribution through Surfactant," *Applied Sciences*, vol. 10, no. 15, p. 5359, Aug. 2020, doi: 10.3390/app10155359.

[206] R. Parveen, A. Datta, and P. Kumar Maiti, "Concentration of Capping Agent Controls Size Selection, Agglomeration and Antimicrobial Action of Silver Nanoparticles," *Journal of Surface Science and Technology*, Apr. 2021, doi: 10.18311/jsst/2020/24875.

[207] C. Vauthier, B. Cabane, and D. Labarre, "How to concentrate nanoparticles and avoid aggregation?," *European Journal of Pharmaceutics and Biopharmaceutics*, vol. 69, no. 2, pp. 466–475, Jun. 2008, doi: 10.1016/j.ejpb.2008.01.025.

[208] J. U. Menon, S. Kona, A. S. Wadajkar, F. Desai, A. Vadla, and K. T. Nguyen, "Effects of surfactants on the properties of PLGA nanoparticles," *J Biomed Mater Res A*, vol. 100A, no. 8, pp. 1998–2005, Aug. 2012, doi: 10.1002/jbm.a.34040.

[209] V. Uskoković, "Factors defining the stability of poly(lactide-co-glycolide) spheres for the sustained release of a cysteine protease inhibitor," *Int J Pharm*, vol. 583, p. 119316, Jun. 2020, doi: 10.1016/j.ijpharm.2020.119316.

[210] N. Grabowski *et al.*, "Toxicity of surface-modified PLGA nanoparticles toward lung alveolar epithelial cells," *Int J Pharm*, vol. 454, no. 2, pp. 686–694, Oct. 2013, doi: 10.1016/j.ijpharm.2013.05.025.

[211] S. K. Sahoo, J. Panyam, S. Prabha, and V. Labhasetwar, "Residual polyvinyl alcohol associated with poly (d,l-lactide-co-glycolide) nanoparticles affects their physical properties

and cellular uptake," *Journal of Controlled Release*, vol. 82, no. 1, pp. 105–114, Jul. 2002, doi: 10.1016/S0168-3659(02)00127-X.

[212] B. Shkodra *et al.*, "Effect of surfactant on the size and stability of PLGA nanoparticles encapsulating a protein kinase C inhibitor," *Int J Pharm*, vol. 566, pp. 756–764, Jul. 2019, doi: 10.1016/j.ijpharm.2019.05.072.

[213] C. J. Martínez Rivas *et al.*, "Nanoprecipitation process: From encapsulation to drug delivery," *Int J Pharm*, vol. 532, no. 1, pp. 66–81, Oct. 2017, doi: 10.1016/j.ijpharm.2017.08.064.

[214] W. Badri, K. Miladi, Q. A. Nazari, H. Fessi, and A. Elaissari, "Effect of process and formulation parameters on polycaprolactone nanoparticles prepared by solvent displacement," *Colloids Surf A Physicochem Eng Asp*, vol. 516, pp. 238–244, Mar. 2017, doi: 10.1016/j.colsurfa.2016.12.029.

[215] E. Trenkenschuh and W. Friess, "Freeze-drying of nanoparticles: How to overcome colloidal instability by formulation and process optimization," *European Journal of Pharmaceutics and Biopharmaceutics*, vol. 165, pp. 345–360, Aug. 2021, doi: 10.1016/j.ejpb.2021.05.024.

[216] G. J. Pillai, M. M. Greeshma, and D. Menon, "Impact of poly(lactic-co-glycolic acid) nanoparticle surface charge on protein, cellular and haematological interactions," *Colloids Surf B Biointerfaces*, vol. 136, pp. 1058–1066, Dec. 2015, doi: 10.1016/j.colsurfb.2015.10.047.

[217] Y. Wang, C. Pi, X. Feng, Y. Hou, L. Zhao, and Y. Wei, "The Influence of Nanoparticle Properties on Oral Bioavailability of Drugs.," *Int J Nanomedicine*, vol. 15, pp. 6295–6310, 2020, doi: 10.2147/IJN.S257269.

[218] M. A. C. Potenza *et al.*, "Single particle optical extinction and scattering allows real time quantitative characterization of drug payload and degradation of polymeric nanoparticles," *Sci Rep*, vol. 5, no. 1, p. 18228, Dec. 2015, doi: 10.1038/srep18228.

[219] F. Danhier, E. Ansorena, J. M. Silva, R. Coco, A. Le Breton, and V. Préat, "PLGA-based nanoparticles: An overview of biomedical applications," *Journal of Controlled Release*, vol. 161, no. 2, pp. 505–522, Jul. 2012, doi: 10.1016/j.jconrel.2012.01.043.

[220] M. Kumar, P. Kulkarni, S. Liu, N. Chemuturi, and D. K. Shah, "Nanoparticle biodistribution coefficients: A quantitative approach for understanding the tissue distribution of nanoparticles," *Adv Drug Deliv Rev*, vol. 194, p. 114708, Mar. 2023, doi: 10.1016/j.addr.2023.114708.

[221] P. Wang, S. M. Henning, and D. Heber, "Limitations of MTT and MTS-Based Assays for Measurement of Antiproliferative Activity of Green Tea Polyphenols," *PLoS One*, vol. 5, no. 4, p. e10202, Apr. 2010, doi: 10.1371/journal.pone.0010202.

[222] M. Trif *et al.*, "Cytotoxicity and intracellular fate of PLGA and chitosan-coated PLGA nanoparticles in Madin–Darby bovine kidney (MDBK) and human colorectal adenocarcinoma (Colo 205) cells," *J Biomed Mater Res A*, vol. 103, no. 11, pp. 3599–3611, Nov. 2015, doi: 10.1002/jbm.a.35498.

[223] D. Cun *et al.*, "High loading efficiency and sustained release of siRNA encapsulated in PLGA nanoparticles: Quality by design optimization and characterization," *European Journal of Pharmaceutics and Biopharmaceutics*, vol. 77, no. 1, pp. 26–35, Jan. 2011, doi: 10.1016/j.ejpb.2010.11.008.

[224] M. Son *et al.*, "Effects of osmolality and solutes on the morphology of red blood cells according to three-dimensional refractive index tomography.," *PLoS One*, vol. 16, no. 12, p. e0262106, 2021, doi: 10.1371/journal.pone.0262106.

[225] N. B. Ghomrasni, C. Chivas-Joly, L. Devoille, J.-F. Hochepied, and N. Feltin, "Challenges in sample preparation for measuring nanoparticles size by scanning electron microscopy from suspensions, powder form and complex media," *Powder Technol*, vol. 359, pp. 226–237, Jan. 2020, doi: 10.1016/j.powtec.2019.10.022.

[226] C. Mohanty and S. K. Sahoo, "The in vitro stability and in vivo pharmacokinetics of curcumin prepared as an aqueous nanoparticulate formulation," *Biomaterials*, vol. 31, no. 25, pp. 6597–6611, Sep. 2010, doi: 10.1016/j.biomaterials.2010.04.062.

[227] C. E. Rapier, K. J. Shea, and A. P. Lee, "Investigating PLGA microparticle swelling behavior reveals an interplay of expansive intermolecular forces," *Sci Rep*, vol. 11, no. 1, p. 14512, Jul. 2021, doi: 10.1038/s41598-021-93785-6.

[228] T. L. Moore *et al.*, "Nanoparticle colloidal stability in cell culture media and impact on cellular interactions," *Chem Soc Rev*, vol. 44, no. 17, pp. 6287–6305, 2015, doi: 10.1039/C4CS00487F.

[229] B. Vuković *et al.*, "Surface Stabilization Affects Toxicity of Silver Nanoparticles in Human Peripheral Blood Mononuclear Cells," *Nanomaterials*, vol. 10, no. 7, p. 1390, Jul. 2020, doi: 10.3390/nano10071390.

[230] Z. R. Stromberg *et al.*, "Formulation of stabilizer-free, nontoxic PLGA and elastin-PLGA nanoparticle delivery systems," *Int J Pharm*, vol. 597, Mar. 2021, doi: 10.1016/j.ijpharm.2021.120340.

[231] R. M. Shah, D. S. Eldridge, E. A. Palombo, and I. H. Harding, "Stability mechanisms for microwave-produced solid lipid nanoparticles," *Colloids Surf A Physicochem Eng Asp*, vol. 643, p. 128774, Jun. 2022, doi: 10.1016/j.colsurfa.2022.128774.

[232] M. Martins, I. M. Aroso, R. L. Reis, A. R. C. Duarte, R. Craveiro, and A. Paiva, "Enhanced performance of supercritical fluid foaming of natural-based polymers by deep eutectic solvents," *AIChE Journal*, vol. 60, no. 11, pp. 3701–3706, Nov. 2014, doi: 10.1002/aic.14607.

[233] M. Pu, K. Liu, M. Zhang, P. Yuan, and J. Cai, "Microparticles and Microcapsules from the Solvent Extraction of Deep Eutectic Solvent-Based Emulsion," *Ind Eng Chem Res*, vol. 59, no. 7, pp. 2892–2898, Feb. 2020, doi: 10.1021/acs.iecr.9b05061.

[234] S. Shrestha, B. Wang, and P. Dutta, "Nanoparticle processing: Understanding and controlling aggregation," *Adv Colloid Interface Sci*, vol. 279, p. 102162, May 2020, doi: 10.1016/j.cis.2020.102162.

[235] O. I. Corrigan and X. Li, "Quantifying drug release from PLGA nanoparticulates," *European Journal of Pharmaceutical Sciences*, vol. 37, no. 3–4, pp. 477–485, Jun. 2009, doi: 10.1016/j.ejps.2009.04.004.

[236] S. S. Ozturk and B. O. Palsson, "Effect of medium osmolarity on hybridoma growth, metabolism, and antibody production," *Biotechnol Bioeng*, vol. 37, no. 10, pp. 989–993, Apr. 1991, doi: 10.1002/bit.260371015.

[237] M. M. El-Hammadi, Á. V. Delgado, C. Melguizo, J. C. Prados, and J. L. Arias, "Folic acid-decorated and PEGylated PLGA nanoparticles for improving the antitumour activity of 5-fluorouracil," *Int J Pharm*, vol. 516, no. 1–2, pp. 61–70, Jan. 2017, doi: 10.1016/j.ijpharm.2016.11.012.

[238] L. Rashidi, F. Ganji, and E. Vasheghani-Farahani, "Fluorescein isothiocyanate-dyed mesoporous silica nanoparticles for tracking antioxidant delivery," *IET Nanobiotechnol*, vol. 11, no. 4, pp. 454–462, Jun. 2017, doi: 10.1049/iet-nbt.2016.0120.

[239] X. Wang, H. Peng, S. Huang, and F. You, "Preparation of Fluorescent Dye-Doped Biocompatible Nanoparticles for Cell Labeling," *J Nanosci Nanotechnol*, vol. 16, no. 4, pp. 3602–3607, Apr. 2016, doi: 10.1166/jnn.2016.11820.

[240] V. Sharma, S. Anandhakumar, and M. Sasidharan, "Self-degrading niosomes for encapsulation of hydrophilic and hydrophobic drugs: An efficient carrier for cancer multi-drug delivery," *Materials Science and Engineering: C*, vol. 56, pp. 393–400, Nov. 2015, doi: 10.1016/j.msec.2015.06.049.

[241] K. Sasaki *et al.*, "Nanoparticle-Mediated Delivery of 2-Deoxy-D-Glucose Induces Antitumor Immunity and Cytotoxicity in Liver Tumors in Mice," *Cell Mol Gastroenterol Hepatol*, vol. 11, no. 3, pp. 739–762, 2021, doi: 10.1016/j.jcmgh.2020.10.010.

[242] T. D. de Oliveira, L. R. Travassos, D. C. Arruda, and D. B. Tada, "Intracellular Targeting of Poly Lactic-Co-Glycolic Acid Nanoparticles by Surface Functionalization with Peptides," *J Biomed Nanotechnol*, vol. 17, no. 7, pp. 1320–1329, Jul. 2021, doi: 10.1166/jbn.2021.3108.

[243] P. Xu *et al.*, "Intracellular Drug Delivery by Poly(lactic- *co* -glycolic acid) Nanoparticles, Revisited," *Mol Pharm*, vol. 6, no. 1, pp. 190–201, Feb. 2009, doi: 10.1021/mp800137z.

[244] Y. Malinovskaya *et al.*, "Delivery of doxorubicin-loaded PLGA nanoparticles into U87 human glioblastoma cells," *Int J Pharm*, vol. 524, no. 1–2, pp. 77–90, May 2017, doi: 10.1016/j.ijpharm.2017.03.049.

[245] P. Franco and I. De Marco, "Nanoparticles and Nanocrystals by Supercritical CO2-Assisted Techniques for Pharmaceutical Applications: A Review," *Applied Sciences*, vol. 11, no. 4, p. 1476, Feb. 2021, doi: 10.3390/app11041476.

[246] S. J. Shepherd, D. Issadore, and M. J. Mitchell, "Microfluidic formulation of nanoparticles for biomedical applications," *Biomaterials*, vol. 274, p. 120826, Jul. 2021, doi: 10.1016/j.biomaterials.2021.120826.

[247] S. Rogstad, M. Boyne, and A. Ruth, "Mass Spectrometry in the Characterization of Complex Drugs," 2019, pp. 139–155. doi: 10.1007/978-3-030-11751-1_8.

[248] Y. Fan, M. Marioli, and K. Zhang, "Analytical characterization of liposomes and other lipid nanoparticles for drug delivery," *J Pharm Biomed Anal*, vol. 192, p. 113642, Jan. 2021, doi: 10.1016/j.jpba.2020.113642.

[249] J. S. Suk, Q. Xu, N. Kim, J. Hanes, and L. M. Ensign, "PEGylation as a strategy for improving nanoparticle-based drug and gene delivery," *Adv Drug Deliv Rev*, vol. 99, pp. 28–51, Apr. 2016, doi: 10.1016/j.addr.2015.09.012.

[250] D. T. Akhter *et al.*, "Oral Delivery of Multicompartment Nanomedicines for Colorectal Cancer Therapeutics: Combining Loco-Regional Delivery with Cell-Target Specificity," *Adv Ther (Weinh)*, vol. 3, no. 2, Feb. 2020, doi: 10.1002/adtp.201900171.

[251] T. Yang *et al.*, "'Targeting Design' of Nanoparticles in Tumor Therapy," *Pharmaceutics*, vol. 14, no. 9, p. 1919, Sep. 2022, doi: 10.3390/pharmaceutics14091919.

[252] R. M. Pearson, H. Hsu, J. Bugno, and S. Hong, "Understanding nano-bio interactions to improve nanocarriers for drug delivery," *MRS Bull*, vol. 39, no. 3, pp. 227–237, Mar. 2014, doi: 10.1557/mrs.2014.9.

2024

Carolina Guerra Neca

UM TÍTULO DE TESE LONGO E IMPRESSIONANTE COM UMA MUDANÇA DE LINHA FORÇADA

NOVA SCHOOL OF SCIENCE & TECHNOLOGY